

Department for International Development

KAR Project R8038

**Impact of CLimate And Sea Level Change in part of
the Indian Sub-Continent (CLASIC)**

Final Report, February 2007

by

Frank Farquharson¹, Fai Fung¹,

Jahir U. Chowdhury²,

Ahmadhul Hassan³,

Kevin Horsburgh⁴ and Jason Lowe⁵

¹Centre for Ecology and Hydrology, Wallingford, UK

²Institute of Water and Flood Management, BUET, Bangladesh

³Center for Environment and Geographical Information System, Bangladesh

⁴Proudman Oceanographic Laboratory, Liverpool, UK

⁵Hadley Centre, Meteorological Office, UK

Contents

- 1 Introduction..... 11**
- 2 Collaboration with partners in Bangladesh 14**
- 3 Water Resources: Modelling..... 16**
 - 3.1 Global Water Availability Assessment (GWAVA) 16**
 - 3.2 Rainfall-Runoff Model..... 16**
 - 3.3 Routing between cells 17**
 - 3.4 Glacier and Snow Model 17**
 - 3.5 Model Resolution 20**
 - 3.6 Water Availability Indices 23**
- 4 Water Resources: Data..... 25**
 - 4.1 Physical Parameters Data 26**
 - 4.2 Water Demands..... 34**
 - 4.3 Climate Data..... 49**
- 5 Water Resources: Calibration..... 56**
 - 5.1 Observed Flows for GBM Model..... 56**
 - 5.2 Calibration of FSB Model 58**
- 6 Water Resources: Calibration..... 60**
 - 6.1 GBM Model..... 60**
 - 6.2 Calibration of FSB Model 64**
 - 6.3 Calibration Results 66**
- 7 Water Resources: Results..... 69**
 - 7.1 Introduction..... 69**
 - 7.2 Climate Change Data..... 69**
 - 7.3 Climate Change Impacts on River Flow 76**
 - 7.4 Flows at Farakka Barrage..... 84**
 - 7.5 Water Availability in the Ganges-Brahmaputra- Meghna Basin..... 86**

7.6	Discussion	91
8	<i>Tropical Storms</i>	92
8.1	Introduction.....	92
8.2	Regional model (RCM) description and scenarios.....	92
8.3	Regional model temperature and surface pressure results	94
8.4	Representation of cyclones in the PRECIS climate model	97
9	<i>Extreme Water Level Modelling</i>	106
9.1	Regional Distribution of Rxtreme Water Levels.....	108
9.2	Local Analysis of Extreme Water Levels.....	115
10	<i>Conclusions</i>	120
11	<i>Dissemination of Results</i>	123
12	<i>References</i>	124
	<i>Appendix A Data Sources for Areas Outside of Bangladesh</i>	1
	<i>Appendix B Provisional programme for final Dissemination Workshop</i>	4
	<i>Appendix C: Land cover to soil capacity conversion</i>	6
	<i>Appendix D: Water Availability Indices for GBM</i>	8

List of Figures

Figure 1 Schematic representation of glacier model: (a) glaciers from DCW (2000) (b) simplified representation of glacier.....	20
Figure 2 Representation of grid resolution for GBM and FSB model.....	20
Figure 3 Fine-scale grid showing MPOs and Bangladesh river system.....	22
Figure 4 Structure of database used in GWAVA.....	25
Figure 5 Drainage network of GBM model.....	26
Figure 6 FSB model drainage network and calibration catchments and gauge stations.....	28
Figure 7 Global land cover characteristics for GBM area.....	30
Figure 8 Major land uses of Bangladesh.....	32
Figure 9 General methodology for correcting raster datasets using country-specific data.....	36
Figure 10 FAO Global map of irrigated areas (GMIA), where darker blues indicate greater fraction of irrigation in cell.....	37
Figure 11 Distribution of rice in 1992 from Ramankutty and Foley (1998). Greener areas have a greater fraction of rice and redder areas less.	38
Figure 12 Annual water demand for GBM (a) Baseline (b) 2050 High Scenario.....	43
Figure 13 Example of mean daily precipitation for baseline climate from HadRM2 simulation of South Asia. Boxes represent rotate polar co-ordinate grid in geographic projection. Circles represent original HadRM2 data and background grid represents values following nearest neighbour interpolation onto a geographic projection grid.....	51
Figure 14 Difference between PRECIS Baseline Ensemble and CRUTS2.1 precipitation: (a) dry Season (b) wet season.....	53
Figure 15 Sub-catchments and gauging station locations in the Ganges-Brahmaputra-Meghna basin.	58
Figure 16 Sub-catchments and gauging station locations in the Ganges-Brahmaputra-Meghna basin.	62
Figure 17 Difference between CRU and UWH annual precipitation (mm).....	64
Figure 18 Daily flows 1979-1999 at Hardinge Bridge (Ganges River).....	66
Figure 19 Daily flows 1979-1993 at Bahadurabad (Brahmaputra River).....	66
Figure 20 Daily flows 1984-1992 at Kaunia (Tista River).....	66
Figure 21 Comparison of modelled and observed discharge for two sub-catchments (a) Atrai sub-catchment Area (b) Gumti sub-catchment.....	68

Figure 22 Absolute differences between UWH and GCMs for mean monthly climate parameters for 1979-1999 for GBM region.	70
Figure 23 Change in dry season precipitation in 2050s for downscaled GCM A2 scenarios compared to 1979-1999.....	71
Figure 24 Change in wet season precipitation in 2050s for downscaled GCM A2 scenarios compared to 1979-1999.....	72
Figure 25 Change in dry season precipitation in 21st century for downscaled GCM A2 scenarios compared to 1979-1999 using HADCM3	73
Figure 26 Change in wet season precipitation in 21st century for downscaled GCM A2 scenarios compared to 1979-1999 using HADCM3	73
Figure 27 Change in precipitation in 2050s for A2 scenario compared to 1979-1999 using a GCM and RCMs from the Hadley Centre.....	75
Figure 28 Mean decad hydrographs for GCMs for 2020s compared to baseline flows at cells near (a) Bahadurabad (b) Hardinge Bridge (c) Kaunia (d) Yangcun.....	77
Figure 29 Mean decad hydrographs for GCMs for 2050s compared to baseline flows at cells near (a) Bahadurabad (b) Hardinge Bridge (c) Kaunia (d) Yangcun.....	78
Figure 30 Percentage changes in mean annual flow for GCMs compared to baseline.....	79
Figure 31 Percentage changes in mean annual flow compared to baseline for Hadley Centre models in (a) 2020s (b) 2050s.....	80
Figure 32 Mean decad hydrographs for Hadley Centre Models for 2020s and 2050s compared to baseline at cells near (a) Bahadurabad (b) Hardinge Bridge (c) Kaunia (d) Yangcun.	82
Figure 33 Changes from baseline for seasonal flows for RCMs in the 2050s.....	83
Figure 34 Mean deacad flows at Farakka barrage for Hadley Centre models	85
Figure 35 Scatter plot of $\overline{q_{dry}^{year}}$ for each cell in GBM region (a) 2025 (b) 2050 (note that baseline values have been plotted along the x-axis).	86
Figure 36 Total water availability index 4 for Hadley Centre climate models.....	87
Figure 37 Number of cells showing stress compared to baseline for Hadley Centre Models.	89
Figure 38 Changes in SWAI-4 for Hadley Centre models where positive values show increase in water stress.	90
Figure 39 Model domains	93
Figure 40 Temperature rise ($^{\circ}\text{C}$) between baseline and future simulation (SRES B2 Scenario)	95

Figure 41 A typical RCM simulated cyclone in the new control simulation. Frames show the evolution at 6 hour intervals. Pressure at mean sea level is in mb.....	96
Figure 42 RCM simulated pressure and fitted Holland model along a line from the centre of the cyclone.....	99
Figure 43 RCM simulated wind and fitted Holland model along a line from the centre of the cyclone.	100
Figure 44: 30 years of modeled cyclone tracks from the Baseline run.....	101
Figure 45: 30 years of modeled cyclone tracks from the A2 run.....	101
Figure 46: 28 years of observed cyclone tracks from the JTWC database	102
Figure 47: Summarising the results of significance testing on the number of storms per year.	103
Figure 48: Division of the coastline into segments.....	103
Figure 49: Significant model bias in the spatial distribution of storms (left) and no significant change in the normalized spatial distribution of storms under the changed climate (right)	104
Figure 50: Global average sea level rise 1990 to 2100 for the SRES scenarios. (Reproduced from IPCC TAR Figure 11.12; see there for full details.).....	108
Figure 51: Percentiles of extreme water levels in the surge domain, showing values from the baseline time slice and changes arising under the two different future scenarios.....	109
Figure 52: As fig 30 but for residual elevation (i.e. after removal of the tide component). ..	110
Figure 53: MSLP anomaly by season between B2 model run and an “idealised B2” derived from linearly interpolated MSLP changes between the baseline and A2 run, taking the mean 1.5 metre temperature over the sea as the independent variable.	112
Figure 54: Modelled Baseline MSLP and changes in MSPL under the A2 scenario	113
Figure 55: Modelled Baseline MSLP and changes in MSPL under the B2 scenario.....	114
Figure 56 Return period curves for baseline and future changes under A2 and B2 scenarios for changes in storminess alone, and changes in time average sea level (neglecting non linear depth effects of mean sea level on surges). Panel 1 is for Cox’s Bazar surge plus tide results. Panel 2 is for Baleswar surge plus tide result. Panel 3 and 4 are as panels 1 and 2 but for surge residuals only.	118
Figure 57: Quantile-Quantile plots for four of the pixels described in Section 9.2. Only extreme water levels above the 99 percentile are shown. Notice that in three cases the extreme water levels are larger under the A2 scenario, as expected, but that at Baleswar in the west of the bay, the opposite is true.	119

List of Tables

Table 1 Summary of water availability indices.....	24
Table 2 Soil classes according to AEZ database.....	29
Table 3 GWAVA soil classes from AEZ soil classes	30
Table 4 Comparison of glacier characteristics	33
Table 5 Total population of Bangladesh in 1990	35
Table 6 Population data for each country for baseline and future horizons.....	41
Table 7 Water Consumption per head (l/head/day)	41
Table 8 Future livestock population.....	42
Table 9 In-stream demand by region.....	44
Table 10 Water Supply Demands by region in 2025	45
Table 11 Surface Water Demand within GIT	46
Table 12 Surface water Demand outside the GIT	46
Table 13 Estimated Agricultural Evaporation in 2025.....	47
Table 14 Net Water Supply Demands by Region in 2025	47
Table 15 Evaporation from Environment, Fisheries and Forests in GIT Area	48
Table 16 Maximum Evaporation from Agriculture in GIT Area.....	48
Table 17 Surface Water Required for Full Irrigation by Region within GIT	49
Table 18 Climate data available for regional climate scenario analysis. Note in addition to the above see Table 20 for available GCM climate data.	49
Table 19 Comparison of mean annual climate variables for baseline period between CRUTS2.1 and mean of PRECIS A, B and C.....	53
Table 20 List of global circulation models available for A2 and B2 scenarios (based on IPCC, 2006).....	55
Table 21 Description of model parameters requiring calibration	56
Table 22 Details of gauged sites used to calibrate the GBM model	57
Table 23 Summary of gauge sites for calibration of FSB model	59
Table 24 Description of model parameters requiring calibration	60
Table 25 Details of gauged sites used to calibrate the GBM model	61
Table 26 Comparison of observed runoff with simple water balance calculation at gauged locations	63
Table 27 Summary of gauge sites for calibration of FSB model	65
Table 28 Key for climate scenario runs. For key to acronyms, see Table 20.	69

Table 29 Modelled mean % changes in precipitation in 2050s compared to 1979-1999 baseline.....	76
Table 30 Changes in number of cells under water stress	86

Abbreviations and Acronyms

GBM	Ganges-Brahmaputra-Meghna (coarse-scale grid)
FSB	Fine-Scale Bangladesh grid
NWMPP	National Water Management Plan Project
NWPo	National Water Policy
NW	North West (hydrological) Region
NC	North Central (hydrological) Region
NE	North East (hydrological) Region
SW	South West (hydrological) Region
SC	South Central (hydrological) Region
SE	South East (hydrological) Region
EH	Eastern Hills (hydrological) Region
RE	Rivers and Estuary (hydrological) Region
GIT	Groundwater irrigated Thanas
SMAAs	Statistical Metropolitan Areas

1 Introduction

The KAR funded project R8038, CLASIC, was initiated at the end of August 2003, with a planned end date of 30 September 2005. The project was funded under Theme W1 of the KAR Programme; Water Resources Management. The Purpose of the project was:

To adapt models and methodologies to assess water resources availability and zones under water stress (lack of water resource or flooding risks) and their likely change due to global warming in regions of monsoon/tropical climate, with special application to case studies in the Indian subcontinent.

The project originally intended to involve partners from both India and Bangladesh. However, there were problems getting Indian Government approval for staff of Indian organisations to participate jointly with Bangladeshi partners in a project concerned with water resources. Therefore, the project finally involved partners in Bangladesh only. However, because the study region covers all of the Ganges-Brahmaputra-Meghna basins, the project had to take account of transboundary river outflows from India into Bangladesh, and also as far as was possible, of consumptive water usage in India and other upstream countries.

Although the project Purpose above focuses primarily on water resources, the project has also studied climate change impacts upon storm surges in the bay of Bengal, which can affect low-lying coastal regions of India just as severely as those in Bangladesh. Thus, although the project only involves participation by staff from Bangladeshi research organisations as partners, the outputs of the project will have wider relevance throughout other parts of the Indian sub-continent.

Thus, the project has studied the impacts of climate change over the Indian sub-continent on three vulnerable areas:

- water resources in Bangladesh,
- to a lesser extent, upon possible fluvial flooding impacts on Bangladesh, and finally,
- upon storm surge impacts on coastal flooding in the Bay of Bengal.

The study has two main components therefore: the land-based study of water resources and fluvial flooding, and the largely separate storm surge studies in the Bay of Bengal, although both strands of the project require use of the same detailed regional climate change scenarios. The following text describing the need for the project is taken from the original project Scope of Work.

The 1998 flood events in Bangladesh and those of 2000 in West Bengal together with the storm surges of 1985, April 1991 *et al*, were dramatic reminders of the vulnerability of the region and the need for research to help limit the damaging effects of such floods. In addition, the Indian subcontinent has one of the highest population densities in the world and the availability of water resources is crucial for the health and economic well-being of this population. There is thus an “*urgent need to take precautionary steps towards improving the data and knowledge necessary to develop a clearer understanding of the likely implications for the future in Bangladesh*” (Warrick & Ahmad, 1996), a need which is widely recognised by stakeholders and governments in the Indian sub-continent. This is reflected for example by programmes and workshops like the National Water Management plan in Bangladesh, started in 1998, and the IOC/WMO/UNESCO (IHP) regional workshop on storm surges (Oct. 1999), both co-funded by local governments. More recently, a 3-year joint Indo/British research programme on impacts of climate change in India was launched aiming to “*build a comprehensive picture of the possible future of impacts of climate change in India*”. Those examples clearly demonstrate the present lack of solution and evidence for demand on more research in the Indian subcontinent. In particular, there is a need for tools and models for water resource assessment and sea level (storm surge) modelling in those regions, and for developing a range of new climate change scenarios whose scale (temporal and spatial) is consistent with the hydrological modelling. Tackling those issues through climate change impact studies should be undertaken as soon as possible for their results to be incorporated into long-term water management planning.

The need for a better understanding of the complexity of the water cycle in Bangladesh led to the funding of the Flood Action Plan, completed in 1995, which aimed to set a foundation to a long-term programme for achieving a comprehensive solution to the flood problem. This did not address climate change issues, nor possible implications of sea level rise, which were considered in a previous project funded by the Ford Foundation and the British ODA (1993-1994). However, significant advances have been made since then in terms of climate change scenarios, water resource and sea-level modelling capabilities, and such progress must be taken into account in any future long-term planning. That is only partly tackled within the 3-

year National Water Management Plan (NWMP; WARPO, Halcrow, 1999) launched in 1998, whose objective is to formulate a long-term water management programme to the year 2025, and to which EGIS provided a major input. However, this is very specific to Bangladesh, and does not consider India, Nepal and other upstream countries where the lack of water resources or an increase in flooding will have severe implications for such a densely populated region. Other works comprise a 3-year joint Indo/British research programme on impacts of climate change, involving both the Hadley Centre and IITM, focused only on India, and a WMO 5-year project aiming to improve flood forecasting and flood warning caused by sea surges induced by cyclones.

2 Collaboration with partners in Bangladesh

The project was initiated by a planning visit to local partners in Bangladesh by the Project Leader, Frank Farquharson, in late 2002. However, the real start of the project was the launch workshop held in Dhaka on 30th January 2003. This workshop was organised by the local partners, and was very well attended by 87 people from 45 separate organisations. The strong message from participants at the workshop was that many governmental, non-governmental and research groups in Bangladesh were very interested in understanding how climate change might affect their country. The CLASIC project was enthusiastically welcomed by all participants. However, despite there having been an initial visit during 2002, and the launch workshop in January 2003, the contract between DFID and CEH was not signed until the end of August 2003, and the 30 month project ended in February 2006.

In October 2004, project partners from Bangladesh were invited to visit UK partners' sites for two weeks. In addition, the visit presented the opportunity to invite a key stakeholder to the UK to enable them to become more involved in the project. Consequently, CEH were able to invite Mr Abdul Baten from the Water Resources Planning Organisation (WARPO) who has been involved in the drawing up of the National Water Management Plan for Bangladesh. Also present during the visit, were Dr Anisul Haque and Mrs Arpana Datta from BUET and Mr Ahmadul Hassan from CEGIS.

The objectives of the visit were threefold:

- to involve participation in the project by a stakeholder, in order establish confidence in the work that is to be carried out;
- to update each of the partners on the progress of each aspect of the project and plan future activities; and
- to continue discussions and make decisions on the remaining technical work.

Aside from the daily meetings used to address the various technical issues, activities also included a visit to the POL site in Bidston and a seminar at CEH involving presentations by each of the project partners.

The visit was invaluable to the progress of the project, as we are now able to involve WARPO in many of the stages of the technical discussions. Following the visit, Mr Baten agreed to work with CEGIS to provide the future demands scenarios for Bangladesh.

3 Water Resources: Modelling

3.1 Global Water Availability Assessment (GWAVA)

The GWAVA model has been used in many regions of the world, including eastern and southern Africa, West Africa, and the Volga River Basin. The GWAVA (Global water availability assessment) model operates on a gridded basis, using a rainfall-runoff model, determining the water balance in each grid cell. To this, components of the water resources system i.e. storage reservoirs, lakes and inter-basin transfers are added and together with estimates of water demand from agriculture, domestic supply and industry a series of indices of water abundance or availability can be produced. Typically, the model is applied at a resolution of 0.5×0.5 degrees (approximately 55×55 km) a resolution which reflects the compromise between fine scale detail of land cover information and soils across the area of interest, the relatively coarse resolution at which climate data are available and the variable resolution at which population data are available.

3.2 Rainfall-Runoff Model

In the GWAVA scheme, a simple rainfall-runoff model, the probability distributed model (PDM) (Moore, 1985) provides estimates of surface runoff in each cell. The distribution term in the model refers to the statistical distribution of soil moisture stores within the catchment or cell bounded by the maximum soil depth, C_{max} . This approach is analogous to the variable source area concept, in which areas close to the streams and in valley bottoms will generate runoff before upslope areas. Surface runoff is routed through a linear reservoir, whilst drainage is allowed to occur at a rate determined by a baseflow coefficient and subsequently routed through another linear reservoir before emerging into the stream.

The PDM parameters defining the soil store; maximum saturation capacity C_{max} , field capacity, fc and rooting depth, rd are linked to soil texture and an indicative land cover, whilst the parameter describing the distribution of stores, b is one that requires calibration. Other model components include the simple empirical daily interception model of Calder (1990) which provides effective rainfall for the PDM and a simple runoff-routing model.

The subsurface flow is represented on the following equation

$$Q_b = k_b S_b^3$$

where Q_b is the baseflow, k_b is a PDM parameter and S_b is the groundwater storage.

3.3 Routing between cells

Runoff is generated in each cell (local runoff) and having had abstractions removed and returns added is routed along the gridded river network to provide an estimate of total runoff. As the overall model time-step is monthly, routing is only generally important in large shallow basins. The method is based upon the simple Muskingham method which provides a time delay and a degree of dispersion of the flood wave and does not require any physical data. A time delay, in days, can be specified for each cell according to:

$$k = 1.5e^{-D/250}$$

where k is the time delay in days and D , the difference in average elevation between cells (in metres).

3.4 Glacier and Snow Model

A significant proportion of the flow arriving in Bangladesh is from glacial and snowmelt originating in the Himalayas. In order to capture these aspects of the hydrological cycle, the glacier model specifically designed for the Himalayas by Rees and Collins (2004) and the snow-pack model by Bell and Moore (1999).

Identified mountain cells were sub-divided into 10 equal-height elevation zones. The distribution of cell area between zones was according to the General Pareto Distribution whose shape and scale parameters were defined by the mean, minimum and maximum elevation of each 20 km cell, as described by the USGS HYDRO1k digital elevation model (USGS, 2001).

The daily temperature in each elevation zone, T_i , was calculated by adjusting the cell's mean daily temperature, T_{mean} , (at the cell's mean elevation, z_{mean}) according to a temperature lapse rate model:

$$T_i = T_{mean} + \alpha(z_{mean} - z_{mid})$$

where z_{mid} is the mid-elevation of the band and α is the temperature lapse rate, which was assumed to have constant value of -5.5 °C/km. Precipitation was assumed to be uniformly distributed across a cell.

For each zone, precipitation is considered to fall as snow whenever the daily temperature of the zone was less than a threshold temperature of 2 °C (T_{snow}). Melting begins when the temperature rises above 1 °C (T_{melt}) at an assumed rate of 4 mm/°C/day (the degree-day-factor for snow, DDF_{snow}). The values assigned to the parameters T_{snow} , T_{melt} , α and DDF_{snow} are consistent with those published elsewhere (viz. Singh and Singh 2001).

The snow-pack model conceptualizes the snow storage in a zone as a “dry” and “wet” store (Bell and Moore 1999). New snow is added to the dry-store, while the wet-store receives water directly as rainfall and as melt from the dry-store, if the daily temperature is above T_{melt} . Meltwater is released from the zone at a rate proportional to the volume of water in the wet-store.

The regional glacier-melt model developed by Rees et al (2004) represents meltwater contribution from many glaciers in a semi-distributed manner. The model assumes that the meltwater contribution from a glacier can be adequately modelled by representing the glacier generically, with an idealised shape and depth. In this study, all glaciers that contribute runoff to an individual cell (i.e. those whose snout falls within the cell) were considered as a single “generic glacier” for that cell (Figure 1). The area of contributing glaciers (i.e. the area of the generic glacier) was obtained from the Digital Chart of the World (ESRI, 1993).

The minimum and maximum elevations of each generic glacier were determined as the minimum and maximum elevations, respectively, of all contributing glaciers, derived from the HYDRO1k DEM. Each generic glacier was subdivided into 20 elevation bands, with the area of ice in each band defined according to a pre-defined shape profile that was considered to

typify how ice-area varies with altitude in the Himalayas. A triangular depth profile was assumed, with a nominal minimum depth of 20 m (water equivalence) set at both extremes and a maximum thickness set at three-quarter distance up the glacier (at band #15). The maximum thickness varied linearly up to a maximum of 500m according to the glacier's area: an assumption based on a previous study of glacier depths (Liu and Ding 1986).

As with the snow-pack model, daily precipitation and temperature are used as inputs to the glacier-melt model. The mean daily temperature in each elevation band is calculated from the cell's mean temperature, using the previous temperature lapse rate model. Ice-melt from an elevation band occurs only when no more snow is present in the band and is calculated using an assumed degree-day-factor of 8 mm/°C/day for ice.

The ice-depth and the ice-melt store in each ice-band are updated daily. At the end of each calendar year, the total volume of snow remaining in the dry snow-store of all elevation bands is redistributed evenly as ice across all bands. Glacier retreat is represented by the depletion of ice-depth from a band. Once the ice-depth in an elevation band has depleted to zero, no further ice-melt originates from the band and any subsequent snow-melt, or rainfall, generated from the band is added directly to the total glacier runoff.

The total volume of runoff from all bands is calculated daily and expressed as a uniform depth of runoff, Q_g , in mm, over the area of the cell. Together with the daily runoff from the glacier-free part of the cell, Q_s , the total daily runoff, Q , for the cell is calculated by:

$$Q = Q_g + (1 - P_{ice}) \cdot Q_s$$

where P_{ice} is the proportion of the cell initially covered by ice.

.

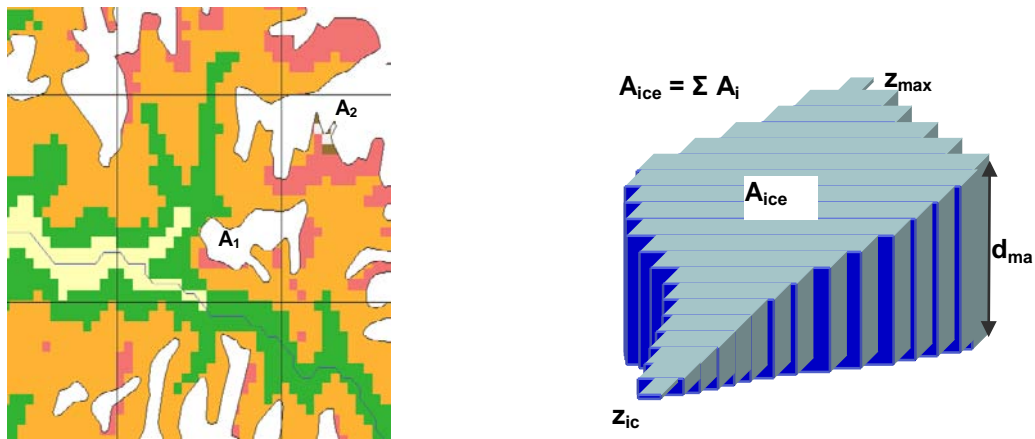


Figure 1 Schematic representation of glacier model: (a) glaciers from DCW (2000) (b) simplified representation of glacier

3.5 Model Resolution

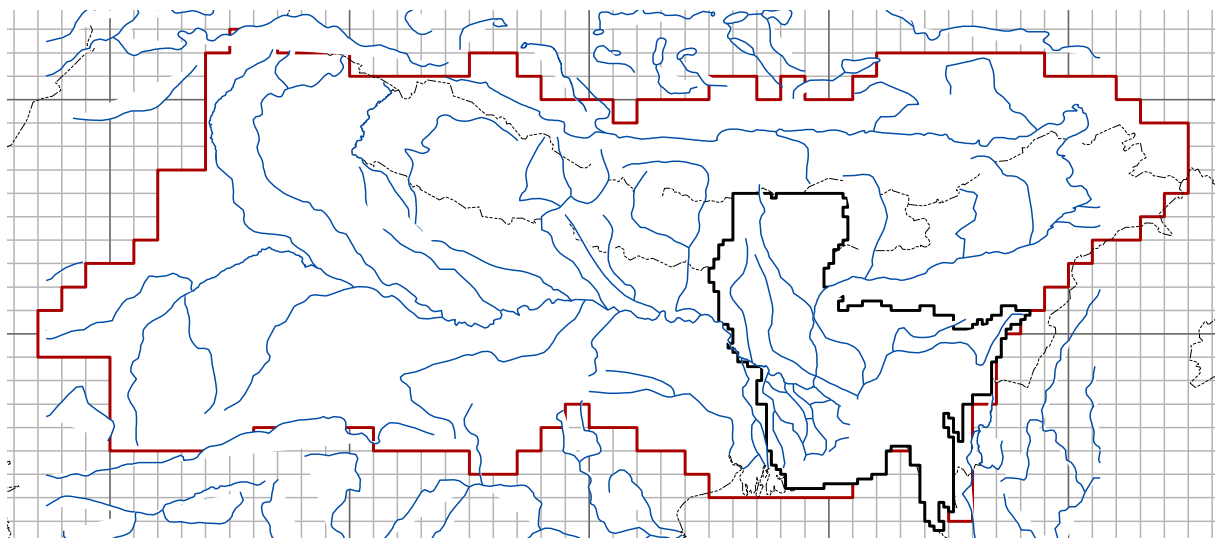


Figure 2 Representation of grid resolution for GBM and FSB model

In the past the GWAVA model has been used on a multi-national scale encompassing many countries at a time. In CLASIC, one of the main focuses has been to make the scale of the results of the simulation process more relevant to the water planner. Therefore the modelling process has been separated into two interlinked approaches (see Figure 2):

1. coarse-scale model at 0.5×0.5 degrees resolution representing the whole of the Ganges-Brahmaputra-Meghna Basin (GBM)
2. fine-scale model at 0.1×0.1 degrees resolution representing Bangladesh (FSB)

The resolution of the FSB model was chosen through a compromise between being able to capture each of the municipal planning organizations (MPO) (see Figure 3), the resolution at which data can be gathered and the validity of the model at a fine resolution.

As the FSB is located at the downstream end of the GBM, there are no feedback processes from the fine-scale to coarse-scale grids. Therefore it is possible to conduct the simulations of the different models independent of each other. Once a GBM run is carry out, the resulting flows are used as the boundary condition which are then fed directly into the fine-scale grid.

In order to minimize the number of points which the coarse-scale flows would enter the fine-scale model, the fine-scale grid was extended outside of Bangladesh to capture trans-national river basins. Two sites were chosen at which the coarse-scale flows are transferred to the fine-scale grid: at Farakka Barrage and at Bahdurabad where gauging stations are also located.

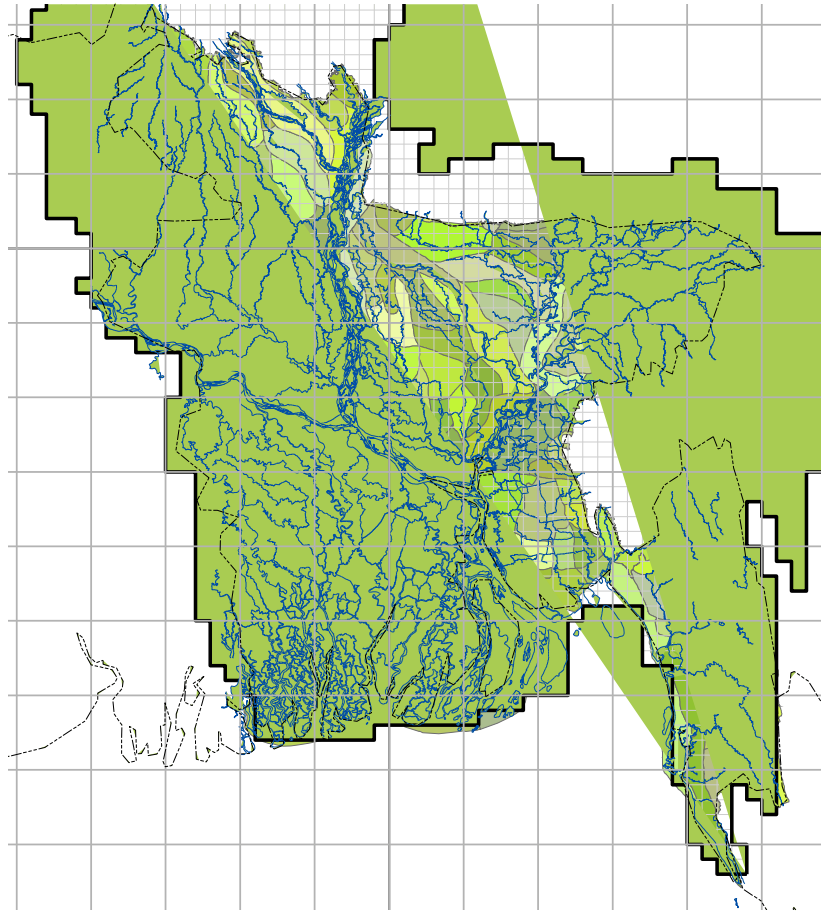


Figure 3 Fine-scale grid showing MPOs and Bangladesh river system

Flooding is a recurring phenomenon in Bangladesh major part of which formed by floodplain. Flooding has many beneficial socio-economic and environmental roles since it recharges soil storage, wetlands and groundwater and performs ecological functions. On the other hand damages caused by occasional large floods is a major concern. The main cause of flooding in Bangladesh is the spilling of rivers due to inflow generated by rainfall at upper part of catchment. Flooded area will be predicted for the model generated peak discharge. The methodology was developed by CEGIS by relating the flooded area with the river water level at representative locations.

3.6 Water Availability Indices

The GWAVA model can be used to generate synthetic streamflows which enable impacts to be explored on the development within areas of the basin on the regime entering the delta. Comparisons on a cell by cell basis, of water yield and demands provide maps showing areas where, for example, water supplies may be insufficient. The comparison can be made in different ways, the simplest (Type 1 Index in GWAVA) being to divide the annual volumetric water yield by the annual volumetric demand, however this does not capture the seasonal or inter-annual variation in water demand and supply. A second method (Type 2) calculates the actual supply available for use, estimated as the driest month in each year which occurs with 90% reliability. This is compared to the minimum monthly demand i.e. assumes demands are constant throughout the year.

Two further indices were developed. The Type 3 index for surface water is found by calculating the 90% reliable flow for each month of the year separately, rather than calculating a single value based on the driest month in each year. The index is then the minimum (over all months in the year) of this value minus the demand in the same month. This index reflects the critical point in the year whether or not there are variable irrigation demands. The index is expressed as a volume, with positive values indicating an excess of supply over demand and negative values a shortfall. An advantage of this index is that it helps to distinguish area where demands are large and there is a large shortfall (for instance) from those where both supply and demands are small and therefore the shortfall is small. Thus, areas of large scale water availability problems are picked out from those where the problems are relatively small scale.

A fourth index was also developed so that results could be expressed as a ratio which ranges from -1 (negligible water available to meet demand), through zero (available water meets demand), to 1 (available water exceeds demand).

The range of water availability indices considered is shown in Table 1.

	Index	Definition
Surface water only	SWAI-type 1	Total annual runoff / Total annual demand
	SWAI-type 2	90% reliable driest month runoff / Minimum monthly demand
	SWAI-type 3	Minimum over all months of: (90% reliable monthly runoff – Demand for that month)
	SWAI-type 4	(SWAI-type 3) / (90% reliable monthly runoff + Demand for that month)
Ground water only	GWAI-type 1	Annual groundwater yield / Total annual demand
	GWAI-type 2	Minimum monthly groundwater yield / Minimum monthly demand
	GWAI-type 3	Minimum over all months of: (Monthly groundwater yield – Demand for that month)
	GWAI-type 4	(GWAI-type 3) / (Monthly groundwater yield + Demand for that month)
Com-bined	TWAI-type 1	(Total annual runoff + Annual groundwater yield) / Total annual demand
	TWAI-type 2	(90% reliable driest month runoff + Minimum monthly groundwater yield) / Minimum monthly demand
	TWAI-type 3	Minimum over all months of: (90% reliable monthly runoff + Monthly groundwater yield – Demand for that month)
	TWAI-type 4	(TWAI-type 3) / (90% reliable monthly runoff + Monthly groundwater yield + Demand for that month)

Table 1 Summary of water availability indices

4 Water Resources: Data

A variety of physiological and human data-sets are required by the model in order to simulate the hydrological processes as well as to assess the availability of water to meet demand. Figure 4 gives an indication to the size of the database required for a simulation run. Because of the size of the region and the resolution of the fine-scale grid, the data collation and generation has been extensive exercise.

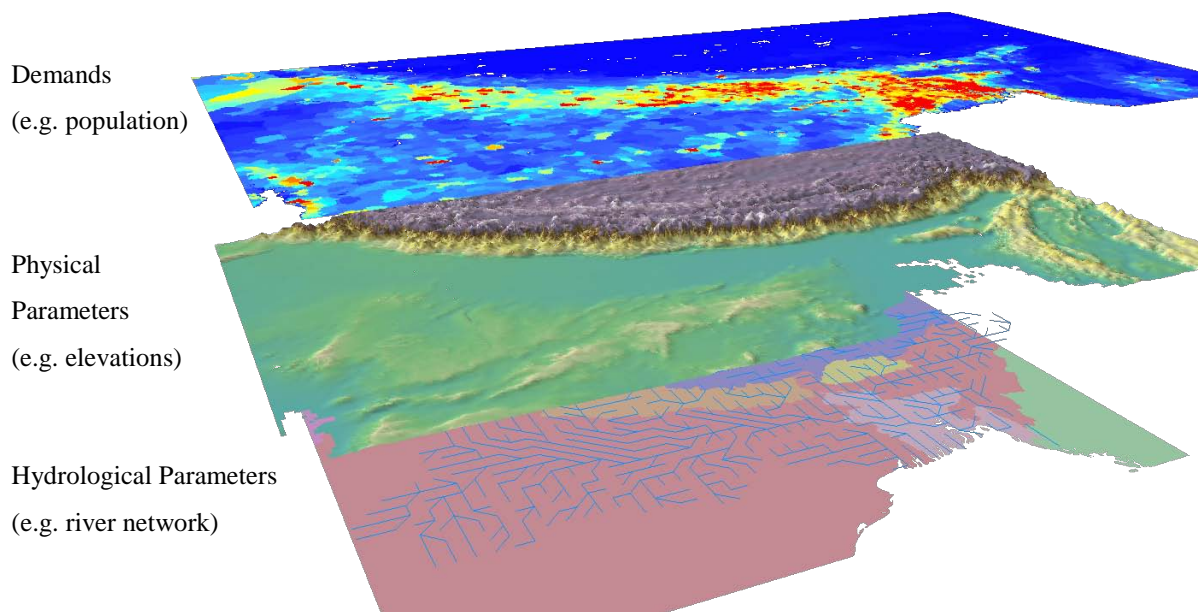


Figure 4 Structure of database used in GWAVA

For the GBM model, which represents the whole of the Ganges-Brahmaputra-Meghna Basins, most of the data has been retrieved from publicly-available resources. There are problems associated with collating data from certain regions in the GBM, as some data are politically sensitive and likely to be unreliable. Data such as irrigation abstractions are very difficult to obtain and therefore methodologies to combat this lack of knowledge have been developed.

Local data sources and knowledge has been used to populate the database for the fine-scale grid. This part of the work has been particularly labour-intensive as most of the data is not available in digitised format.

In the following section, a brief summary of the data requirements, their sources and the techniques used to convert them into a usable form is presented.

A large component of the work has been to build the database required by GWAVA for the input data. This data ranges from physical parameters such as soil type, land-use type and topography, to demands statistics such as population numbers, irrigation abstractions and reservoir operations.

4.1 Physical Parameters Data

Drainage Directions – GBM Model

The GBM grid was based on and Siebert *et al* (2001) who based their work on Hydro1k drainage maps produced by USGS (2001). These drainage directions were checked using Jet Navigation and Pilot Charts and altered accordingly, particularly around the Himalayan region. Using local expertise and comparisons with known catchment areas, the drainage directions were updated. The final drainage map is presented in Figure 5.

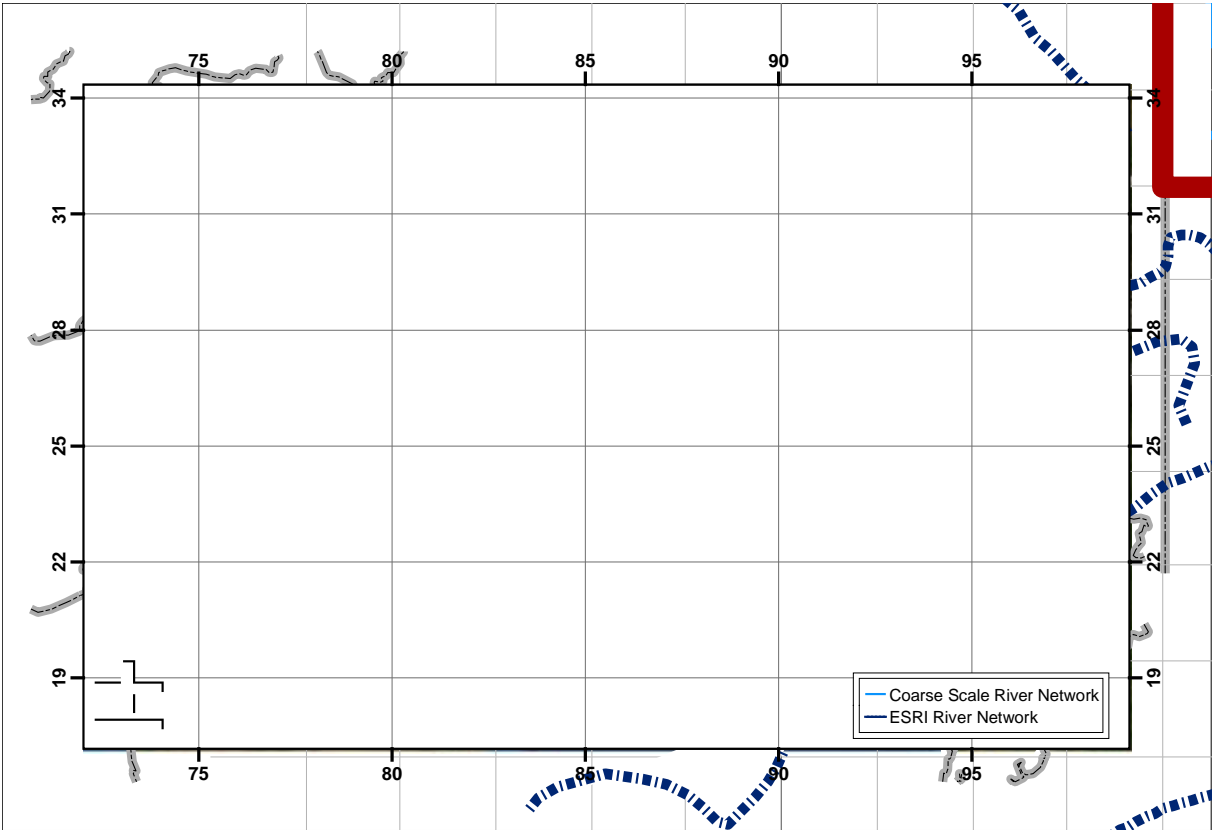


Figure 5 Drainage network of GBM model

Drainage Directions - FSB Model

The FSB model area has been covered by a network of 2317 grid cells of resolution $0.1^{\circ} \times 0.1^{\circ}$ (see Figure 6). The size of a grid cell is approximately 11km x 11km. The grid network was extended beyond the borders of Bangladesh in order to capture the catchments of trans-boundary rivers other than two large rivers, the Ganges and the Brahmaputra. This minimizes the number of points at which the boundary condition data are to be obtained from the GBM model. River water withdrawal/diversion by water control structure (e.g. pump station and barrage) at a cell has also been represented in the model.

The cell to cell drainage directions were set by over laying maps of grid network, elevation contour and river system. The contour map was based on digital elevation model of 300m x 300m resolution. The river system map provided guidance regarding drainage pattern in the complex Ganges-Brahmaputra-Meghna delta having inter-connected river network and very small slope. Topographic information on the area outside of Bangladesh was obtained from Tactical Pilotage Charts published by the Defence Mapping Agency Aerospace Center, USA.

A deltaic characteristic of the drainage system is the presence of distributaries of the main rivers. There are 13 grid cells where discharge ratios have been specified in order to calculate divisions of flow between the main river and its distributary. The discharge ratios are functions of month and have been estimated by analyzing available data on river cross-sections, local bed slope and bed resistance. Some of the oftakes of the distributaries become dry if the flow in the main rivers drop below certain magnitudes.

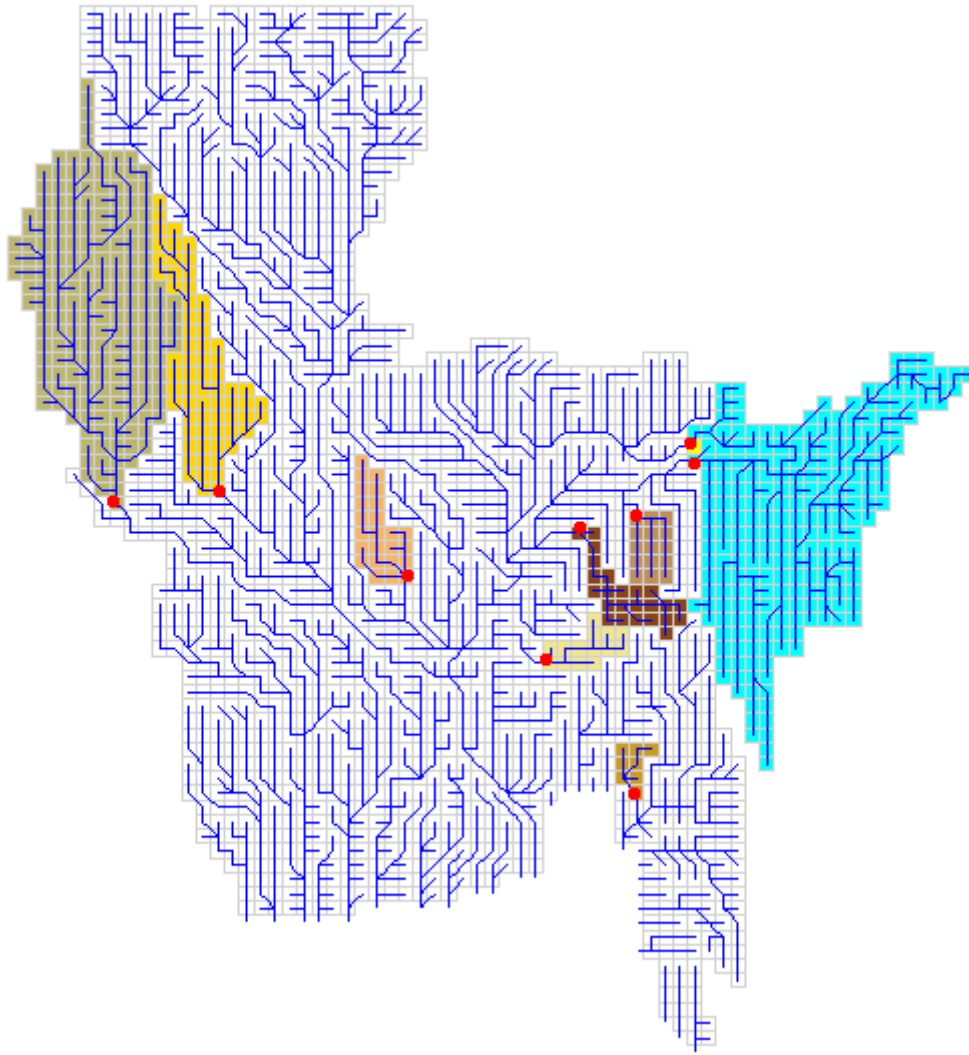


Figure 6 FSB model drainage network and calibration catchments and gauge stations

Field and Saturated Capacities using Land Use Data and Soil Textures

Land use and soil texture data were combined to calculate field and saturated capacities required by the PDM. Dominant soil texture classes were calculated from the *FAO Soil Map of the World* (FAO, 1995) for areas outside of Bangladesh.

Within Bangladesh, local information was used: The Bangladesh Agricultural Research Council (BARC) have developed a database, known as the Agro ecological Zone (AEZ) database system of Bangladesh, which was based on reconnaissance soil resource information generated by the Soil Resources Development Institute (SRDI). The Land Resources Inventory (LRI) database was developed by SRDI was not geographically referenced. The AEZ database under land resources inventory (LRI) has derived detail classification of soil

texture are given in Table 2. From the table, the soil structure information was converted to GWAVA soil classes as shown in Table 3.

Soil association spatial data layer representing the whole Bangladesh by dividing it into 1049 polygons having different identifying codes called as ‘AEZCODE’ with the information of various important characteristics of soil were prepared by SRDI. The soil association data were digitized under the AST (Agriculture Sector Team) project in SPANS format. Later FPCO (1993) converted the soil association data into Arc Info GIS format. The digitized soil data was converted to 0.1 degrees grid scale. Some grid cells contain soil texture from two or more polygons. Hence dominant soil texture class in a grid cell was determined after conversion of soil data to fine scale grid.

The fractions of sand and clay in each soil texture class were then calculated using Saxton *et al* (1986).

AEZ Code	Description	AEZ Code	Description
0	Mixed	11	Silt Loam
1	Sand	12	Gravelly Clay Loam
2	Loamy Sand	13	Silty Clay Loam
3	Loamy Fine Sand	14	Clay Loam
4	Sandy Loam	15	Silty Clay
5	Fine Sandy Loam	16	Clay
6	Very Fine Sandy Loam	17	Mucky Clay
7	Gravelly Sandy Clay Loam	18	Muck
8	Sandy Clay Loam	19	Peaty Muck
9	Loam	20	Peat
10	Silt		

Table 2 Soil classes according to AEZ database

GWAVA soil ID	Soil Texture	AEZ texture code
1	sand	1,2,3
2	sandy loam	4,5,6
3	silt loam	9,10,11
4	clay loam	7,8,12,13,14
5	clay	15,16,17
6	others	0
7	organic	18,19,20

Table 3 GWAVA soil classes from AEZ soil classes

There are four land use types currently used in GWAVA, of which the data was obtained from the *Global Land Cover Characteristics Database* (USGS, 2005) for areas outside of Bangladesh (see Figure 7). In order to make use of this publicly available dataset, the data has previously been translated into 12 universal land cover types. This was then translated to six classes: bare soil, grass, shrub, tree, water and wetland for use in GWAVA (see Table).

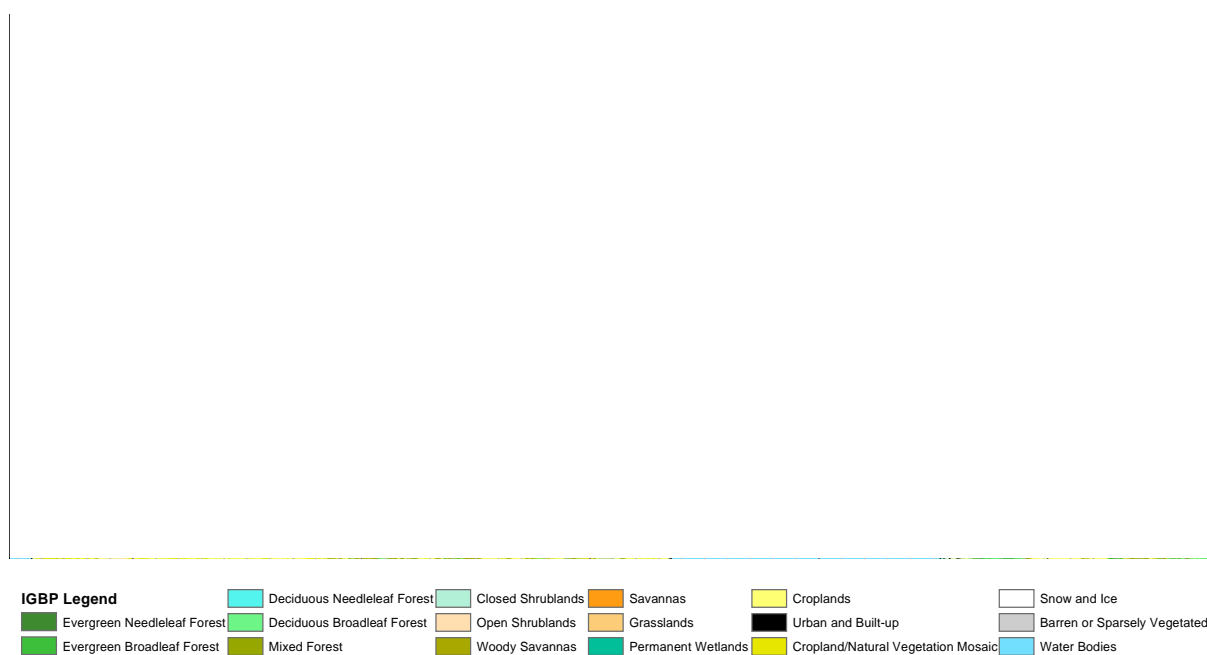


Figure 7 Global land cover characteristics for GBM area

For the fine scale region within Bangladesh, land use data in the National Water Resources Database (NWRD) are based on SPOT 89 image, LANDSAT 97 image and IRS 98 image. Topographic maps collected from Survey of Bangladesh (SoB) and Irrigation map collected

from Bangladesh Water Development Board have also been used to update the data layer. The land use map provided by CEGIS is shown in Figure 8. Digitised land use maps were converted to 0.1 degrees grid scale. Agricultural land, deciduous forest, mangrove forest, tea, orchard, homesteads, water bodies, etc. are major land uses of Bangladesh, almost 65% of which is agricultural land. These land uses are divided into six classes for use in GWAVA model. The croplands, village homesteads are considered as grasses and shrubs respectively.

The field and saturated soil capacities for each rooting depth in each soil texture class were then calculated using Vörösmarty *et al* (1989). The resulting capacities can be found in Appendix C.

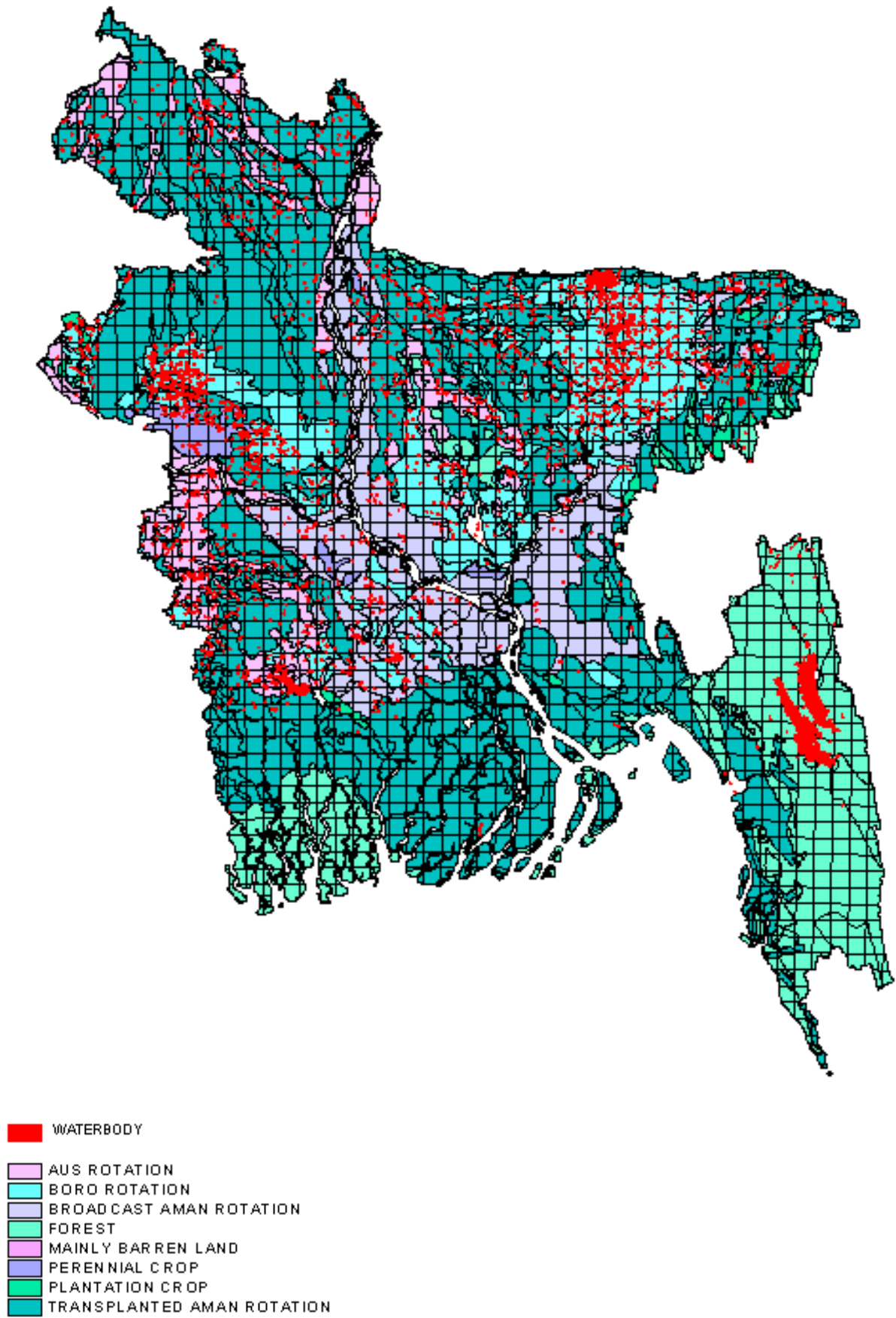


Figure 8 Major land uses of Bangladesh

Mountain/Glacier Cells

The mountain and glacier cells had to be identified in order to mark the cells in which snow and glacier melt module is to be activated.

Cells in which snowmelt occurs are identified by marking cells that have a mean elevation greater than 2000m above sea level. As the drainage network from Döll and Lehner (2000) was based on USGS (2001), the Hydro1k digital elevation model (DEM) was used to determine the elevations required for the snowmelt/glacier cells.

Glaciers were identified, categorised and their features calculated according to the procedure described in Section 3.4. However, in addition to the Digital Chart of the World (DCW) and for consistency, the USGS (2005) Global Land Cover Characteristics (GLCC) dataset was also used (see Table 4 for a comparison of the glacier characteristics)

Data Source	No. of Glacier Cells	Total Glacier Area (km ²)
GLCC	143	25,519
DCW	65	33,546

Table 4 Comparison of glacier characteristics

There are distinct differences between the two datasets, with the total glacier area differing over 20%. For consistency, it was deemed appropriate to use the GLCC dataset in line with the soil capacity calculations detailed above.

Reservoir Information

There is only one reservoir in Bangladesh, at Kaptai, Chittagong which is used for hydro-power generation. Reservoir operation data were extracted from Noman (1997).

4.2 Water Demands

The fundamental difference between GWAVA and all other hydrological models is the inclusion of the anthropogenic influence on the hydrological cycle. Although net consumption of water may only account for a very small percent of water during the monsoon season, it is the spatial and temporal variations of supply and demand during the seven month dry season that are of interest to water planners, policy makers and various stakeholders alike. This section describes the various types of data used to calculate demands for the GBM model according to the GWAVA formulation. Human and livestock populations are required for each model cell to estimate domestic water use. Water demand for irrigation and industry are also required.

Note that the methods described below at the coarse-grid resolution, was also applied at the fine-grid resolution for regions outside of Bangladesh.

Total/Urban/Livestock Populations

In order to make use of all data that is available in the public domain, a methodology was required to convert national statistics to spatially-distributed GIS data. The total, urban, rural and livestock populations were all calculated using very similar methodologies:

- Obtain spatially-distributed data
- Resample the data according to required resolution
- Calculate total value for each country using the appropriate country masks, e.g. for Gridded population of the world, the GPW country masks were used. A mask of each country was then re-sampled at the required resolution. At the boundaries, a percentage area was used to represent the country in that cell.
- Apply factor to spatially-distributed data that will bring the total value in line with the national statistic for each country.

For each cell:

$$f_{GPW}^{UNDP} = \frac{Population_{total}^{UNDP}}{\sum_{mask} Population_{total}^{GPW}}$$

$$Population_{total} = Population_{total}^{GPW} \times f_{total}^{UNDP}$$

Sum all population data for all countries to produce regional map of values.

This method is similar to that described in Gaffin *et al* (2004) for GDP calculations and is illustrated in Figure 9.

A similar approach was also used to determine the urban population. However, the method was altered slightly in order to make use of the spatially-distributed rural population dataset from FAO (2001). The GPW and FAO total population datasets are not identical and so instead of using the FAO rural population directly, the urban population was determined by firstly normalising the rural population data with the total population, thereby creating a grid of rural population fraction. This was then multiplied by the GPW total population grid, i.e.

For each cell,

$$Population_{rural}^{GPW} = \frac{Population_{rural}^{FAO}}{Population_{total}^{FAO}} \times Population_{total}^{GPW}$$

The FAO total population set was not used directly as it was found that the GPW datasets agreed better with the FAO/UNHABITAT national statistics.

Data Source	Total Population (1000's)
UNHABITAT	109,466
UNDP/FAOSTAT	109,402
FAO (2001) at 0.5°	87,356*
GPW grid at 0.5°	106,456

* based on LandScan Global Population Database 1998, version unknown.

Table 5 Total population of Bangladesh in 1990

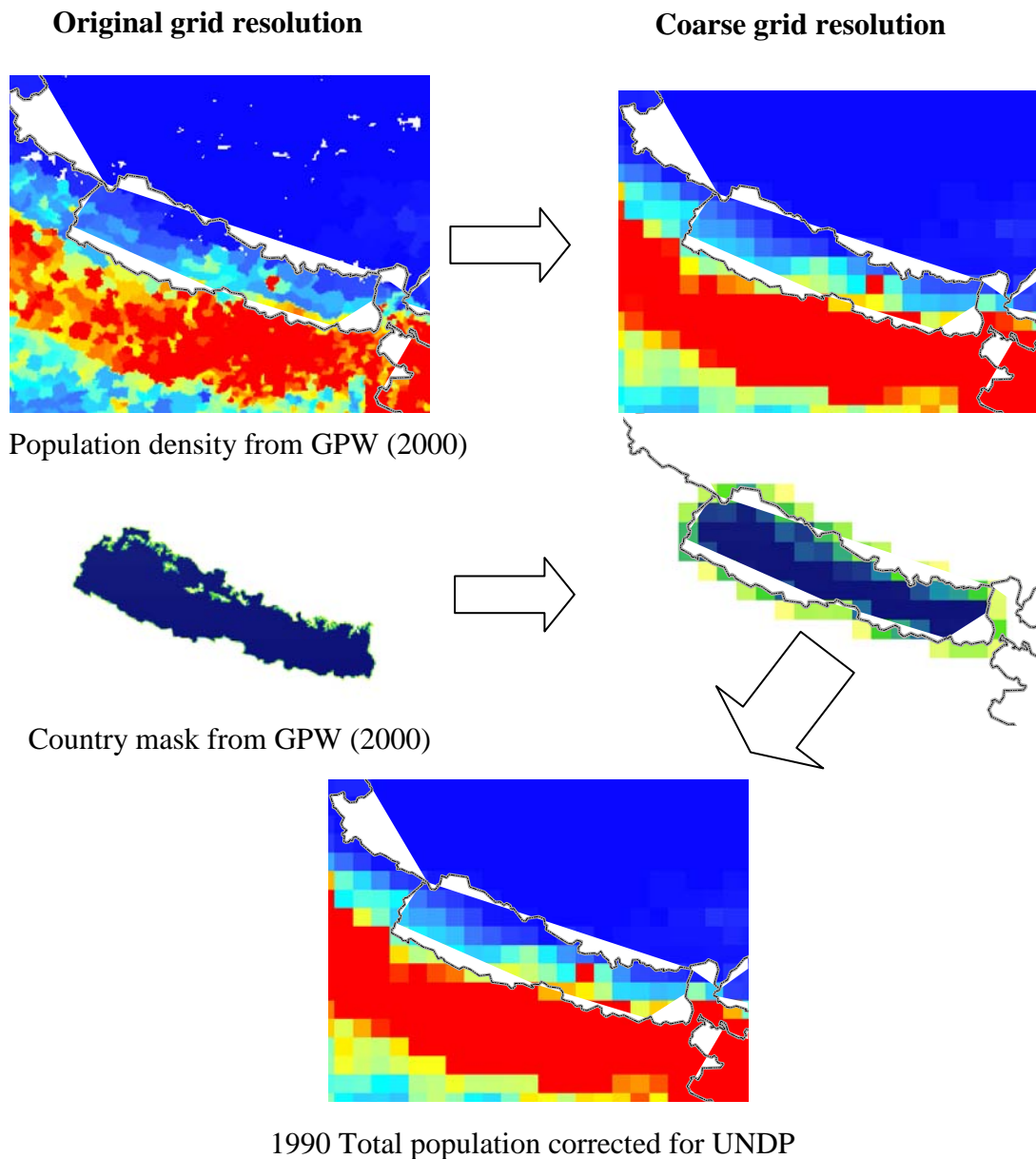


Figure 9 General methodology for correcting raster datasets using country-specific data

For the FSB model within Bangladesh, Thana wise total and urban human population data were obtained from NWRD at WARPO. Thana wise livestock population was in hard form. Manual entry of these data made from BBS (1998). CEGIS digitized the Thana map and converted it to 0.1 degrees grid scale. Some grid cells contain some parts of two or more Thanas. So total human population in a cell is the sum of population provided according to the percentage of a Thana in that cell. The urban and livestock population were also given in each cell using the same procedure. Urban and rural water demand as well as livestock water demand data were obtained from Ahmed and Rahman (2000).

Industrial Water Use Data

The industrial water use was based on the urban population distribution and calculated in a similar way to the total population. Industrial water use data in each hydrological region were extracted from NWRD of Bangladesh. The digitised regional map of Bangladesh was converted to 0.1 degrees grid scale to obtain industrial water use in a grid cell.

Irrigation data – Outside of Bangladesh

A combination of methods was used to determine the irrigation water use, due to the lack of cohesive information from all the countries represented in the Ganges-Brahmaputra basin. For Bhutan, Nepal and the Tibetan plateau, little crop data was found for resolutions less than country-wide. However, as the irrigation water use is relatively low in comparison to that along the Ganges, resolutions at a national scale are not expected make a significant impact.

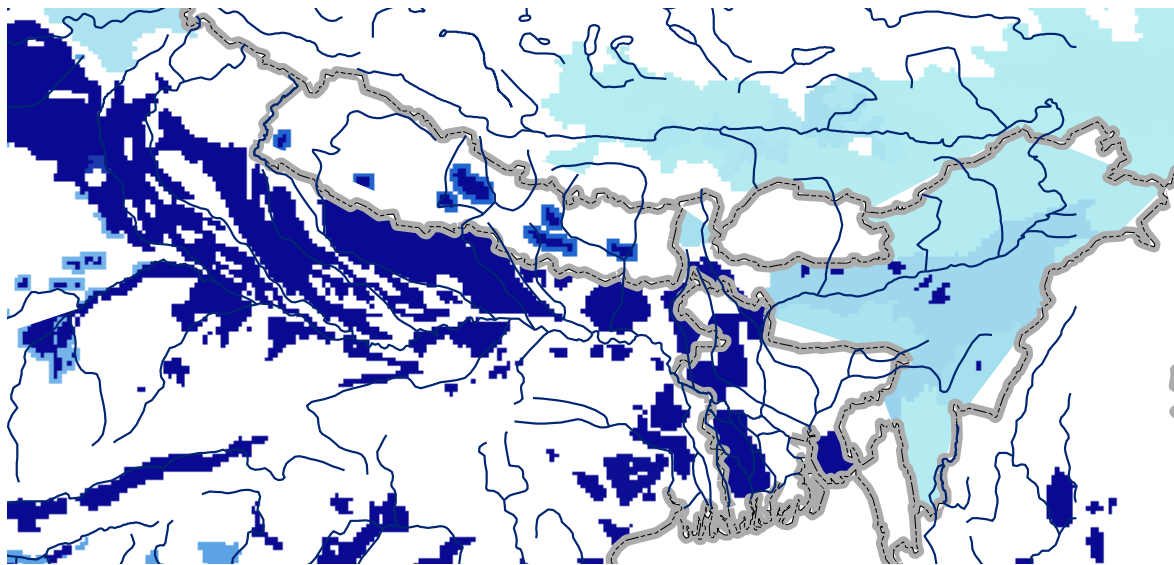


Figure 10 FAO Global map of irrigated areas (GMIA), where darker blues indicate greater fraction of irrigation in cell

The majority of the river basin is located in India, for which a lot of agricultural data on a state-wise scale is available from DES (2004).

The Global Map of Irrigated Areas (GMIA) (see Figure 10) was used as a basis to locate and size the irrigation schemes. Superimposed onto this information, crop data on a national scale

was used for Bhutan, Nepal and Tibet from FAOSTAT, and state-wise statistics for India from DES (2004). The distribution of this crop data was then determined using Ramankutty and Foley (1998), an example of which is shown in Figure 11.

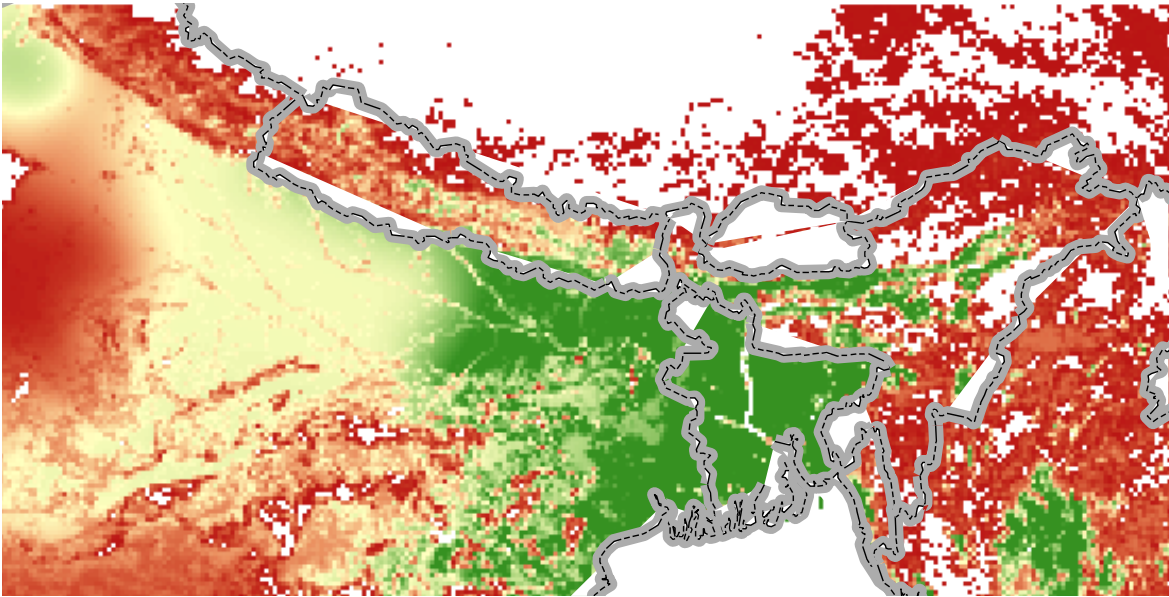


Figure 11 Distribution of rice in 1992 from Ramankutty and Foley (1998). Greener areas have a greater fraction of rice and redder areas less.

The method used was similar to the population calculations using the GMIA as the spatial distribution and the FAOSTAT/DES (2004) information as the national/state-wise statistic

For each cell,

$$\text{Irrigated Area}^{GMIA} = (\text{Irrigated Fraction}) \times \text{Cell Area}$$

$$\text{Irrigated Area}^{FAO/DES} = \frac{\text{Irrigated Area}^{FAO/DES}_{country/state}}{\sum_{mask} \text{Irrigated Area}^{GMIA}} \times \text{Irrigated Area}^{GMIA}$$

where

GMIA	- Döll and Lehner (2001)
FAO	- FAOSTAT (2005)
DES	- DES (2000)

Irrigation data – within Bangladesh

For the FSB model within Bangladesh, the irrigation scheme of the country is divided into two: major irrigation and minor irrigation. Major irrigation projects provide mainly supplementary irrigation in the monsoon season while minor irrigation is for the dry season.

The digitised map of major irrigation projects was obtained from CEGIS. The major irrigation project data layer has been captured from the published maps (prepared by ECDS) of 1991 at 1:50,000 scales. The digitisation has been done under Arc/Info GIS environment volume wise and then all the coverage has been appended for making national level data layer. After data capturing, map features were adjusted manually with respect to the river database (captured from LANDSAT 97 with 30m resolution). The attribute information derived from BWDB has been incorporated to the spatial data layer. Manual editing has also been done using the river, Thana boundary and road data layers of National Water Resources Database (NWRD). The digitised map was converted to 0.1degree grid scale and irrigation water use in a cell was obtained according to percent of project area in a grid cell.

Water withdrawal was calculated considering hydraulic structures such as pump station and barrage and number of irrigation equipments such as Shallow Tube Wells (STW), Deep Tube Wells (DTW) and Low Lift Pumps (LLP), their capacities and operating hours. Minor irrigation data were not in digitised form. Manual entry of this data was made from survey report on minor irrigation (BADC, 2003). Thana-wise minor irrigation data were converted to 0.1 degrees grid scale and the percentage of a Thana in a cell was determined. Irrigation water use in a Thana was calculated considering the number of irrigation equipments (LLP, DTW, STW etc.), their capacities and operating hours. Cell-wise major and minor irrigation water use were summed to obtain total irrigation water use in a cell.

Information on cropping patterns in each fine grid cell was obtained using digitised agricultural land use maps of Bangladesh. The digitised soil map of SRDI, as mentioned earlier, was linked to the LRI database to produce different national outputs including agricultural land use maps. Further SRDI produced GIS based agricultural land use maps in 1:100,000 scale. The digitised agricultural land use map was converted to a 0.1 degrees grid to get the crop pattern in each grid cell. Decadal crop coefficients for calculation of

evapotranspiration were provided by MPO (1987).

Surface Water to Ground Water Use

Total surface or total ground water use is the sum of water used for irrigation, industrial and domestic purposes. Irrigation water use for each cell from two sources were determined considering major irrigation and minor irrigation projects as mentioned in the previous section. Industrial water use from two sources was extracted from NWRD of Bangladesh. Domestic water use from two sources was estimated using a database of water supply of Bangladesh (DPHE, 1998; DPHE, 2002).

Future Water Demand – Outside of Bangladesh

To determine the effect of the changing climate on water resources, it is also necessary to include the effects of socio-economic changes. Two future horizons, at a timescale relevant to water planners were looked at: 2025 and 2050.

Future water demands scenarios were developed using future population data from various sources. The spatial variation was assumed to be the same as that of the baseline. The annual increase rates were assumed to be the same between 2000-2025 and 2025-2050 and based on the increases given in UNPD (2005). The result of the exercise is presented in Table 6. These values were then used in the procedure described in the previous paragraphs on a country-by-country basis to produce a spatially-varying map of population.

Country	Rural Population (000s)		Urban Population (000s)	
	2025	2050	2025	2050
Bangladesh	134,085	133,821	74,183	86,500
Bhutan	3,061	3,220	640	810
China	618,089	572,903	836,052	886,962
India	852,105	830,525	517,178	586,052
Nepal	27,943	28,764	9,888	11,976

Table 6 Population data for each country for baseline and future horizons

Industrial demands have been set arbitrarily to 25% of the urban demand and 50% of the urban demand for the low and high scenarios respectively. Water consumption per head was also developed for two different scenarios as presented in Table 7.

	Rural	Urban	Special Urban
Baseline	25	60	140
Low scenario	50	140	200
High Scenario	75	190	250

Table 7 Water Consumption per head (l/head/day)

Changes in livestock populations were calculated as a function of the change in rural population for each country following Meigh *et al* (1998), as no forward projections of livestock populations could be found. The relationship between rural population and livestock changes was determined by fitting a linear function for quinennial changes provided by UNPD (2005) and FAO (2005) respectively. The result of these calculations is presented in Table 8.

Country	Bovine Population (000s)		Small Rudiments Population (000s)	
	2025	2050	2025	2050
Bangladesh	26,980	26,629	45,151	43,952
Bhutan	410	420	73	76
China	92,064	89,608	215,142	203,496
India	208,607	204,094	211,894	202,576
Nepal	8,007	8,188	9,385	9,826

Table 8 Future livestock population

The combination of all these factors is presented in Figure 12, where the annual water demand is presented. As noted previously, agriculture is the main user of water in the catchment and the areas of high water demand in Figure 12 follow that of the irrigated areas.

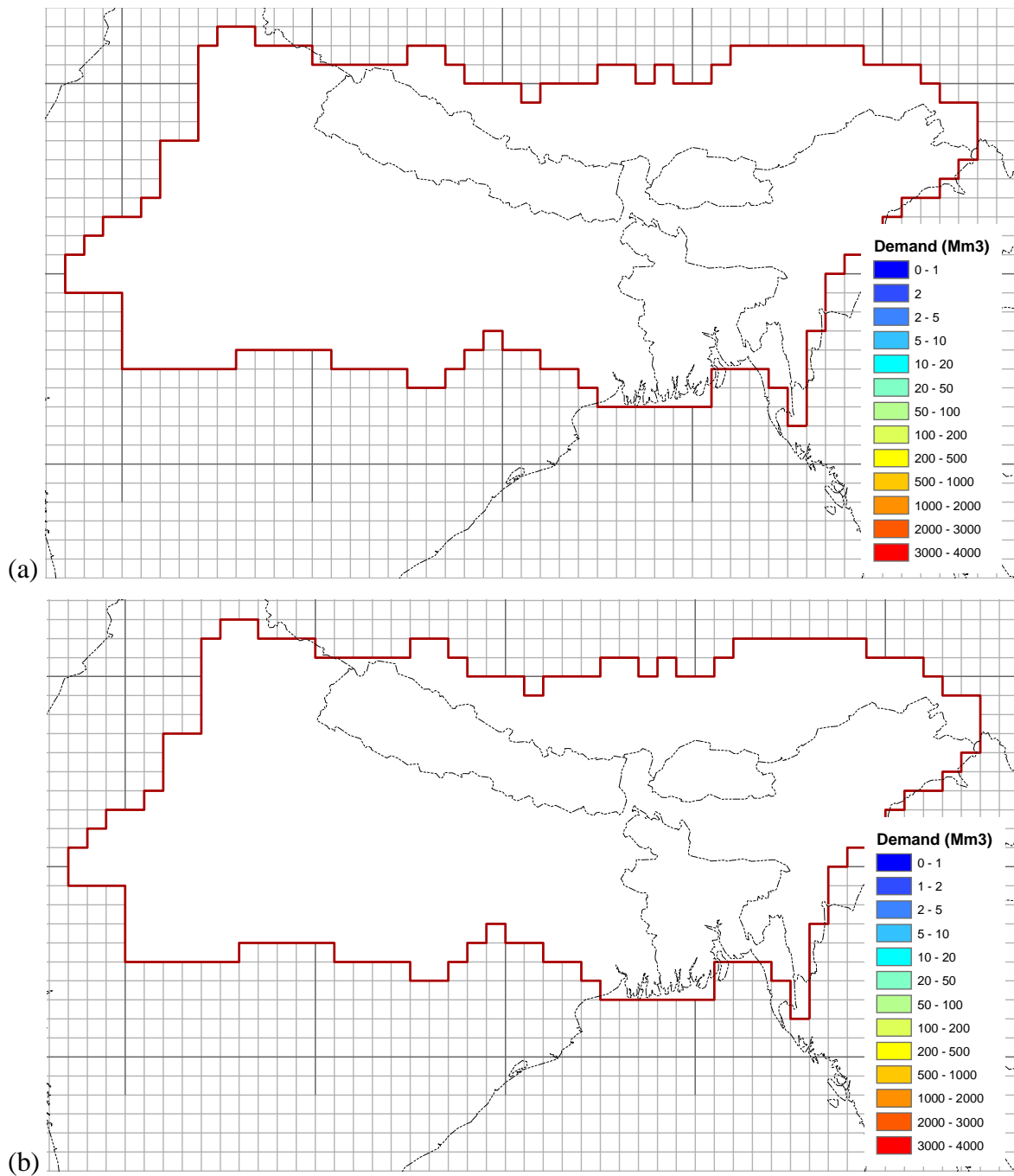


Figure 12 Annual water demand for GBM (a) Baseline (b) 2050 High Scenario

Future Water Demand within Bangladesh - National Water Management Plan

National Water Management Plan Project (NWMPP), 2000 has estimated water demand of different regions of Bangladesh in various sectors. The water demands are described according to sources as follows.

SURFACE WATER DEMAND

In NWMPP, surface water demand is calculated in different sectors such as in-stream water demand, irrigation demand, rural and urban water supply.

a) *IN-STREAM WATER DEMAND:*

As noted in the National Water Policy (NWPo), meeting in-stream demands is the priority call on surface water. These demands have been summarized in Table 9 below by region.

	NW	NC	NE	SW	SC	SE	EH	RE	Total
Salinity Control (m ³ /s)	0	0	0	400	1,000	56	36	1,000	2,492
Navigation and Fisheries (m ³ /s)	56	195	76	12	0	0	0	0	339
Dilution (m ³ /s)	0	50	10	20	0	0	20	0	100
Environment (m ³ /s)	119	9	89	11	823	23	29	925	2,028
Adopted (m³/s)	119	195	89	400	1,000	56	36	1,000	2,895
Salinity Control (Mm ³ /Season)	0	0	0	7,335	18,338	1,027	660	18,338	45,699
Navigation and Fisheries (Mm ³ /Season)	1,027	3,576	1,394	220	0	0	0	0	6,217
Dilution (Mm ³ /Season)	0	917	183	367	0	0	367	0	1,834
Environment (Mm ³ /Season)	2,179	167	1,635	210	15,101	414	523	16,956	37,183
Adopted (Mm³/Season)	2,179	3,576	1,635	7,335	18,338	1,027	660	18,338	53,089

Table 9 In-stream demand by region

b) *DOMESTIC DEMAND (RURAL AND URBAN WATER SUPPLY):*

Demands for water supply have been estimated, based on projected rural and urban populations in the year 2025.

	Population in million				
Region	SMA's	Other Towns	Rural Areas	Total Population	Demand m ³ /s
SW	2.4	4.5	16.4	23.3	1
SC	-	3.4	10.6	14	0
NW	2.3	11	28.9	42.2	1
NC	26.8	6	17.6	50.4	14
NE	-	3.5	14.1	17.6	0
SE	-	4	14.2	18.2	0
EH	6.1	3.2	6	15.3	3
Total	37.6	35.6	107.8	181	19

Table 10 Water Supply Demands by region in 2025

c) COMMERCIAL AND INDUSTRIAL DEMANDS:

Commercial and industrial needs are additional to domestic demand. Firm data for such users is not available but World Bank data indicates that, for piped distribution systems, commercial consumption is typically 8 to 11% and industrial consumption 10 to 15% of the total supply. Accordingly, NWMP have estimated commercial demand as 10%, and industrial demand as 15%, of domestic urban demand.

The total of domestic, commercial and industrial demands in 2025, as estimated by NWMPP and expressed in national average per capita terms, is 146 l/c/d. Total demands for populations in the SMA's (202 l/c/d), in Other Towns (166 l/c/d) and in Rural Areas (112 l/c/d). The resulting expected national average of 146 l/c/d in 2025 might be high by international standards. The figure of 146 l/c/d adopted by NWMPP may be considered to be conservative.

d) *IRRIGATION DEMAND:*

Irrigation Demand for groundwater irrigated Thanas (GIT):

Safety Factor	90%
Demand in SW	59 m ³ /s
Demand in NW	76 m ³ /s
Total	135 m ³ /s

Table 11 Surface Water Demand within GIT

Irrigation Demand outside the GIT: The irrigation demand in areas outside the GIT have been calculated by region using the efficiencies appropriate to each region (75% in coastal areas and 100% elsewhere) and assuming dependable rather than average rainfall.

Region	No. of Thanas	Irrigable Area Km ²	Efficiency %	Irrigation Demand		Static Water Mm ³	Net Demand m ³ /s	Return Flow m ³ /s
				Mm ³	m ³ /s			
SW	29	3,370	75	2,779	152	313	135	51
SC	36	6,328	75	4,027	220	382	199	73
NW	9	909	100	466	25	61	22	-
NC	20	565	100	272	15	185	5	-
NE	41	8,880	100	3,066	167	2,740	18	-
SE	15	2,753	75	1,570	86	282	70	29
EHCa	14	1,410	75	975	53	160	44	18
EH Ib	38	2,789	100	1,243	68	588	36	-
Total	202	27,003		14,397	785	4,712	528	170

a Coastal Thanas in EH Region
b Inland Thanas in EH Region

Table 12 Surface water Demand outside the GIT

The regional distribution of future water demands for agriculture set out below is based on maximum irrigable area and the distribution of land type in 2025 as shown in Table 13 below.

Region	Area	Irrigable Area	Irrigable Demand		Rainfed Area	Rainfed Demand		Total Area	Total Demand	
	(km ²)	(km ²)	(mm)	(Mm ³)	(km ²)	(mm)	(Mm ³)	(km ²)	(mm)	(Mm ³)
SW	24,689	12,705	442	5,619	1,066	76.3	81.3	13,771	414	5,701
SC	13,034	8,477	323	2,737	4,388	49.7	21.8	8,915	309	2,759
NW	33,794	22,081	435	9,614	2,523	106	266.5	24,604	402	9,881
NC	17,199	9,477	330	3,129	915	66.2	60.6	10,392	307	3,189
NE	20,038	13,162	270	3,551	1,362	38.2	52.1	14,525	248	3,603
SE	11,240	6,804	283	1,928	290	45.3	13.1	7,093	274	1,941
EH	19,820	4,200	326	1,367	528	80.2	42.3	4,728	298	1,409
Total	139,813	76,906	363	27,946	7,121	75.5	537.7	84,027	339	28,483

Table 13 Estimated Agricultural Evaporation in 2025

GROUND WATER DEMAND

a) DOMESTIC, COMMERCIAL AND INDUSTRIAL DEMANDS

The NWPo accords a high priority to these demands and accordingly, although they are relatively small, they are considered first. Detailed calculations of expected demand in the year 2025. These estimates have been converted into a depth in mm for the dry season over the Thana, based on the expected urban and rural populations. Average figures for each region are presented in Table 14.

Region	Population in million				Demand	Area	Demand
	SMAs	Other towns	Rural areas	Total	Mm ³ /season	km ²	mm/season
SW	2.4	4.5	16.4	23.3	289	24,689	12
SC	-	3.4	10.6	14.0	179	13,034	14
NW	2.3	11.0	28.8	42.1	539	33,794	16
NC	26.8	6.0	17.6	50.5	566	17,199	33
NE	-	3.5	14.1	17.6	222	20,038	11
SE	-	4.0	14.2	18.2	232	11,240	21
EH	6.1	3.2	6.0	15.3	181	19,820	9
Total	37.6	35.7	107.7	181.0	2209	139,813	16

Table 14 Net Water Supply Demands by Region in 2025

b) *EVAPORATIVE DEMANDS FOR THE ENVIRONMENT, FISHERIES AND FORESTS*

Demands on groundwater resources arise from evaporation from the areas under environmental use, fisheries and forests. These are met from soil moisture, residual surface storage at the end of the monsoon and from irrigation returns that would otherwise have returned to the groundwater reservoir. They are very often overlooked in demand estimates, but need to be specifically allowed for in any study of groundwater behaviour. Table 15 shows the summary for the GIT by region.

Region	Environment		Fisheries		Forest		Total		
	GIT Area	Area	Demand	Area	Demand	Area	Demand	Area	Demand
	km ²	km ²	Mm ³						
SW	14,299	2,350	35	633	287	1,150	297	4,132	620
SC	3,527	788	6	146	43	191	39	1,125	88
NW	32,358	5,885	140	1,459	628	1,636	522	8,979	1,290
NC	15,860	3,595	42	576	190	1,792	406	5,963	637
NE	6,090	901	12	204	63	417	95	1,522	170
SE	6,495	1,415	16	382	107	366	71	2,162	194
Total	78,629	14,934	251	3,399	1,319	5,551	1,430	23,884	2,999

Table 15 Evaporation from Environment, Fisheries and Forests in GIT Area

c) *AGRICULTURAL DEMAND*

Agricultural demand will arise from both rainfed and irrigated agriculture. These demands will arise on the Net Cultivated Area (NCA).

	Irrigated		Rainfed		Total		
	Area	Demand	Area	Demand	Area	Demand	Depth
	Km ²	Mm ³	Km ²	Mm ³	Km ²	Mm ³	mm
SW	9,335	4,135	832	61	10,167	4,196	413
SC	2,149	639	253	12	2,402	652	271
NW	21,072	9,339	2,306	245	23,378	9,548	410
NC	9,012	3,023	884	59	9,897	3,082	311
NE	4,283	1,341	285	16	4,568	1,357	297
SE	4,051	1,145	283	13	4,333	1,158	267
Total	49,903	19,622	4,842	406	54,745	20,028	366

Table 16 Maximum Evaporation from Agriculture in GIT Area

Region	Shortfall on GW availability	Area irrigable with available GW	Further area irrigable with additional water	Total Irrigable Area
	Mm ³	Km ²	Km ²	Km ²
SW	151	8,993	342	9,335
NW	171	20,687	385	21,072
Total	322	29,680	727	30,407

Table 17 Surface Water Required for Full Irrigation by Region within GIT

4.3 Climate Data

The climate data comes from various sources and therefore a number of tools had to be developed to extract the data and convert it to a format that GWAVA can read.

Code	Time Frame	Source, Description
BMD	1961-1990	BMD/BWDB, observed dataset
CRUCL1.0	1961-1990	New <i>et al</i> (1999), observed dataset
CRUTS2.1	1961-1990	Mitchell <i>et al</i> (2000), observed dataset
UWH	1978-1999	Adam <i>et al</i> (2006), corrected observed dataset
PRECISBASA	1961-1990	IITM (2005), baseline simulation
PRECISBASB	1961-1990	IITM (2005) , baseline simulation
PRECISBASC	1961-1990	IITM (2005) , baseline simulation
PRECISERA-15	1979-1993	IITM (2005), baseline simulation using ERA-15 boundary conditions
HADRM2CON	2041-2060	Hassell and Jones (1999) control simulation assuming fixed carbon dioxide (CO ₂) emissions
HADRM2PERT	2041-2060	Hassell and Jones (1999) perturbed simulation assuming 1% increase in CO ₂
PRECISA2	2070-2100	IITM (2005), simulation assuming A2 emissions

Table 18 Climate data available for regional climate scenario analysis. Note in addition to the above see Table 20 for available GCM climate data.

For a more detailed description of the Hadley Centre climate data using the PRECIS software see Section 8.2.

CRU data

Extraction and formatting is straight-forward as the projection of the data is the same as that required by GWAVA. The precipitation and temperature data were extracted directly and the potential evaporation was calculated using the Penman-Monteith equation with the following data items provided in the CRU data collection:

- Cloud cover
- Solar radiation
- Wind speed
- Vapour Pressure

Note that the CRU dataset only provides monthly data and so a random precipitation generator was used based on the precipitation and number of rain-days per month. Temperature was also processed through a random generator.

Rainfall Data for FSB Model

To capture rainfall pattern within Bangladesh in the FSB model, observed daily rainfall data from 1961 to 1990 from the Bangladesh Meteorological Department (BMD) were used. A total of 29 stations of BMD were used for interpolating rainfall in each grid cell within Bangladesh. Observed rainfall data of Bangladesh Water Development Board (BWDB) were used to fill any missing data of BMD. The rainfall for grid cells outside of Bangladesh were extracted from CRUCL1.0 rainfall data.

Hadley Centre data

The data provided by the Hadley Centre for its regional climate model of South Asia is at a daily resolution and in rotated polar co-ordinates. A number of different methods to interpolate the data onto the Geographic projection were considered and it was found that interpolation methods smoothed out a lot of the extreme values which should be preserved. Therefore a nearest neighbour approach was used, as presented in Figure 13.

Once again, the potential evaporation was calculated using the Penman-Monteith equation, using the following items:

- Net downward short wave radiation
- Net downward long-wave radiation
- Mean/Max./Min. temperature
- Wind speed
- Relative humidity

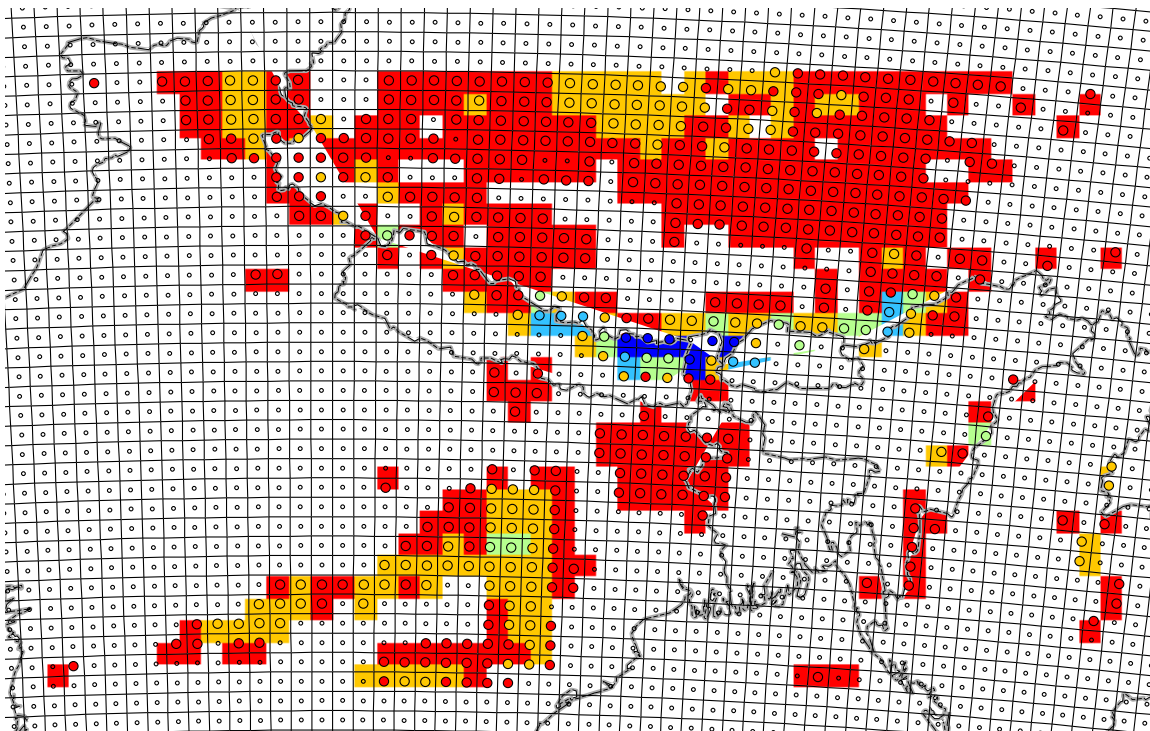


Figure 13 Example of mean daily precipitation for baseline climate from HadRM2 simulation of South Asia. Boxes represent rotate polar co-ordinate grid in geographic projection. Circles represent original HadRM2 data and background grid represents values following nearest neighbour interpolation onto a geographic projection grid.

The baseline climates using observed data from CRU and the Hadley Centre's PRECIS show some large spatial variations in rainfall spatially (see Figure 13). In fact, the magnitude of the rainfall in the PRECIS model runs is much larger than the CRU data (see Table 19). There appears to be much higher rainfall during the dry season to the south of the Himalayas. The Tibetan plateau also appears to be much drier than the observed data series. This pattern is also observed in the HadRM2 dataset.

Future Climate

The future climate scenario data using regional climate models are presented in Table 18. With the inclusion of the glacier model, described in Section 3.4, climate data is required from the end of the baseline period up to the end of the future scenario in order to determine the progress of the de/glaciation. Therefore in order to calculate the water availability indices for the future horizons of 2025 and 2050, climate variables had to be generated from 1991 to 2060. In fact, to use PRECISA2 data representing 2070-2100, some processing is required to provide the climate variables required by the GWAVA runs for future horizons.

Average changes in monthly precipitation, temperature and potential evaporation between the future climate and the baseline (or control climate for HadRM2) were calculated. This value was assigned to the midpoint of the future period, for example for PRECISA2 the average change was assigned to 2085. An annual incremental increase in the monthly values of each of the three climate variables were then applied to the baseline climate dataset used to calibrate the model, i.e. the CRU TS2.1 dataset. This procedure was also followed by Rees *et al* (2005).

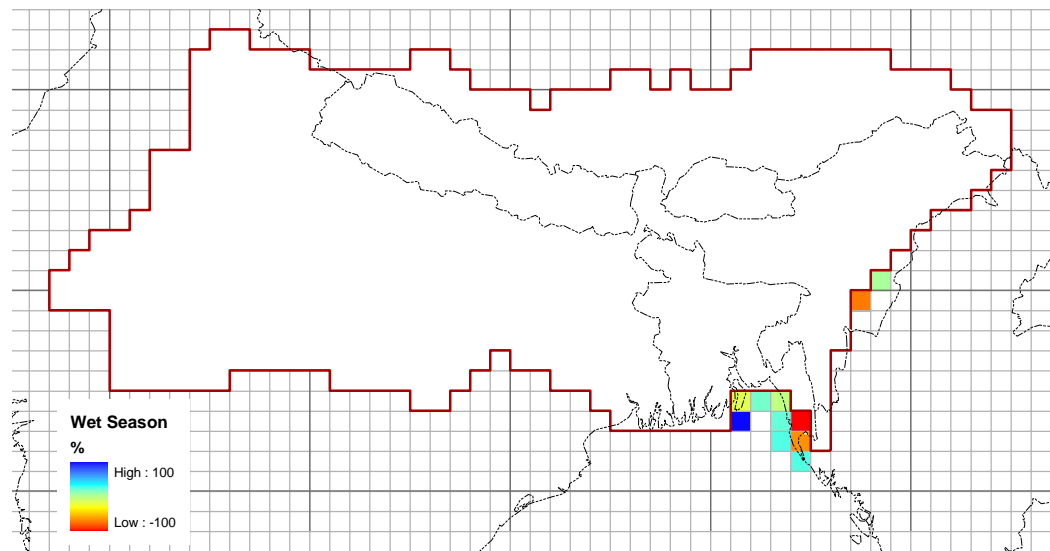
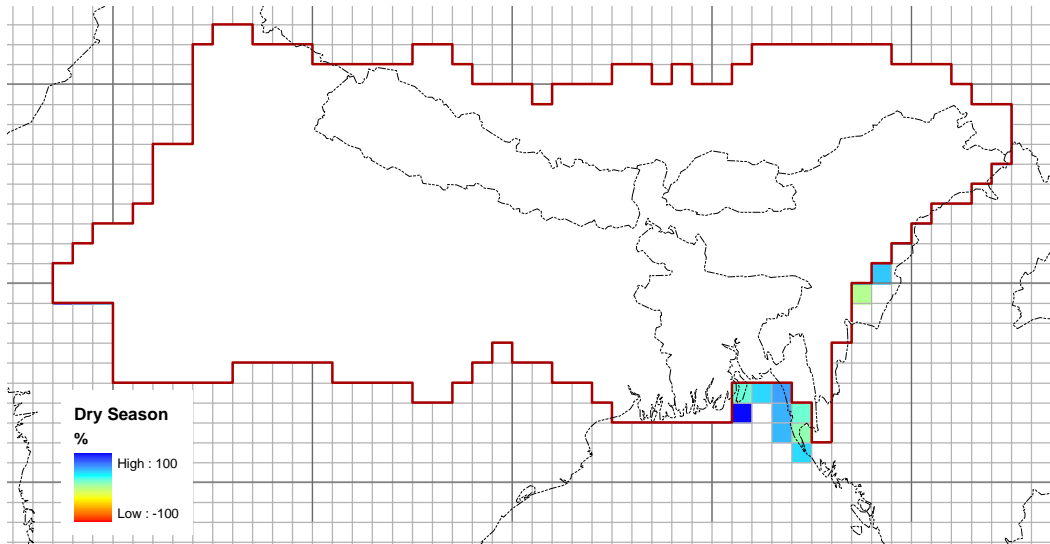


Figure 14 Difference between PRECIS Baseline Ensemble and CRUTS2.1 precipitation: (a) dry Season (b) wet season

	Mean annual precipitation (mm)	Mean annual Evaporation (mm)	Mean annual Number of Rain days
Observed	1,338	1,454	2.76
Modelled	1,685	1,691	8.92

Table 19 Comparison of mean annual climate variables for baseline period between CRUTS2.1 and mean of PRECIS A, B and C.

Access to data on Future Climates

A key input to both the water resources and storm-surge modelling work is fine-scale (50 x 50 km) climate change scenario data. The source of this data was to be from the Hadley Centre's PRECIS model simulations for South Asia (PRECIS stands for **P**roviding **R**egional **C**limates for **I**mpacts **S**tudies). The PRECIS modelling work was to be undertaken by a variety of groups within the region, and results fed through to the CLASIC team members during the first part of 2005. However, there were delays in getting access to the regional climate change data from participants within the Indian sub-continent. These climate modelling groups operate outside of the CLASIC project (and are funded by a related Dfid funded project, the Comprehensive Disaster Management Plan). Thus the CLASIC project has no real 'leverage' over these groups. Fortunately for the water resources modelling, some of the PRECIS results were generated and available in the spring of 2005 by the Indian Institute of Tropical Meteorology (IITM).

Unfortunately, the storm-surge modelling requires data at a smaller time resolution than that generated by IITM. PRECIS data at the relevant time-scale was then expected through the DFID funded Comprehensive Disaster Management Program (CDMP) in Bangladesh, however this project was fraught with difficulties and delays. It was learnt that PRECIS simulations were finally commenced in Bangladesh, however useful results would not be available until mid this year, which is too late to be used by the CLASIC project team.

Consequently CEH and the Hadley Centre conducted PRECIS simulations in the UK. Although this option has been available to the project team for some time, it was not possible to start running PRECIS in the UK until late last year because of agreements between the Hadley Centre and Defra and DFID, who had funded the development of the PRECIS model. The original intention was that PRECIS should be used exclusively by scientists in developing countries in order to generate local 'ownership' of the scenarios generated. However, it was difficult to ascertain who established this principle, and after discussing the issue with staff of DFID, it was agreed that the project team should run the model in the UK in order to enable the CLASIC project to complete its work.

However, the CLASIC project's work has been significantly delayed due to the slow take-up of the PRECIS model within Bangladesh and surrounding countries. Unfortunately the

CLASIC project team effectively had no influence over this matter since we were not providing funding, training, or any other input to these regional modelling groups. Consequently, as a direct result of the very slow provision of suitable regional climate change scenario results from these regional modelling groups, the CLASIC project was some months behind schedule. The project team have now acted to develop the necessary regional climate change scenarios directly by running the PRECIS model at the Hadley Centre and at CEH Wallingford and POL

Additional Climate Model Data

Due to the difficulties encountered and that climate change studies directing towards ensemble runs, it was decided that as many climate scenario runs should be used given the time available. This included both global circulation model (GCM) and regional climate model (RCM) data other than PRECIS, i.e. HadRM2 mentioned in above.

The associated problems with using large-scale GCMs are well-known, especially when looking at regional impact models. However, it was deemed necessary to look at a few of available scenarios from the Data Distribution Centre (DDC) from the Intergovernmental Panel on Climate Change (IPCC) website (see Table 20) in order to give some indication as to the possible spread of results.

<i>Research Centre</i>	<i>Acronym</i>	<i>Model</i>
Hadley Centre for Climate Prediction and Research	HCCPR	HADCM3
National Centre for Atmospheric Research	NCAR	NCAR-CSM
Geophysical Fluid Dynamics Laboratory	GFDL	R30
Canadian Center for Climate Modelling and Analysis	CCCma	CGCM2
Center for Climate System Research/ National Institute for Environmental Studies	CCSR/NIES	CCSR/NIES AGCM

Table 20 List of global circulation models available for A2 and B2 scenarios (based on IPCC, 2006)

5 Water Resources: Calibration

5.1 Observed Flows for GBM Model

Whilst many of the model parameters are linked to physical attributes, some model calibration is still necessary. The remaining parameters requiring calibration are detailed in Table 21. Observed monthly flow data are required for the baseline period of 1961 – 1990 are available at locations across the basin. With a grid-based model it would be possible to alter the properties of each cell and achieve a perfect fit however for the results to be meaningful cells are grouped into sub-catchments and calibrated as a single unit.

Parameter	Description
<i>vfact</i>	Multiplier applied to the storage parameters (C_{max} & fc)
<i>b</i>	PDM parameter
<i>grout</i>	Slow response routing parameter
<i>srout</i>	Fast response routing parameter
<i>bf power</i>	Baseflow recession equation – power term
<i>ploss</i>	Transmission loss (percentage of monthly flow)
<i>k</i>	Routing parameter (days)

Table 21 Description of model parameters requiring calibration

As well as selecting stations with long and reliable flow records, it is important to select flow stations that map correctly on to the gridded river network which underpins the accumulation of runoff in the model i.e. gauging stations should be situated corresponding to a cell outlet and lie on the main river and not an adjacent tributary. Unfortunately restricted by the resolution of the grid, the gridded network does not align well with number of stations located along the smaller tributaries of the Ganges in Nepal. However, the records in Nepal are very short and therefore have been discarded. A list of the stations used is presented Table 22.

Location	River	Start Year	End Year	Type
Bahadurabad	Brahmaputra	1965	1995	Daily
Benighat	Karnali	1963	1993	Mean Monthly
N.T. Road Crossing	Bhareli	1958	1979	Monthly
Chisapani	Karnali	1962	1993	Mean Monthly
Devghat	Narayani	1963	1993	Mean Monthly
Farakka	Ganges	1949	1973	Monthly
Hardinge Bridge	Ganges	1965	1998	Daily
Kaunia	Tista	1985	1992	Daily
Manas	Mathanguri	1955	1974	Monthly
Pandu	Brahmaputra	1956	1979	Monthly
Turkeghat	Arun	1976	1986	Mean Monthly
Yangcun	Yalong Zangbao	1956	1982	Daily

Table 22 Details of gauged sites used to calibrate the GBM model

Cells have been flagged as belonging to particular sub-catchments (Figure 15) enabling calibration for particular zones. The basin and sub-catchments do not fit perfectly onto the gridded scheme as a result of the shape of internal boundaries and hence error in the areas arises. It can be clearly seen from Figure 15 that there are no gauging stations in India for the Ganges. The political sensitivity of discharge data in the region and the lack of involvement with India in the CLASIC project means that this situation is unlikely to change. Although not particularly satisfactory, the only station that can be used for calibrating the most of the Ganges is at the Farakka Barrage.

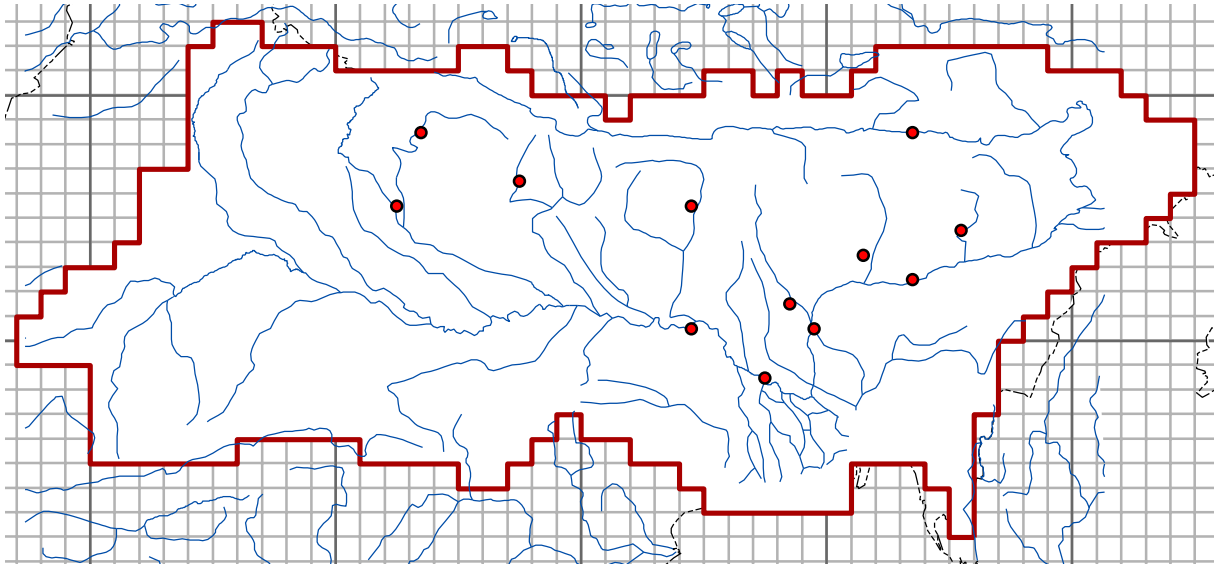


Figure 15 Sub-catchments and gauging station locations in the Ganges-Brahmaputra-Meghna basin.

The first stage of the model calibration was to compare mean annual runoff (MAR), calculated over calendar years to fit the overall water balance which was achieved chiefly by adjustments to the parameter ν_{fact} and b . Further refinements to the model fit were made by adjusting the remaining parameter and comparing mean monthly flows. The sub-catchments are calibrated successively beginning with those uppermost in the catchment and moving downstream.

5.2 Calibration of FSB Model

Calibration requires selection of sub-catchments that have gauging stations at the outlet. The sub-catchments should be within the model area covered by FSB model. A total of eight sub-catchments have been identified (Figure 6), and a summary of gauge sites is given in Table 23. A reasonable agreement is to be achieved between modelled and observed discharges by adjusting calibration parameters.

Bunded agricultural land is the dominant land use in Bangladesh. Because of the bund height of 15-20 cm, a substantial portion of local rainfall-runoff is retained in the agricultural land, and this retention storage is lost by evapo-transpiration and groundwater recharge. Another hydrologic characteristic is the temporary detention of river floodwater by the extensive floodplain, and large portion of this detention storage returns to the river during recession

phase. As a result of retention of local runoff by bunded agricultural land and detention of river floodwater by floodplain, outflow from a cell during monsoon is substantially less than that would be without these storages. The water balance calculation algorithm of GWAVA does not have provision for accounting these two surface water storages. Higher value of the soil storage parameter v_{fact} is used in the case of the catchment with extensive floodplain to achieve agreement for wet season flow. Agreement for dry season flow is chiefly achieved by adjusting the base flow routing parameter $grout$. Agreement for time of flow is chiefly achieved by adjusting the storage constant in the Muskingum routing method.

Location	River	Catchment Area (km ²)	Start Year	End Year	Type
Atrai Railway Bridge	Atrai	8,228	4/1/1964	3/31/1991	Daily
Mirjapur	Bangshi	2,904	4/1/1965	3/31/1991	Daily
Panchpukuria	Halda	968	4/1/1965	3/31/1991	Daily
Comilla	Gumti	1,694	4/1/1965	3/31/1991	Daily
Sheola	Kushiyara	29,282	4/1/1964	3/31/1991	Daily
Kanairghat	Surma		4/1/1969	3/31/1991	Daily
Manu Railway Bridge	Manu	1,815	4/1/1982	3/31/1995	Daily
Shaestataganj	Khowai	2,904	4/1/1964	3/31/1991	Daily
Chapainawabgoni	Mahananda	23,837	5/5/81	12/31/90	Daily

Table 23 Summary of gauge sites for calibration of FSB model

6 Water Resources: Calibration

6.1 GBM Model

Observed Flows

Whilst many of the model parameters are linked to physical attributes, some model calibration is still necessary. The remaining parameters requiring calibration are detailed in Table 21. Observed monthly flow data are required for the baseline period at locations across the basin. With a grid-based model it would be possible to alter the properties of each cell and achieve a perfect fit however for the results to be meaningful cells are grouped into sub-catchments and calibrated as a single unit.

Parameter	Description
<i>vfact</i>	Multiplier applied to the storage parameters (C_{max} & fc)
<i>b</i>	PDM parameter
<i>grout</i>	Slow response routing parameter
<i>srout</i>	Fast response routing parameter
<i>bf power</i>	Baseflow recession equation – power term
<i>ploss</i>	Transmission loss (percentage of monthly flow)
<i>k</i>	Routing parameter (days)

Table 24 Description of model parameters requiring calibration

As well as selecting stations with long and reliable flow records, it is important to select flow stations that map correctly on to the gridded river network which underpins the accumulation of runoff in the model i.e. gauging stations should be situated corresponding to a cell outlet and lie on the main river and not an adjacent tributary. Unfortunately restricted by the resolution of the grid, the gridded network does not align well with a number of stations located along the smaller tributaries of the Ganges in Nepal. However, the records in Nepal are very short and therefore have been discarded. A list of the stations used is presented Table 22.

Location	River	Start Year	End Year	Type
Bahadurabad	Brahmaputra	1965	1995	Daily
Benighat	Karnali	1963	1993	Mean Monthly
N.T. Road Crossing	Bhareli	1958	1979	Monthly
Chisapani	Karnali	1962	1993	Mean Monthly
Devghat	Narayani	1963	1993	Mean Monthly
Farakka	Ganges	1949	1973	Monthly
Hardinge Bridge	Ganges	1965	1998	Daily
Kaunia	Tista	1985	1992	Daily
Manas	Mathanguri	1955	1974	Monthly
Pandu	Brahmaputra	1956	1979	Monthly
Turkeghat	Arun	1976	1986	Mean Monthly
Yangcun	Yalong Zangbao	1956	1982	Daily

Table 25 Details of gauged sites used to calibrate the GBM model

Cells have been flagged as belonging to particular sub-catchments (see Figure 15) enabling calibration for particular zones. The basin and sub-catchments do not fit perfectly onto the gridded scheme as a result of the shape of internal boundaries and hence error in the areas arises. It can be clearly seen from Figure 15 that there are no gauging stations in India for the Ganges. The political sensitivity of discharge data in this region and the lack of involvement with India in the CLASIC project means that this situation is unlikely to change; river flow data within the Ganges basin is not available to parties outside of India. Although not particularly satisfactory, the only station that can be used for calibrating the most of the Ganges is at the Farakka Barrage.

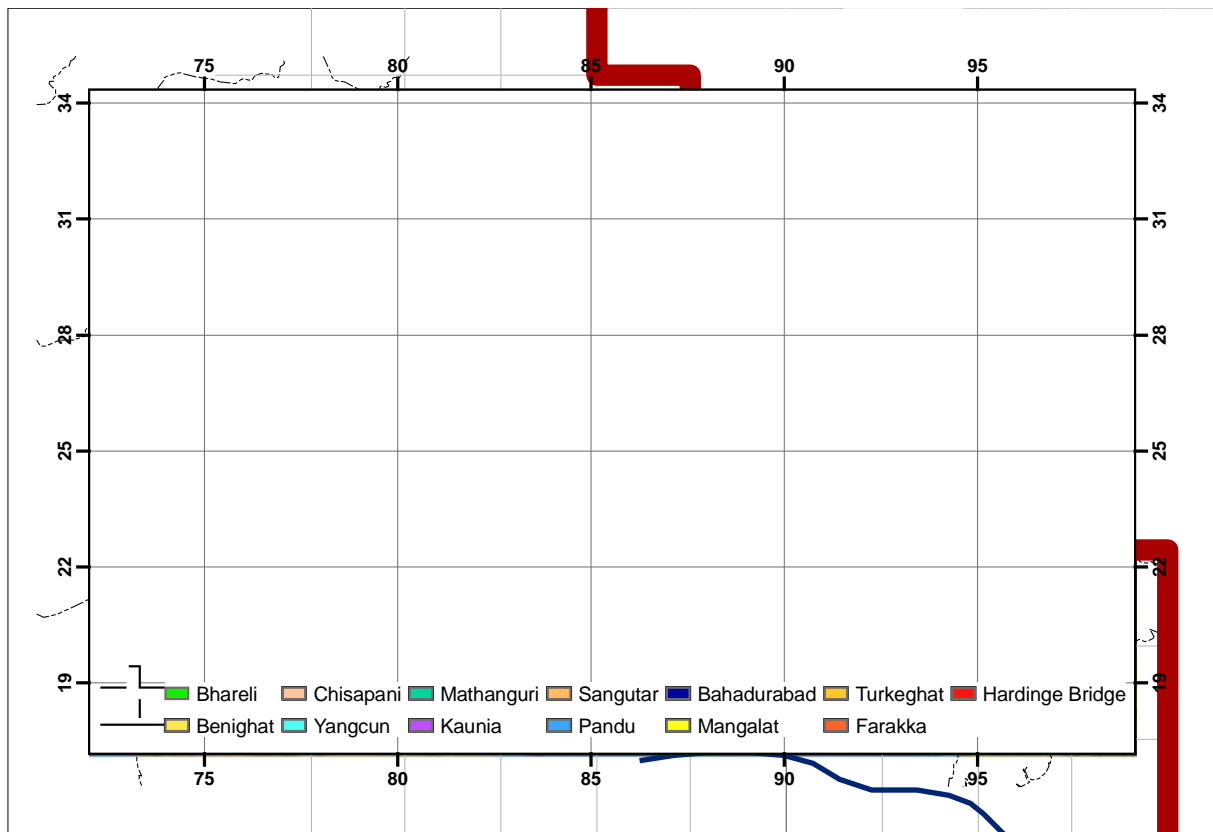


Figure 16 Sub-catchments and gauging station locations in the Ganges-Brahmaputra-Meghna basin.

The first stage of the model calibration was to compare mean annual runoff (MAR), calculated over calendar years to fit the overall water balance which was achieved chiefly by adjustments to the parameter v_{fact} and b . Further refinements to the model fit were made by adjusting the remaining parameter and comparing mean monthly flows. The sub-catchments are calibrated successively beginning with those uppermost in the catchment and moving downstream.

Application of “Observed” Climate Data

The overall water balance for the region can be found in Table 1, where large shortfalls in rainfall can be seen clearly for the CRU dataset. This has also been identified in previous work e.g. Nijssen *et al* (2001). This does present a serious problem to the overall model, as unless a method was found to adjust the climate data in some way, there would have been a discrepancy in the absolute values of water flow. In fact, this problem was identified while carrying out an extensive exercise attempting to locate the source of calibration difficulties.

<i>Variable</i> (10^3 mm/yr)	<i>Bahadurabad</i>		<i>Hardinge Bridge</i>		<i>Kaunia</i>	
	<i>CRU</i>	<i>UWH</i>	<i>CRU</i>	<i>UWH</i>	<i>CRU</i>	<i>UWH</i>
Rain	255	336	378	436	15	17
Evaporation	183	184	556	557	7	7
Computed Runoff	334	630	193	332	23	31
Observed Runoff	611	611	321	321	30	30
Computed / Observed	0.55	1.03	0.60	1.03	0.75	1.04

Table 26 Comparison of observed runoff with simple water balance calculation at gauged locations

The problems mentioned above has recently been looked at by Adam *et al* (2006) where they applied a correction factor to a gridded global precipitation set by Willmot and Matura (2001) for orographic effects. They argue that gridded global precipitation is generally underestimated due to systematic bias and the fact that stations are generally at low elevations. The product provided by Adam *et al* (2006) from the University of Washington (UWH) spans between 1979 and 1999. A simple water balance calculation and computed water flows are presented in Table 26, showing that the UWH dataset improves the agreement between the computed and observed flows significantly. However, it must be noted that this would be expected as Adam *et al* (2006) use observed discharges to calibrate their factors.

The difference between annual rainfalls can be found in Figure 17. As can be seen the areas south of the Himalayas and in the Arunachal Pradesh have a much increased rainfall. The rainfall on the Tibetan plateau is greatly reduced, however as the rainfall is low in this region, any small absolute changes in rainfall result in a high relative change. This agrees very well with the problems that were encountered in the calibration process using the CRU dataset.

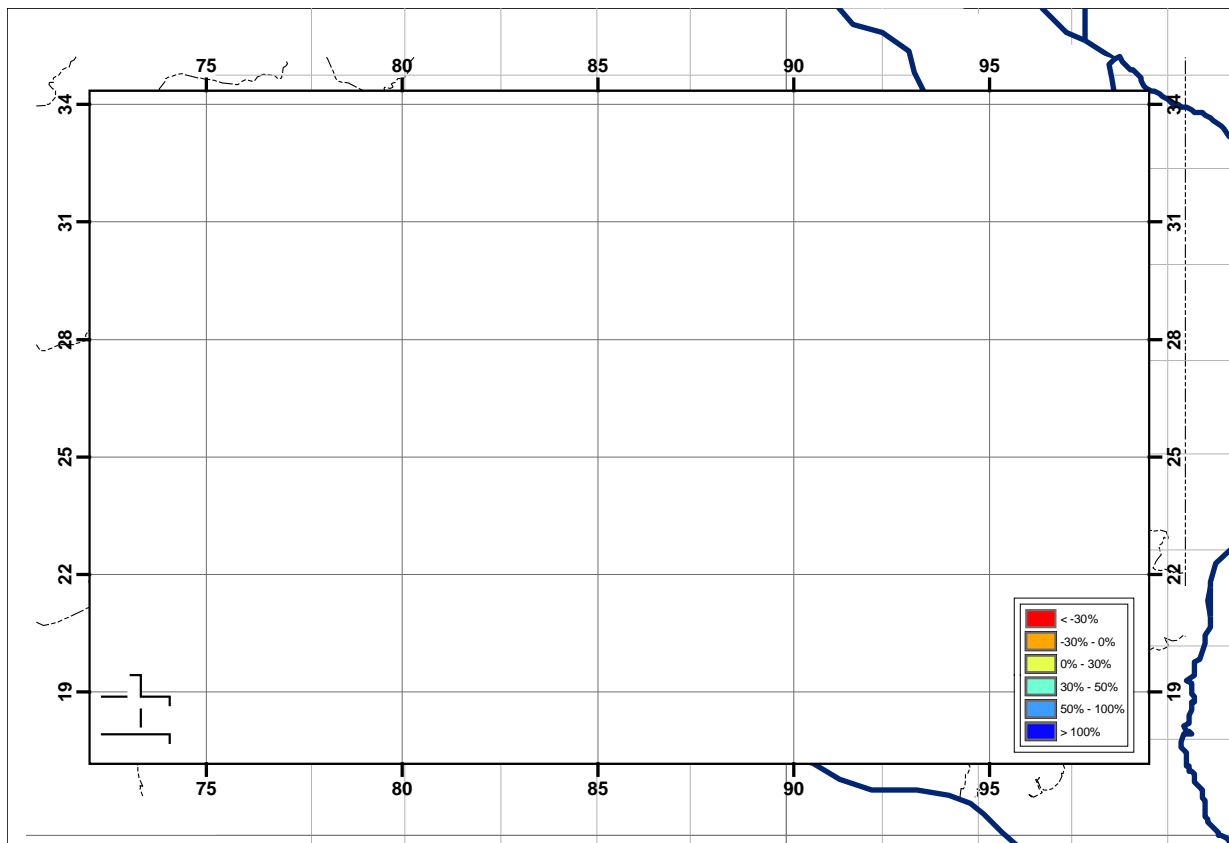


Figure 17 Difference between CRU and UWH annual precipitation (mm)

6.2 Calibration of FSB Model

Calibration requires selection of sub-catchments that have gauging stations at the outlet. The sub-catchments should be within the model area covered by FSB model. A total of eight sub-catchments have been identified (see Figure 6), and a summary of gauge sites is given in Table 23. A reasonable agreement is to be achieved between modelled and observed discharges by adjusting calibration parameters.

Bunded agricultural land is the dominant land use in Bangladesh. Because of the bund height of 15-20 cm, a substantial portion of local rainfall-runoff is retained in the agricultural land, and this retention storage is lost by evapo-transpiration and groundwater recharge. Another hydrologic characteristic is the temporary detention of river floodwater by the extensive floodplain, and large portion of this detention storage returns to the river during recession phase. As a result of retention of local runoff by bunded agricultural land and detention of

river floodwater by floodplain, outflow from a cell during monsoon is substantially less than that would be without these storages. The water balance calculation algorithm of GWAVA does not have provision for accounting these two surface water storages. Higher value of the soil storage parameter *vfact* is used in the case of the catchment with extensive floodplain to achieve agreement for wet season flow. Agreement for dry season flow is chiefly achieved by adjusting the base flow routing parameter *grout*. Agreement for time of flow is chiefly achieved by adjusting the storage constant in the Muskingum routing method.

Location	River	Catchment Area (km ²)	Start Year	End Year	Type
Atrai Railway Bridge	Atrai	8,228	4/1/1964	3/31/1991	Daily
Mirjapur	Bangshi	2,904	4/1/1965	3/31/1991	Daily
Panchpukuria	Halda	968	4/1/1965	3/31/1991	Daily
Comilla	Gumti	1,694	4/1/1965	3/31/1991	Daily
Sheola	Kushiyara	29,282	4/1/1964	3/31/1991	Daily
Kanairghat	Surma		4/1/1969	3/31/1991	Daily
Manu Railway Bridge	Manu	1,815	4/1/1982	3/31/1995	Daily
Shaestataganj	Khowai	2,904	4/1/1964	3/31/1991	Daily
Chapainawabgoni	Mahananda	23,837	5/5/81	12/31/90	Daily

Table 27 Summary of gauge sites for calibration of FSB model

6.3 Calibration Results

Flow Calibration – GBM model

A Nash and Sutcliffe (1970) assessment of fit was used in the calibration procedure and Figure 18 to Figure 20 show the results of the process. Using these corrected values for rainfall, the calibration of the coarse-grid model showed marked improvement compared to that using the CRU dataset. Overall the flows appear to be reproduced well at Hardinge Bridge and Kaunia, although low flows appear to be consistently lower for Bahadurabad.

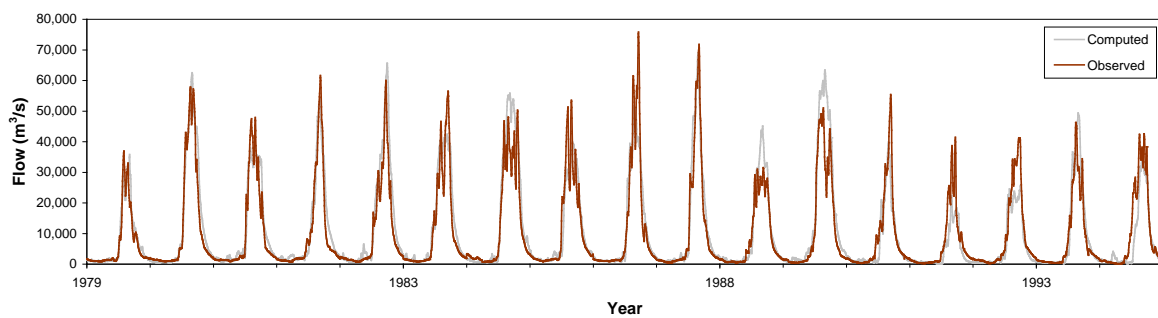


Figure 18 Daily flows 1979-1999 at Hardinge Bridge (Ganges River)

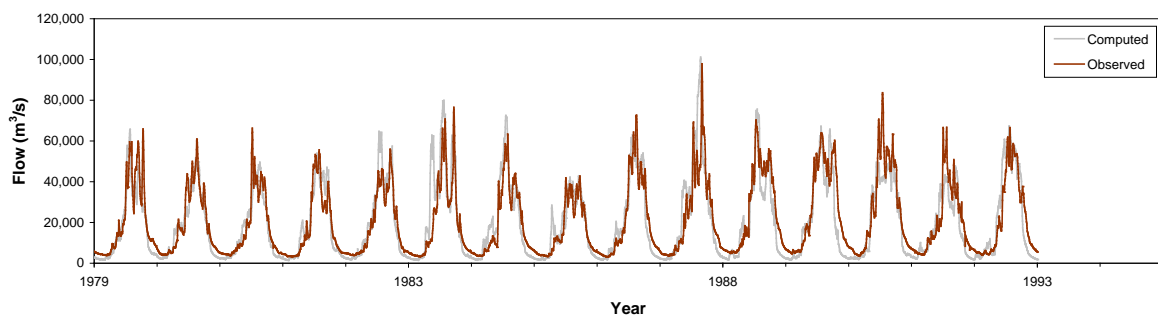


Figure 19 Daily flows 1979-1993 at Bahadurabad (Brahmaputra River)

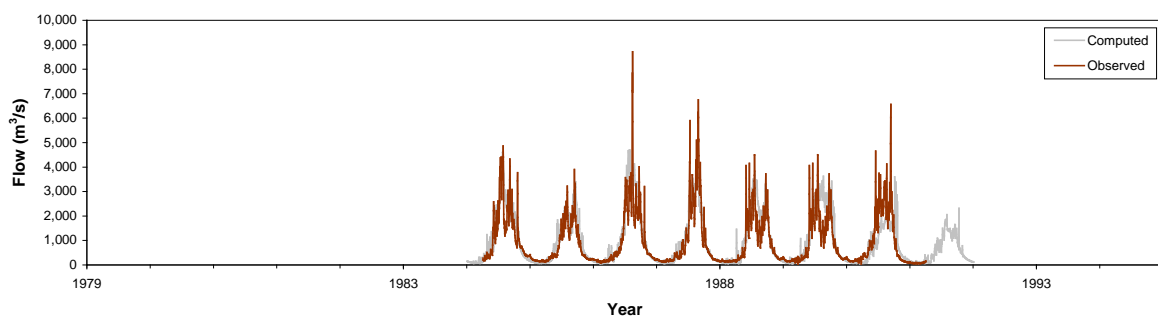


Figure 20 Daily flows 1984-1992 at Kaunia (Tista River)

The results presented are also testament to a more realistic glacier model. Attempts were made using a previous implementation of the glacier model (a model that was used for modelling the Caspian Sea), producing very large glacier melt. This was due to the fact that the glaciers represented an infinite source of water, unlike the current regional glacier model, which can disappear with time. This shows how the annual change in glacier area is very important in the modelling of the Himalayan glaciers.

Flow calibration - FSB model

A comparison of modelled and observed discharges is given in Figure 21 for two sub-catchments, one at the western side of model region while the other at the eastern side. The comparisons are shown for decadal average discharges by selecting a high flood year, an average flood year and a low flood year. Water resources planning and design studies in Bangladesh is carried out on the basis of decadal flow. The Ganges Water Treaty for sharing of Ganges water between India and Bangladesh is also based on decadal flow. There are three decads in each month, the first two being each of 10 days duration, and the third one the remaining days of the month. The duration of the last decadal in a month is 11 days for January, March, May, July, August, October and December, 10 days for April, June, September and November, and 9 or 8 days for February depending on leap year or not.

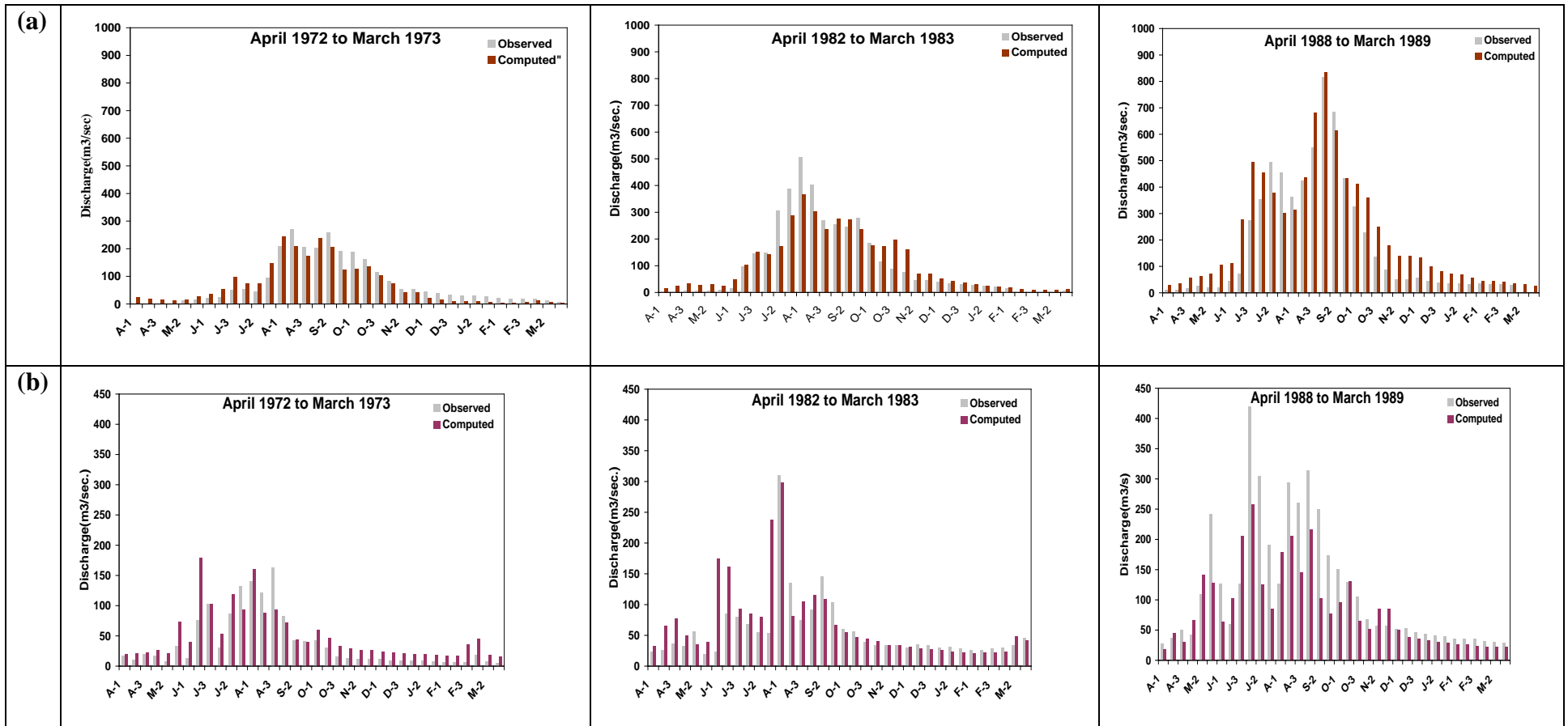


Figure 21 Comparison of modelled and observed discharge for two sub-catchments (a) Atrai sub-catchment Area (b) Gumti sub-catchment

7 Water Resources: Results

7.1 Introduction

In order to interpret the results from an impacts assessment, it is important to identify the key drivers and sensitivities of the water resources system. In the following sections, the sensitivities in the hydrological system and water demand to climate change are identified and then used to explain the impacts on water resources in the region. A key for the abbreviations used to describe the scenarios is provided in Table 28.

Model	Climate Model Used	Emissions Scenario
CCCma A2	CCCma's GCM, CGCM2	A2
CCSRNIES A2	CCSR/NIES's GCM, CCSR/NIES AGCM	A2
GFDL A2	GFDL's GCM, R30	A2
HadCM3 A2	Hadley Centre's GCM, HadCM3	A2
PRECIS A2	Hadley Centre's RCM, PRECIS	A2
CCCma B2	CCCma's GCM, CGCM2	B2
CCSRNIES B2	CCSR/NIES's GCM, CCSR/NIES AGCM	B2
GFDL B2	GFDL's GCM, R30	B2
HadCM3 B2	Hadley Centre's GCM, HadCM3	B2
HadRM2	Hadley Centre's RCM, HadRM2	1%/year increase in CO ₂ from 1990 onwards

Table 28 Key for climate scenario runs. For key to acronyms, see Table 20.

7.2 Climate Change Data

GCM Data

Mean monthly climate parameters are presented in Figure 22, showing that the differences between the different GCMs are significant and their representation of observed climate in this region of the world is rather inconsistent. The figure demonstrates the uncertainty in the absolute values and their use directly in impacts assessments must be considered carefully. However, this result should not be cause for alarm, as it has been long established that there is

great uncertainty in GCM results. In fact, one of the objectives of the current work is to raise these issues and to attempt to overcome them.

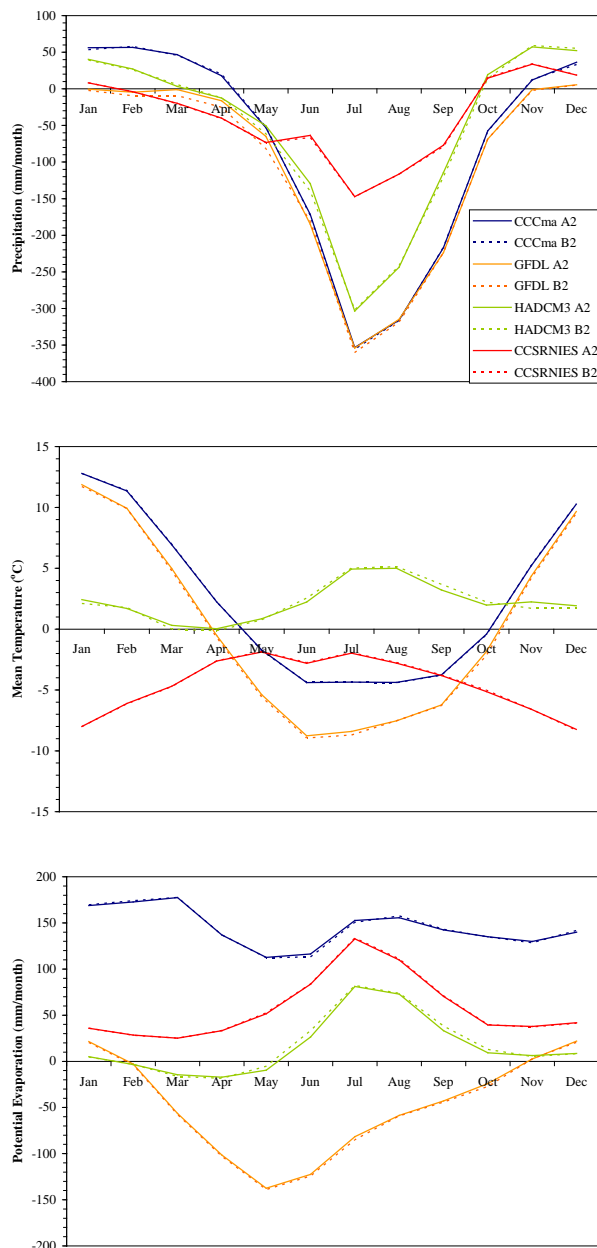


Figure 22 Absolute differences between UWH and GCMs for mean monthly climate parameters for 1979-1999 for GBM region.

For the above analysis, linear interpolation was used to downscale the climate variables from the GCMs to the grid resolution of the GWAVA model and the spatial variation of these mean monthly climate parameters are presented in Figure 23 and Figure 24.

The GCMs consistently underestimate the amount rainfall during the monsoon and overestimate during the dry season. HADCM3 appears to demonstrate behaviour much closer to that of the UWH data compared to other models.

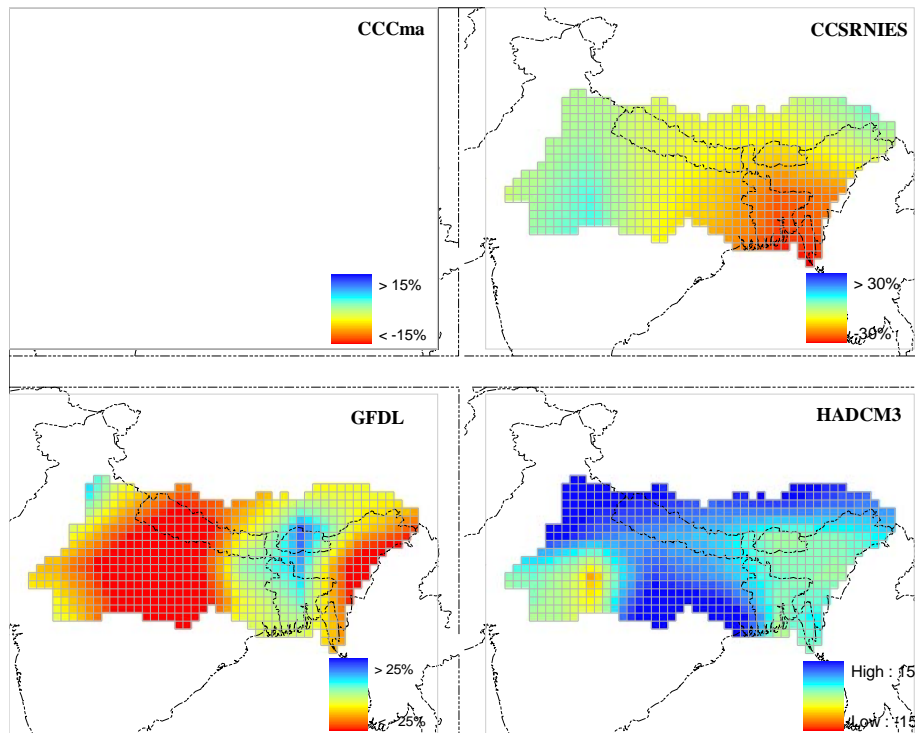


Figure 23 Change in dry season precipitation in 2050s for downscaled GCM A2 scenarios compared to 1979-1999.

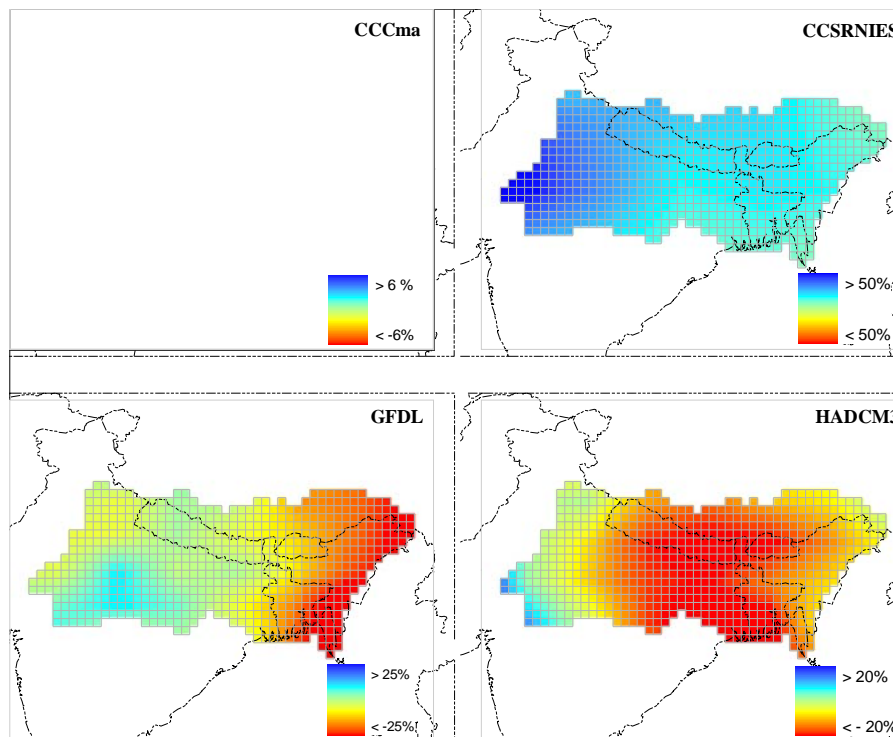


Figure 24 Change in wet season precipitation in 2050s for downscaled GCM A2 scenarios compared to 1979-1999.

In hydrological models, it is possible to look at relative changes only as in the SAGARMATHA project. However, GWAVA requires quantitative comparisons between flows and water demands. As the magnitude of the climate parameters from the GCMs don't appear to be representative of the observed climate, it was deemed necessary to calculate the changes in climate for each scenario and then apply these to the observed climate as an incremental annual change. The result of this exercise is presented in Figure 25 and Figure 26.

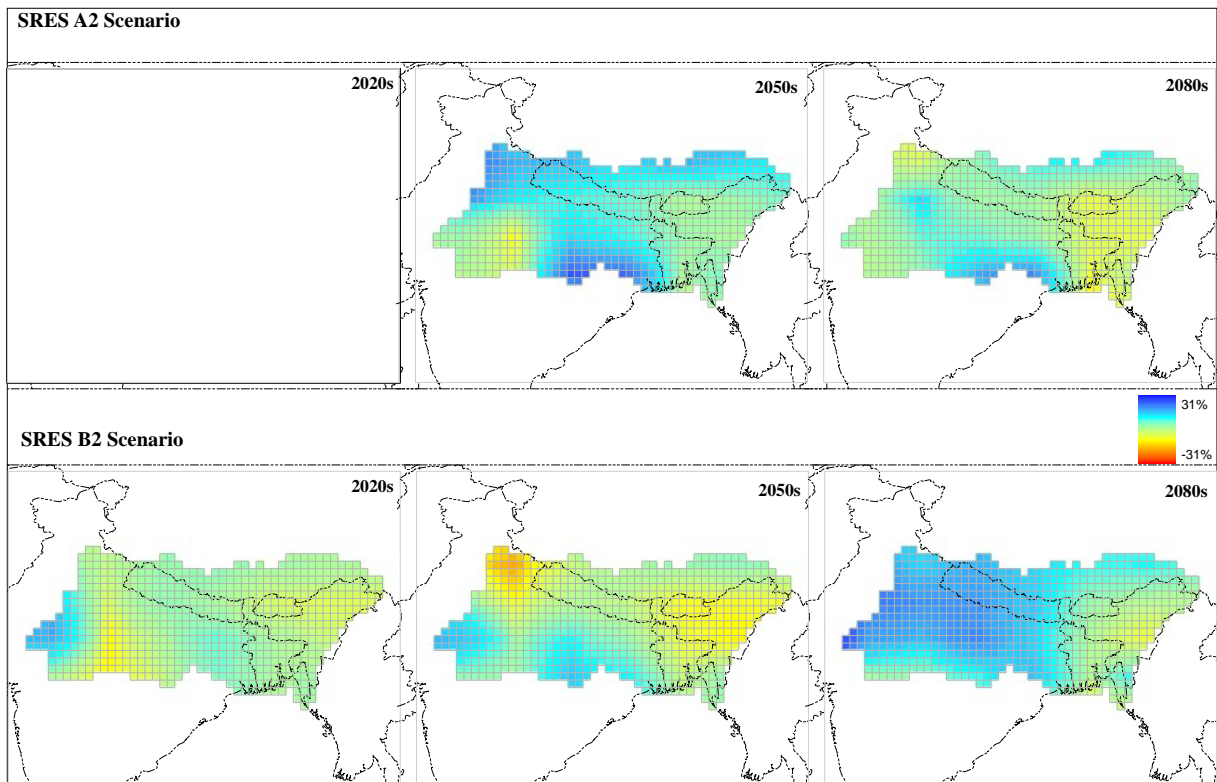


Figure 25 Change in dry season precipitation in 21st century for downscaled GCM A2 scenarios compared to 1979-1999 using HADCM3

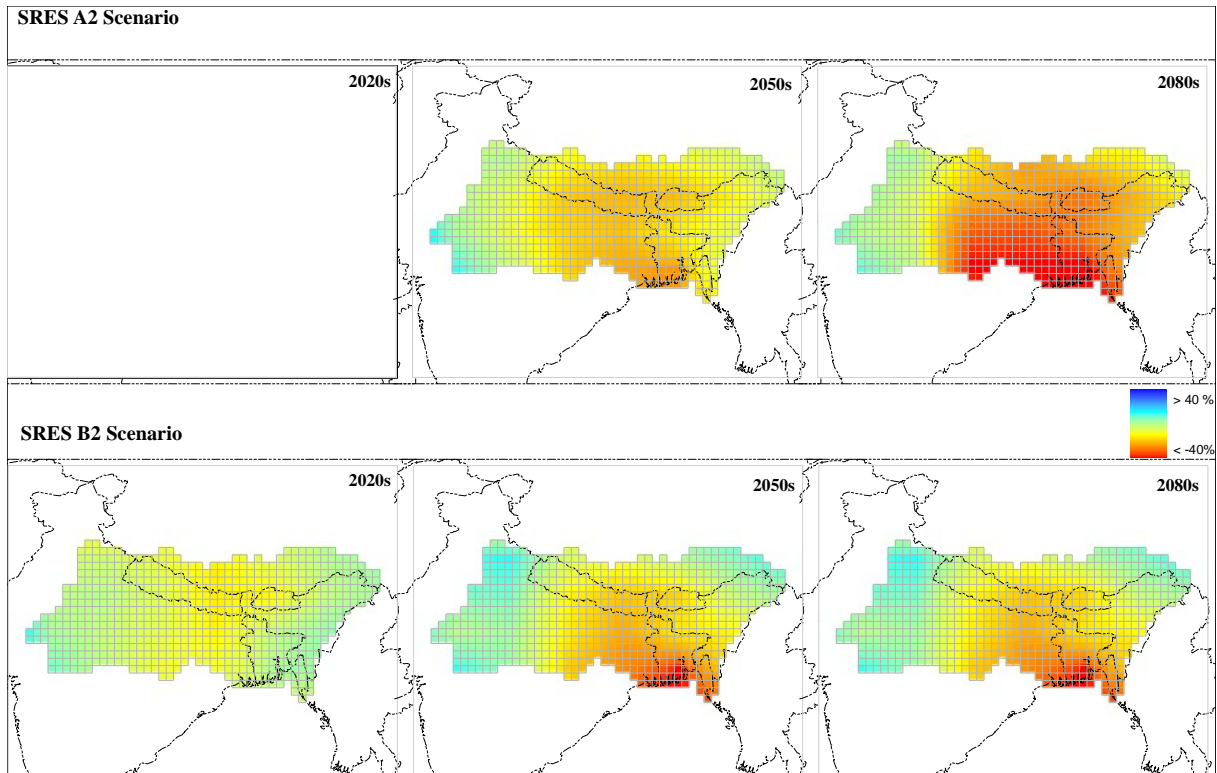


Figure 26 Change in wet season precipitation in 21st century for downscaled GCM A2 scenarios compared to 1979-1999 using HADCM3

Regional Climate Models

Downscaling by linear interpolation can filter out extreme values and therefore may provide an unrealistic representation of the spatial variability of the climate. There are a number of other methods available for downscaling including

- dynamical downscaling, based on physical/dynamical links between the climate at the large scale and at smaller scales;
- statistical downscaling that uses empirical relationships between large-scale atmospheric variables and observed daily local weather variables, e.g. rainfall (Prudhomme, 2006).

The dynamical downscaling approach has been covered in this work by the use of the two Regional Climate Models (RCM) from the Hadley Centre: PRECIS and HADRM2. Unfortunately, the resources have not been available to apply the statistical downscaling approach but could be an area for future work.

At the initial stage of the project, it was thought that the PRECIS daily data could be used directly in the GWAVA model. However, following some analyses, it was found that the problems with the magnitude of the rainfall in GCMs were also present in RCMs. Hence, as with the GCMs, climate changes were applied to the observed climate.

In Figure 27, the differences between the RCM and GCM precipitation data are presented and it can be clearly seen that the RCMs can capture the effects of the Himalayas. This is a response that would not be expected using both the coarse resolution of the GCMs and the linear interpolation technique.

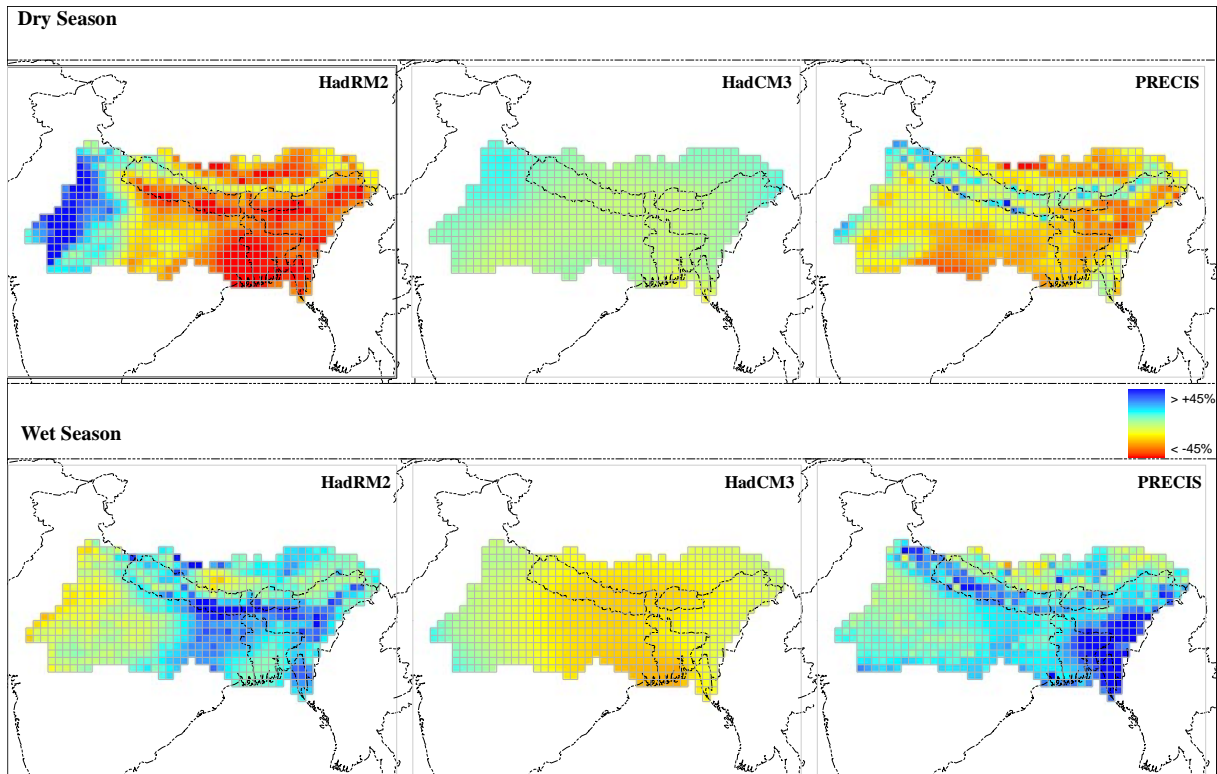


Figure 27 Change in precipitation in 2050s for A2 scenario compared to 1979-1999 using a GCM and RCMs from the Hadley Centre

A summary of the changes in the precipitation patterns in the 2050s are presented in Table 29. As mentioned previously, there is no consistent signal from each of the GCM models. There also appears to be some discrepancy between the Hadley Centre's GCM and RCM models, even with the direction of the change.

Model	Dry Season	Wet Season
CCCma A2	3.4	-0.3
CCSRNIES A2	-7.8	22.0
GFDL A2	-13.9	-7.3
HadCM3 A2	7.9	-12.9
PRECIS A2	-14.8	16.1
CCCma B2	1.4	-5.5
CCSRNIES B2	1.17	21.5
GFDL B2	-6.3	4.5
HadCM3 B2	0.1	-3.3
HadRM2	-17.3	10.9

Table 29 Modelled mean % changes in precipitation in 2050s compared to 1979-1999 baseline

7.3 Climate Change Impacts on River Flow

An ensemble of runs were performed using the suite of climate models described in the previous section. The mean decadal flow centred on the 2020s and 2050s are presented in Figure 28 and Figure 29 respectively for a select number of grid cells, showing that for most scenarios, there is a strong positive signal at Hardinge Bridge and Kaunia. At Bahadurabad and Yangcun, there does not appear to be any significant trends. As expected, the differences between the flows from each scenario are greater in the 2050s than the 2020s.

It is interesting to observe that although there is some spread in the flow values, the seasonal changes are similar for all cells and scenarios, i.e. there are no dramatic changes in the flow regime. However, the point at which the hydrograph begins to rise, an event which marks the change in crop to be grown, starts earlier in all scenarios and is most notable for Hardinge Bridge.

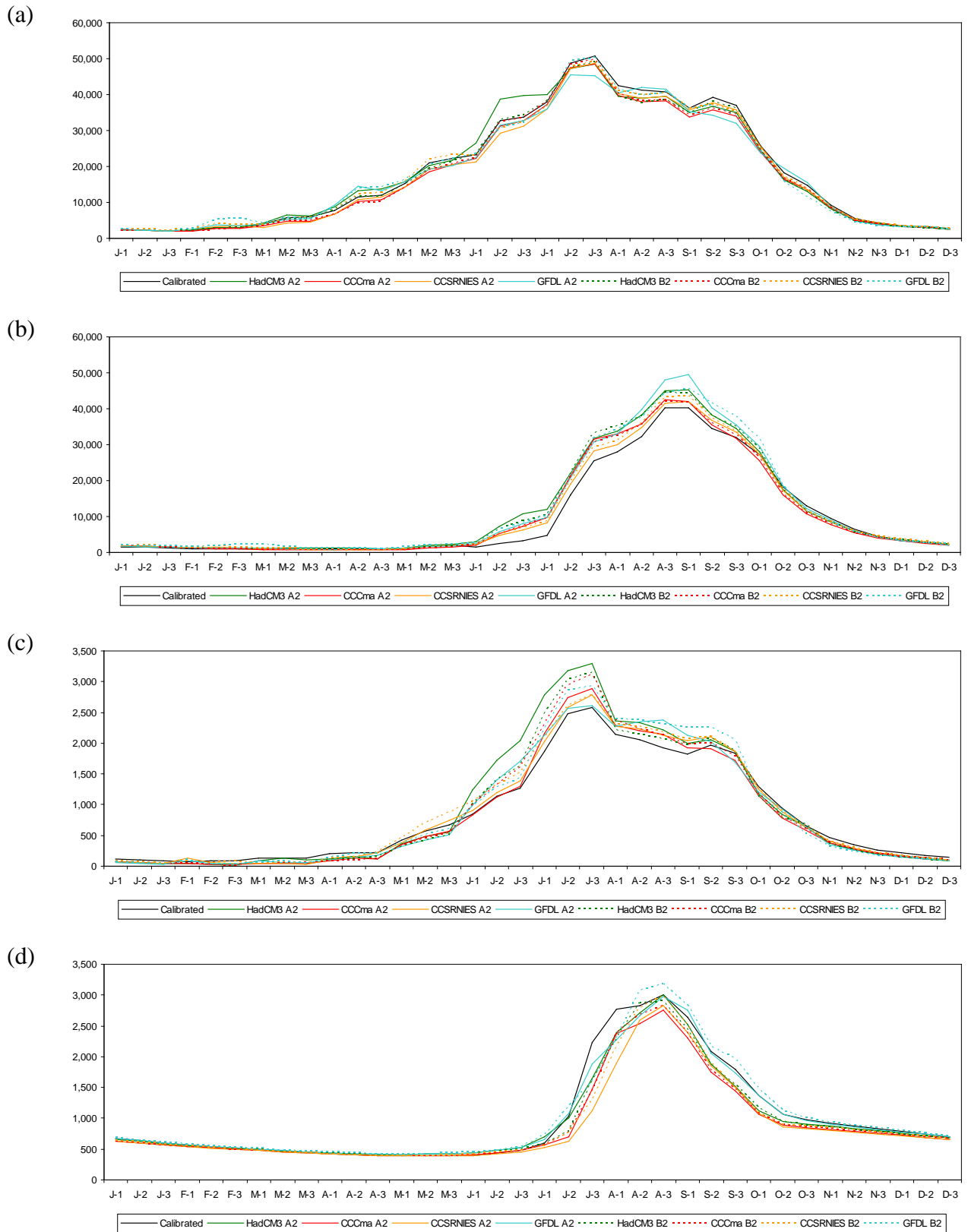


Figure 28 Mean decadal hydrographs for GCMs for 2020s compared to baseline flows at cells near (a) Bahadurabad (b) Hardinge Bridge (c) Kaunia (d) Yangnua

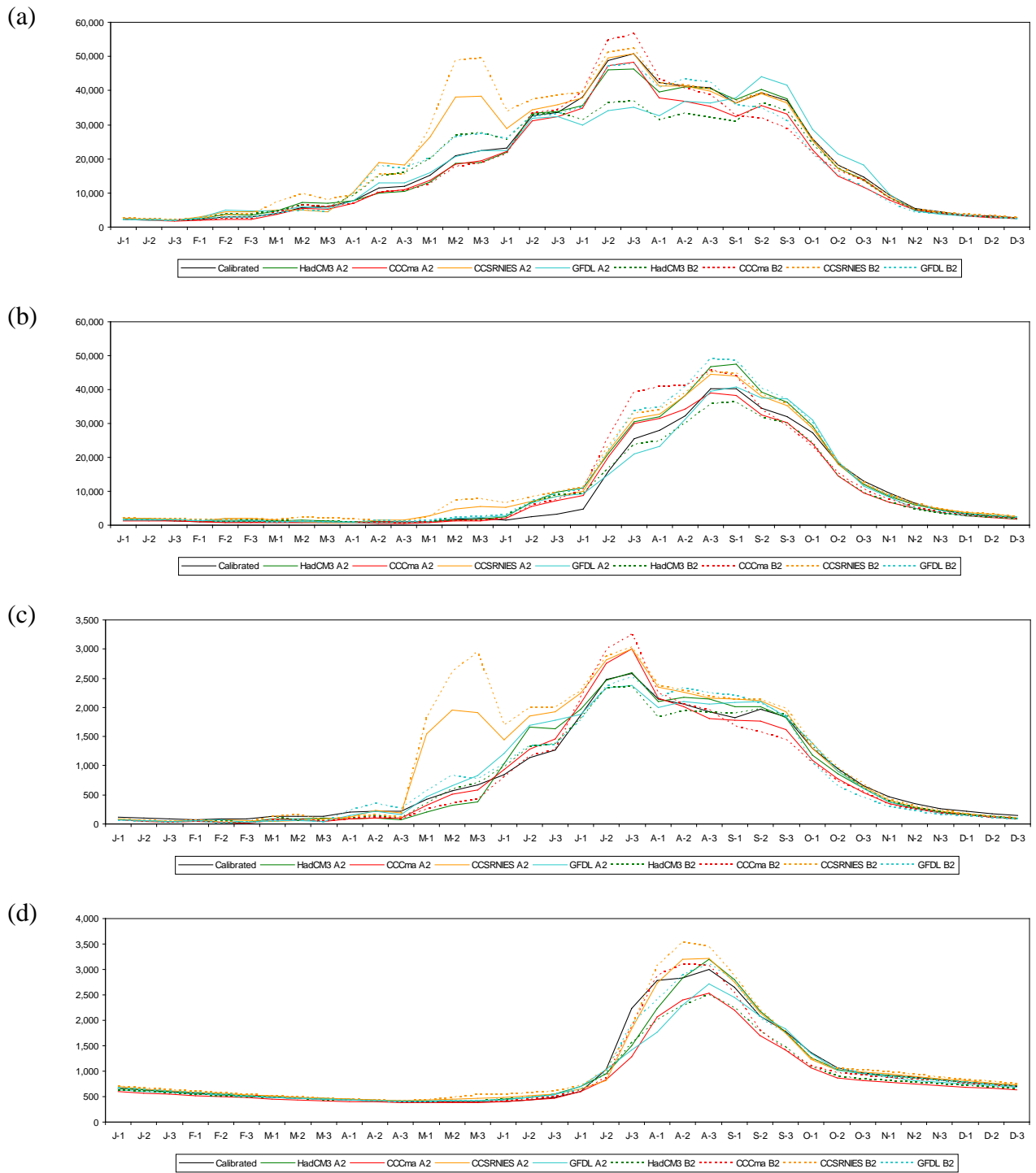
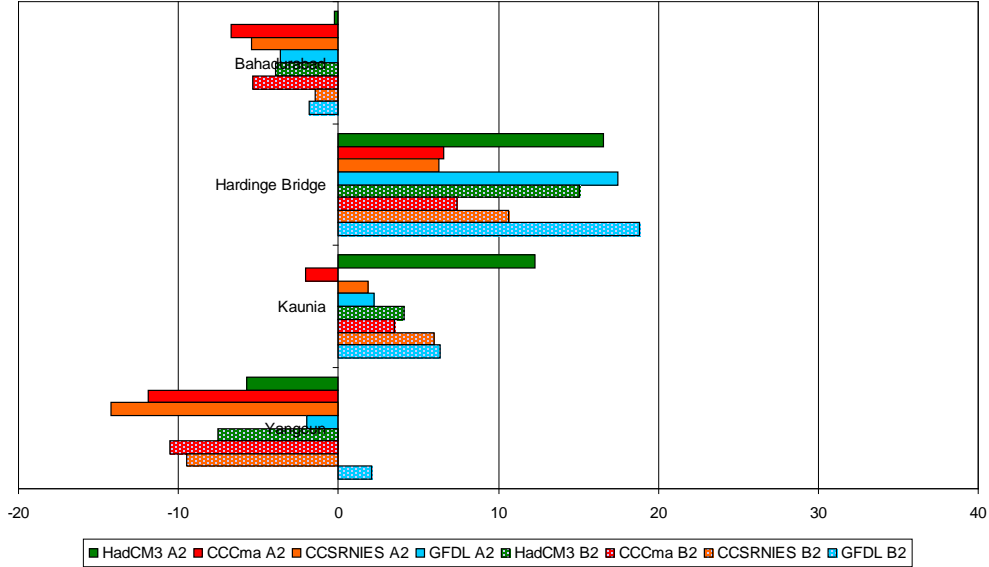


Figure 29 Mean decadal hydrographs for GCMs for 2050s compared to baseline flows at cells near (a) Bahadurabad (b) Hardinge Bridge (c) Kaunia (d) Yangcun

The changes in mean annual flow compared to the baseline flows for each of the selected grid are presented in Figure 30. The changes confirm the result observed above, where signals for each scenario tend to be in the same direction, although the magnitude of the changes vary greatly between scenarios. General agreement between the GCMs that flows will decrease along the Brahmaputra in the future should be of some concern.

Time horizon: 2020s,



Time horizon: 2050s,

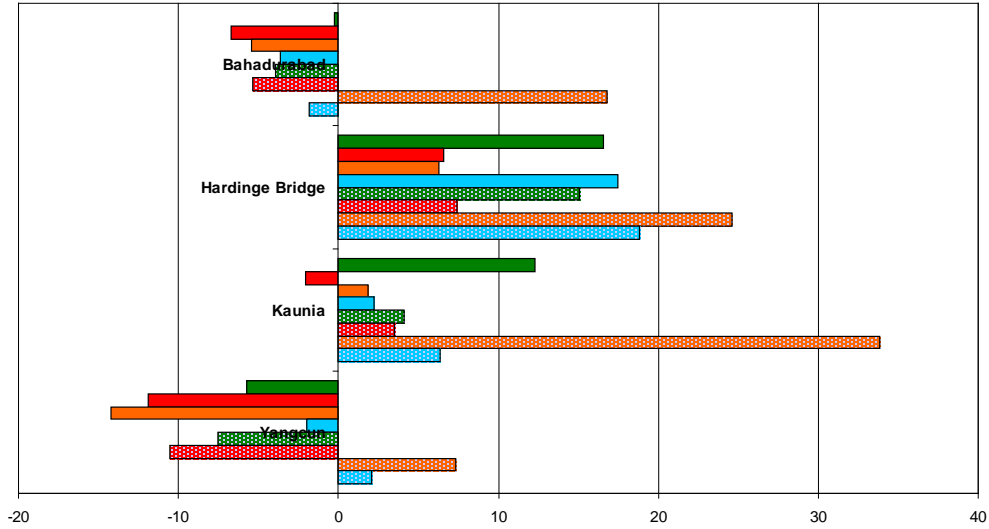


Figure 30 Percentage changes in mean annual flow for GCMs compared to baseline.

Because of the similar behaviour of the climate models from the Hadley Centre, they have been compared against each other on their own for the two future time horizons (see Figure 31). It must be noted that for this part of the analysis, although the HadCM3 and PRECIS models are being used for the A2 emissions scenarios, the HadRM2 model uses a different emissions scenario (see Table 28). As observed for the GCM results, the differences between models are much larger than the differences between emissions scenarios for each of the models. Therefore the aim of this work is to analyse a range of results from a variety of different models to gauge the possible range of future outcomes. While interpreting these results, the emissions scenarios used must be kept in mind.

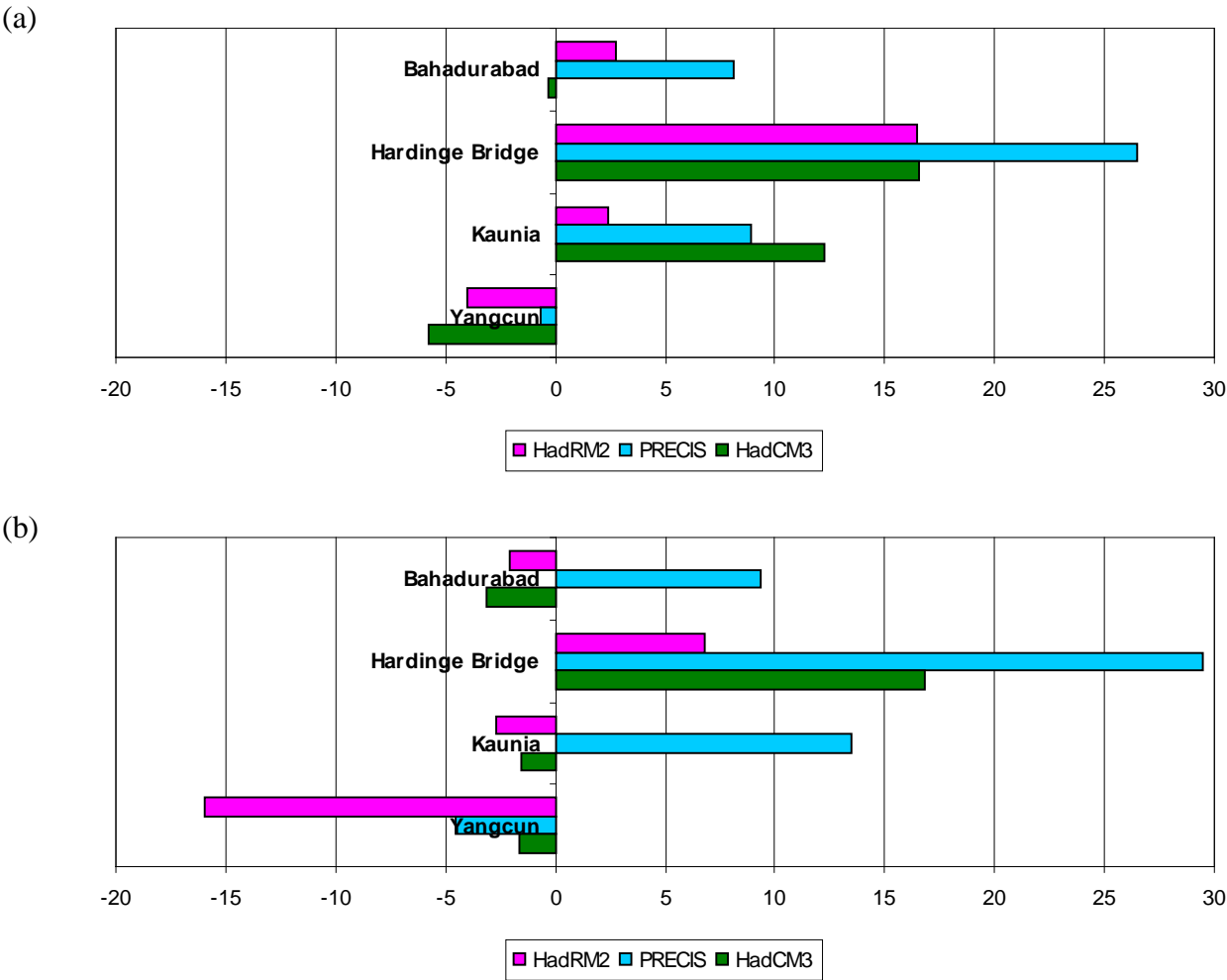


Figure 31 Percentage changes in mean annual flow compared to baseline for Hadley Centre models in (a) 2020s (b) 2050s.

As commented on previously, the direction of change between the GCM and the RCMs appear to be different. For example, at Bahadurabad, the RCMs show an increase of the peak during the monsoon in the future, whereas the GCM shows a decrease. In Figure 32, once again, at Hardinge Bridge, the beginning of the rise in the hydrograph starts earlier in the future.

An interesting feature demonstrated in Figure 31 and Figure 32, is that for Bahadurabad and Hardinge Bridge, there is a distinct increase in the mean annual flow in the future. Due to the very low flows during the dry season at baseline and future time slices, the change in mean annual flow is mainly due to increases in wet season flows.

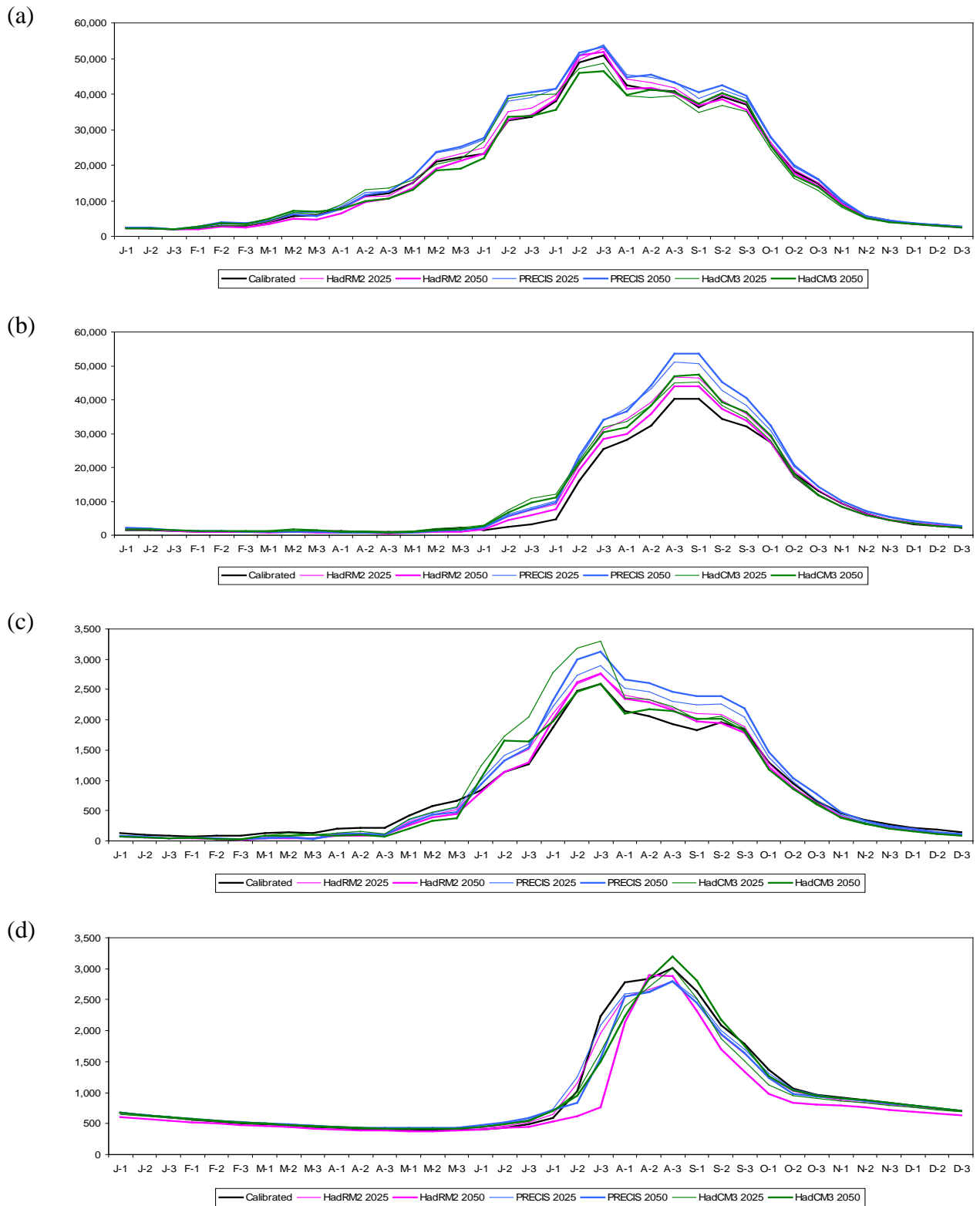


Figure 32 Mean decadal hydrographs for Hadley Centre Models for 2020s and 2050s compared to baseline at cells near (a) Bahadurabad (b) Hardinge Bridge (c) Kaunia (d) Yangcun

The Yalong Zangbo (Brahmaputra River in Tibet) is mainly fed by glacier melt rather than precipitation and therefore for the HadRM2 scenario, the large decrease in flow at Yangcun and the subsequent changes in flow at Bahadurbad can possibly be attributed to the large decreasing glacier areas in the region.

For water resources and flooding issues, the seasonal flows are very important: the changes in these are presented in Figure 33. The smaller values involved in the dry season flows leads it to larger percentage changes. However, it is clear that along the Gangetic plain where there is a lot of flow abstraction for irrigation, there appears to be a reduction in flow in the 2050s. Indeed, this can be seen in both RCMs and a less marked way for the GCM.

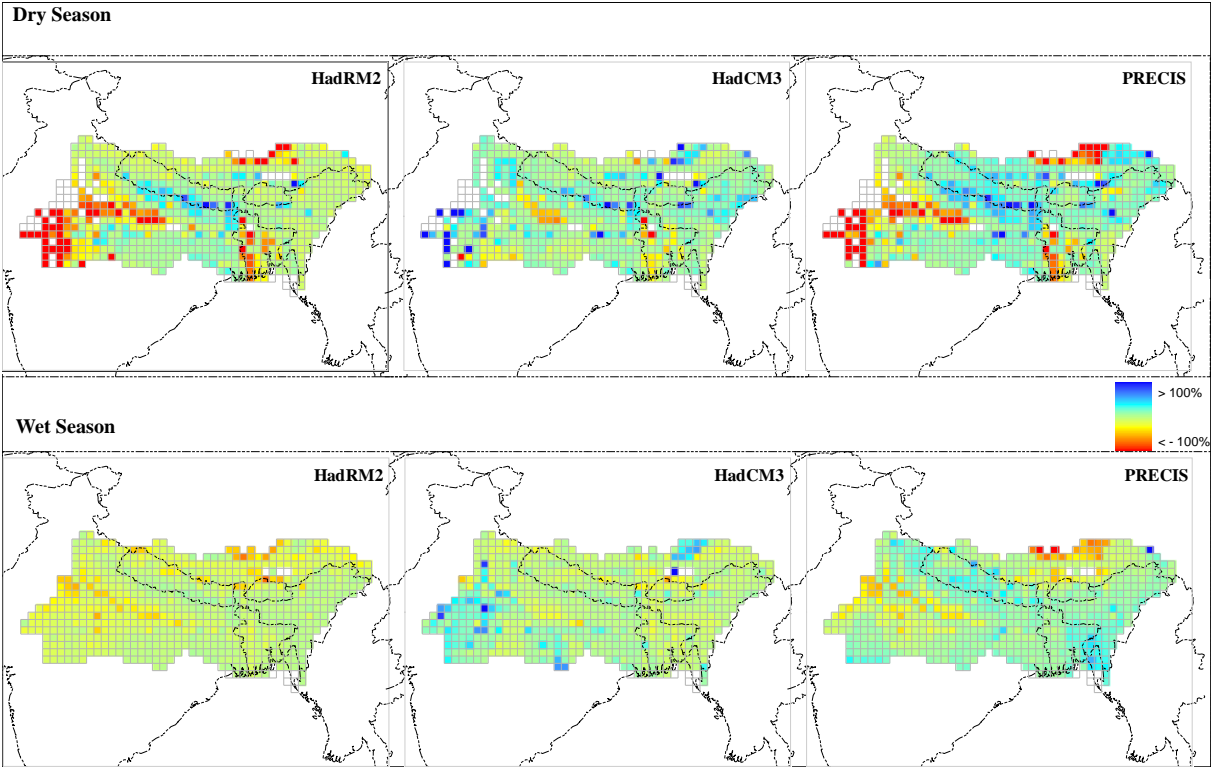


Figure 33 Changes from baseline for seasonal flows for RCMs in the 2050s

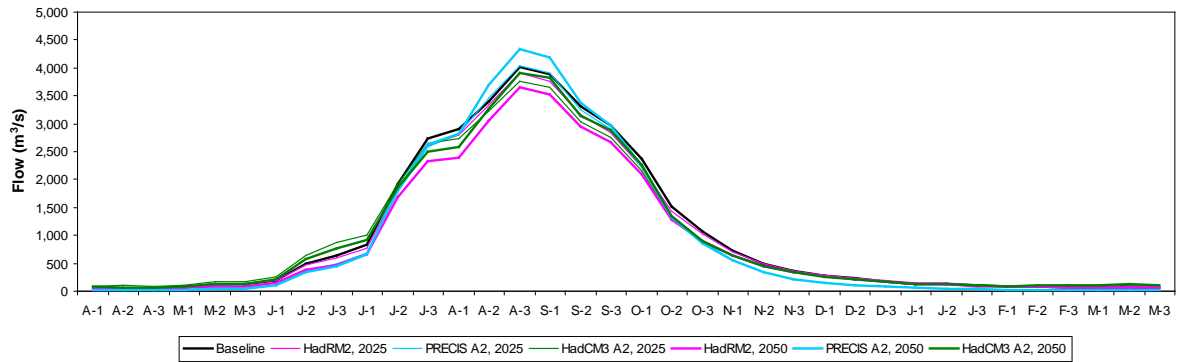
7.4 Flows at Farakka Barrage

The Water Sharing Agreement between India and Bangladesh is a highly controversial one and a source of many conflicts of water use. Figure 34 shows the mean decadal flow at the Farakka Barrage where the flow is controlled according to the agreement. The figure also includes plots at different scales in order to focus on the seasonality of the flows.

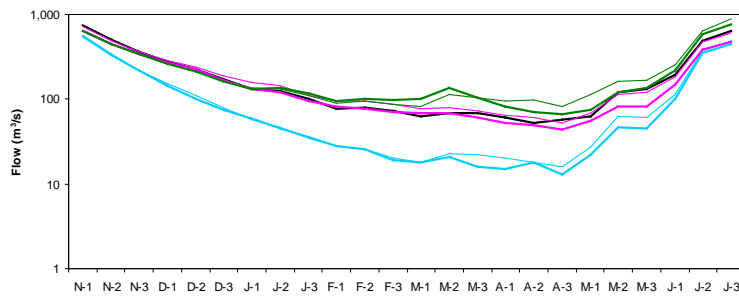
It can be seen clearly that under HadRM2 and HadCM3 A2, the dry season flows are of a similar magnitude to that of the baseline, but for PRECIS A2, the flows are substantially lower. During the wet season, the peak of the hydrograph for PRECIS A2 is steeper than the baseline peak for both time horizons and is higher during the 2050s. However, all other scenarios show a reduction in the peak flow.

The flows into the Hugli river system shows that the dry season flows will be significantly reduced for the PRECIS A2 model whereas flows for other scenarios are not significantly different from current conditions. Should this scenario come to pass, this will have some bearing on the Water Sharing Treaty and the flows required by India to divert into the Hugli River System.

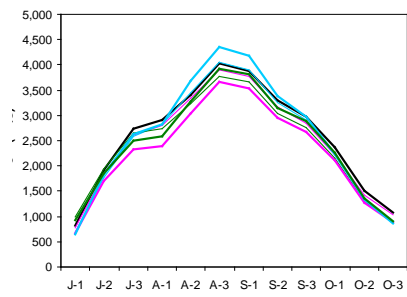
(a) Flows into Bangladesh



(b) Dry season flow



(c) Flood peak



(b) Flows diverted to Hugli river system

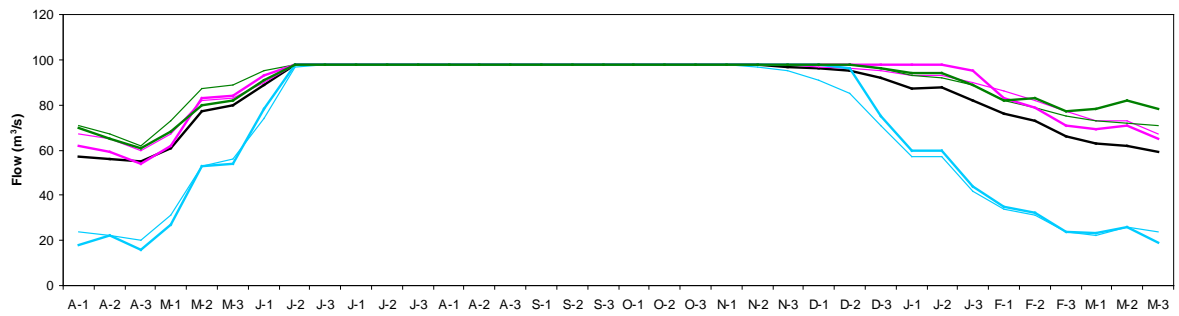


Figure 34 Mean decadal flows at Farakka barrage for Hadley Centre models

7.5 Water Availability in the Ganges-Brahmaputra- Meghna Basin

One of the indicators produced by GWAVA to look at water flows during periods of possible water stress is the $\overline{q_{dry}^{year}}$, which is the mean driest monthly flow for the period centred on *year*. In Table 29, values of $\overline{q_{dry}^{year}}$ are presented for the Hadley Centre models and shows that the number of cells with a reduction in $\overline{q_{dry}^{year}}$ increases through the 21st Century, i.e. the potential that more cells are under water stress is greater.

Climate Scenario	No. of Cells with reduction in $\overline{q_{dry}^{2025}}$	Mean reduction in $\overline{q_{dry}^{2025}}$	No. of Cells with reduction in $\overline{q_{dry}^{2050}}$	Mean reduction in $\overline{q_{dry}^{2050}}$
HadCM3 A2	387	0.89	334	0.89
HadRM2	229	0.93	328	0.80
PRECIS A2	87	0.84	149	0.60

Table 30 Changes in number of cells under water stress

The changes in $\overline{q_{dry}^{year}}$ for cells with low flows can be viewed more clearly in Figure 35. The figure shows that for the RCMs, the low flows appear to be decreasing and the large flows appear to be increasing. As the 21st Century progresses, this trend becomes more apparent.

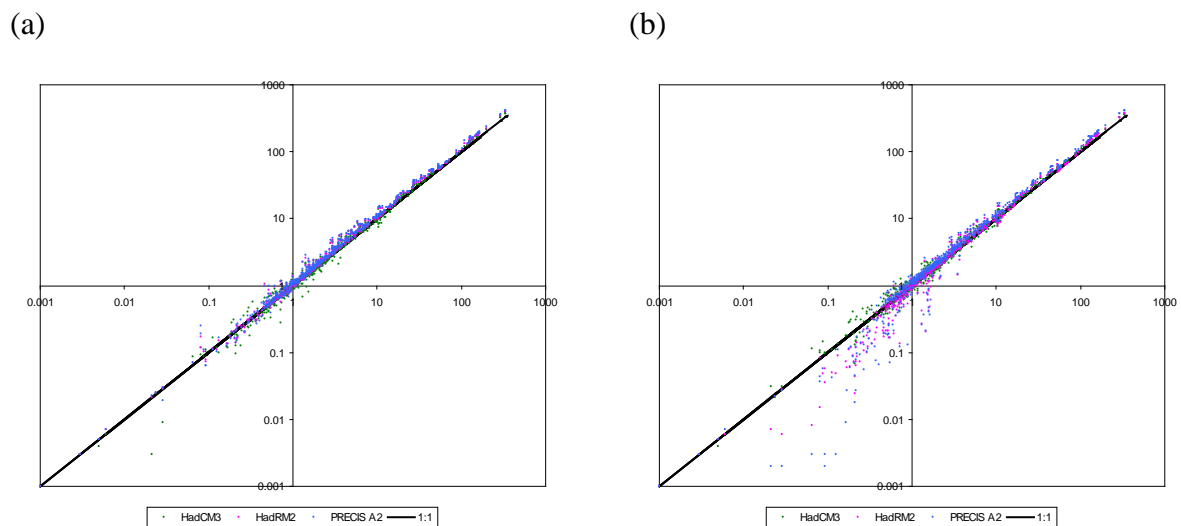


Figure 35 Scatter plot of $\overline{q_{dry}^{year}}$ for each cell in GBM region (a) 2025 (b) 2050 (note that baseline values have been plotted along the x-axis).

Although flows are important, it is not an issue for areas where there is little demand for the water. The water availability indices are most useful for identifying regions of water stress and are presented in Figure 36. At first glance, there appears to be little change in the index for each scenario and time horizon when compared to the baseline. In fact, the spatial pattern of regions of water stress does not appear to change.

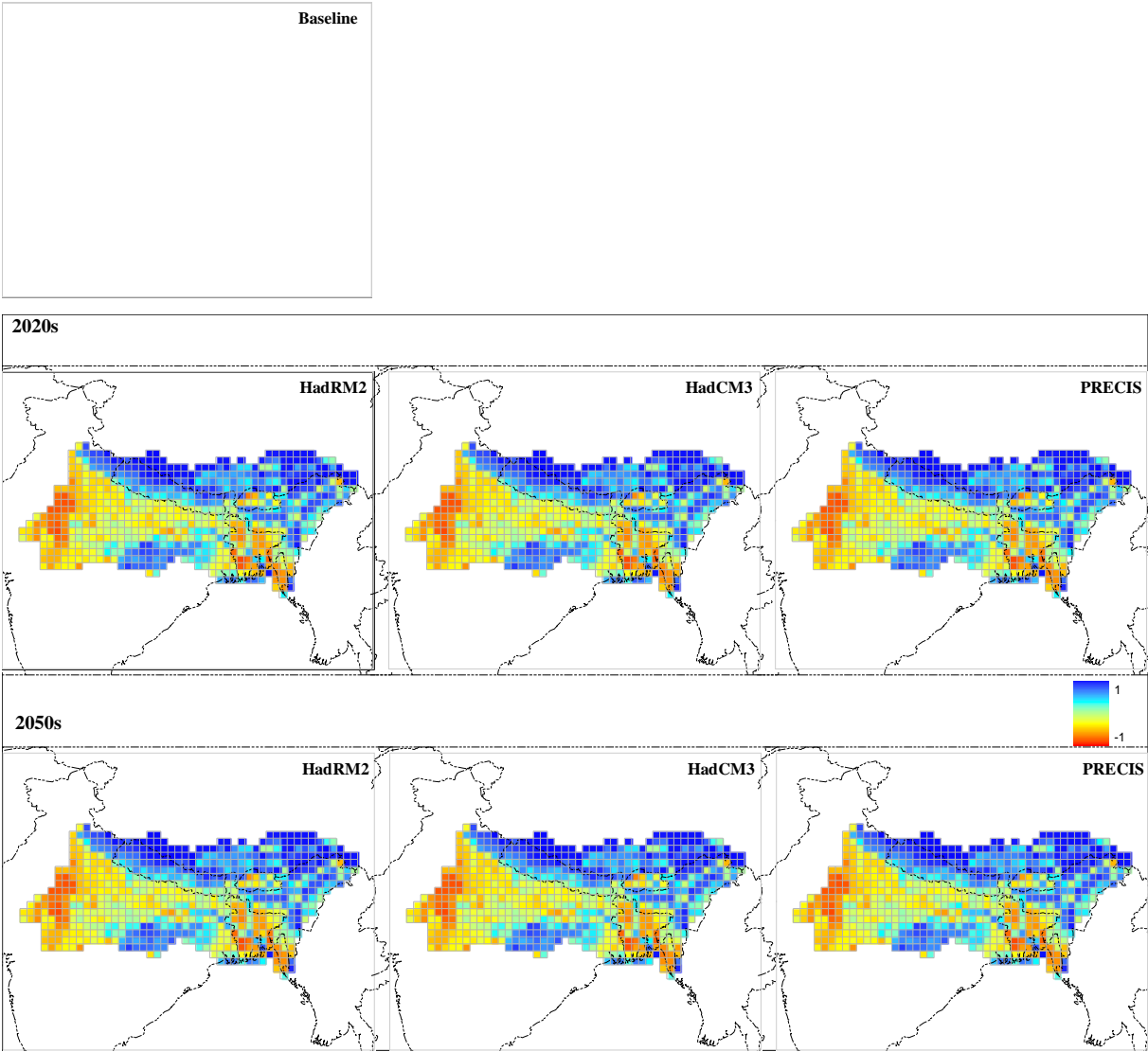


Figure 36 Total water availability index 4 for Hadley Centre climate models

A more detailed analysis of the number of cells that become more stressed in the future is shown in Figure 37. In fact, this figure shows that only a few cells compared to the number of cells in the region (a total of 660 cells) flip from being water rich to water stressed. The reason for this behaviour is that those cells that are already under stress will also tend to be stressed in the future. Indeed most cells in the region show an

increase in water stress as demonstrated spatially in

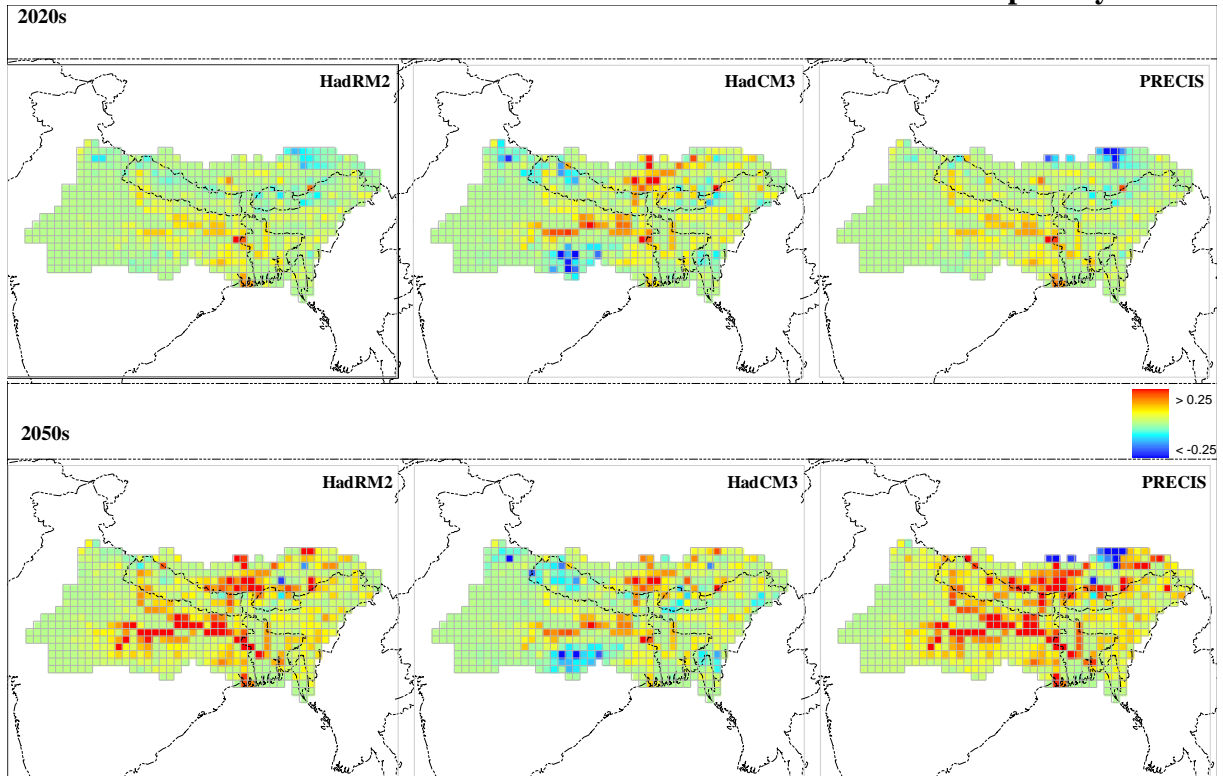
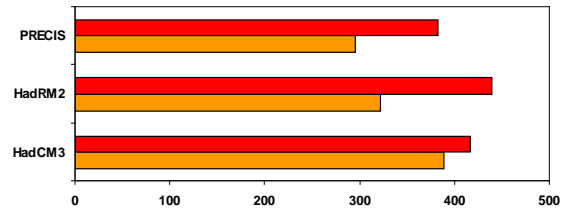
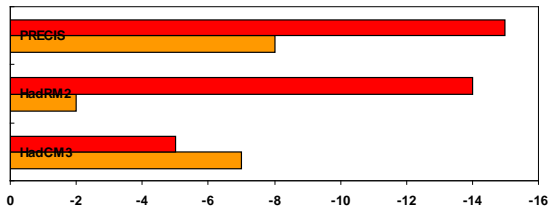
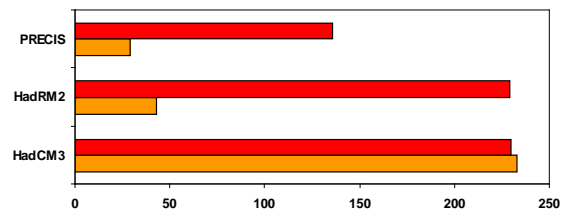
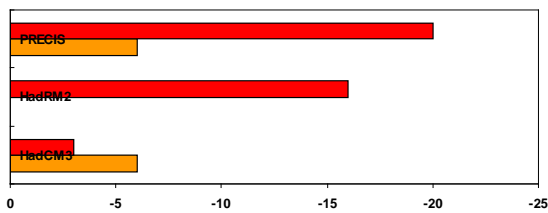


Figure 38.

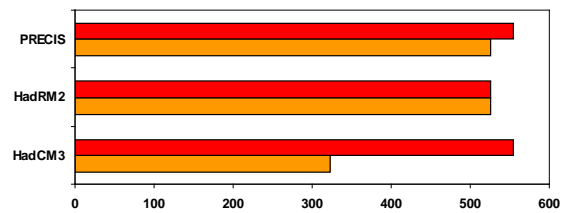
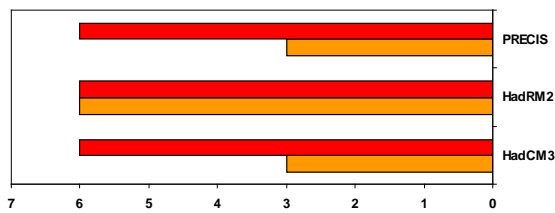
Total Water Availability:



Surface Water Availability:



Groundwater Availability:



Change in number of cells under stress

Number of cells showing increasing stress

Figure 37 Number of cells showing stress compared to baseline for Hadley Centre Models.

In fact, this pattern is observed for all the indices available to GWAVA (see Appendix D for a series of surface water indices). This situation highlights the fact that the current water demand outstrips the available water in many regions of the GBM region.

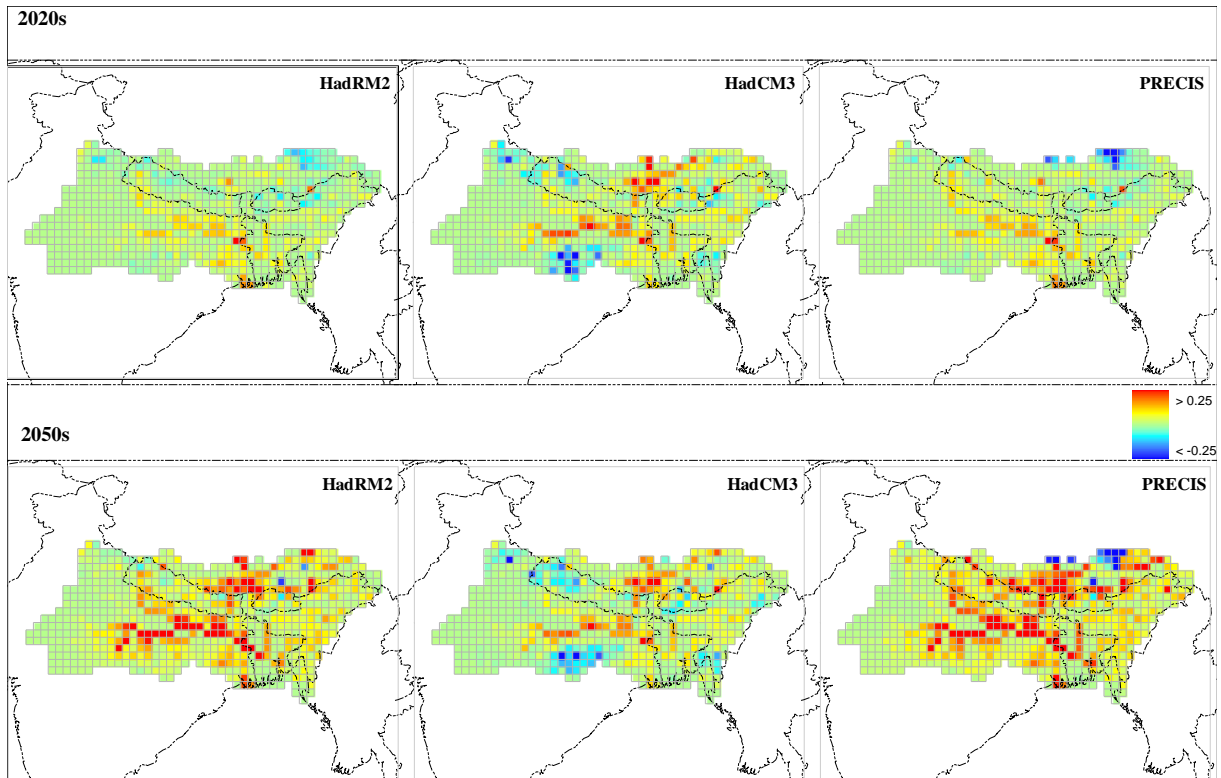


Figure 38 Changes in SWAI-4 for Hadley Centre models where positive values show increase in water stress.

7.6 Discussion

The main parameter of water resources modelling is precipitation and unfortunately, this is the very parameter that is the most difficult for climate modellers to predict. It is clear that with the increasing temperatures, there will be earlier glacial melt in the Himalayas, triggering an earlier rise in the hydrograph of glacier-fed rivers entering Bangladesh. It looks like the effect of this will not be seen until late in the 21st Century and for medium-term planning, this should not be an issue. However, these glaciers are not an infinite source and planners should take note of this while drawing up water management plans. Much monitoring is still required in this area and the fate of the glaciers is still relatively unknown.

As observed in this study, the climate data used to drive many models can be conflicting and trying to interpret their use is very difficult. A range of possible scenarios for the climate have been looked at and an assembly of sound water demands scenarios for the future have been attempted. It can be seen from the results that although the climate is a large driver and has a large impact on water flows and possibly flooding, the main problem is the dry season flow and the water extraction during this season. Most of the areas that are already stressed will remain stressed and with the large increases in population predicted by UN agencies, this situation can only be exacerbated in the future.

A large proportion of the water used in the Gangetic plain and Bangladesh is supplied by groundwater and although there is some treatment of groundwater in GWAVA, a more sophisticated model will be required to look at this aspect of water resources in greater detail.

Plans for the inter-linking river project are underway for Indian rivers and significant changes could be in store for the major rivers that enter Bangladesh. Unfortunately, details of the projects are still unknown and it was not possible to look at the effects of these plans on Bangladesh water resources in this study. However, as can be seen in the scenarios that do already exist, drought problems already exist in the area and with the projections for population growth and the increase in the standard of life for the Indian population, one can only assume that demand for water will increase and problems during the dry season can only worsen.

8 Tropical Storms

8.1 Introduction

At tropical latitudes severe cyclonic storms often cause significant damage to property and loss of life. At the coast, the detrimental effects of these powerful storms result from high winds and rainfall, and the storm surges driven by the high winds and low atmospheric pressure. The coastline surrounding the shallow northern section of the Bay of Bengal is particularly vulnerable to damage by storm surges, especially when they occur concomitantly with a tidal maximum. In Bangladesh alone, approximately 30 million people live within 3 m of current mean sea level (Houghton, 1997) and during the past 40 years there have been a number of major storm surge disasters in this region. The CLASIC project aims to produce new scenarios of climate driven changes in tropical cyclones and the resulting storm surges.

The simulation of storm surges requires high spatial and temporal resolution driving data from regional climate models. This was to be provided from the PRECIS climate model (**P**rediction of **R**egional **C**limate for **I**mpact **S**tudies, developed by the Hadley Centre and not funded as part of the CLASIC project) from researchers using the model in the Indian Sub Continent. Unfortunately, as explained in Section 4.3, data of suitable temporal resolution to drive the storm surge models did not become available and this caused a significant delay in this part of the project. The UK partners (CEH, Hadley Centre and the Proudman Oceanographic Laboratory [POL]) have produced this driving data themselves on a no cost basis for CLASIC.

8.2 Regional model (RCM) description and scenarios

The PRECIS climate model is an atmospheric and land surface model of limited area and high resolution which is locatable over any part of the globe (The region used in CLASIC is shown in Figure 39, along with the POL surge model domain). Dynamical flow, the atmospheric sulphur cycle, clouds and precipitation, radiative processes, the land surface and the deep soil are all treated within the model.

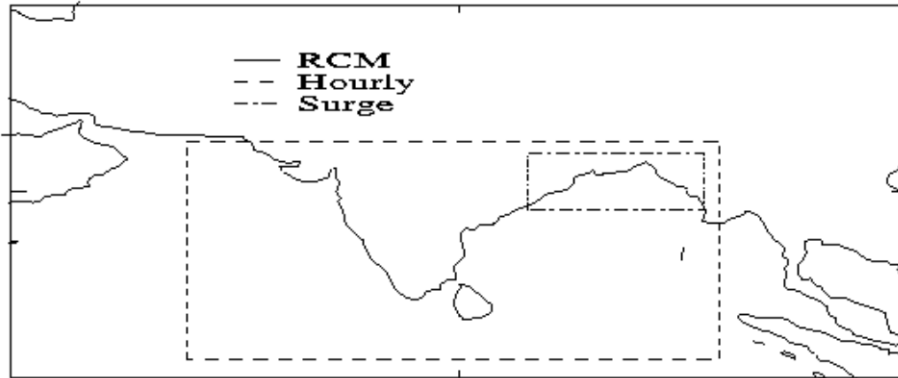


Figure 39 Model domains

The PRECIS model requires prescribed surface (over water only) and lateral boundary conditions. Surface conditions over land are calculated directly by PRECIS. Lateral boundary conditions provide dynamical atmospheric information at the latitudinal and longitudinal edges of the model domain. The boundary conditions in this study are sourced from global climate model experiments. We have also performed some experiments, not reported here, using boundary conditions from the ERA reanalysis product (a reanalysis of 1979-2001 global climatic data produced by the European Centre for Medium-Range Weather Forecasts).

The atmospheric component of the PRECIS model is a hydrostatic version of the full primitive equations, i.e. the atmosphere is assumed to be in a state of hydrostatic equilibrium and hence vertical motions are diagnosed separately from the equations of state. It has a complete representation of the Coriolis force and employs a regular latitude-longitude grid in the horizontal and a hybrid vertical coordinate. There are 19 vertical levels, the lowest at ~ 50m and the highest at 0.5 hPa with terrain following sigma coordinates (sigma = pressure/surface pressure) used for the bottom four levels, purely pressure coordinates for the top three levels and a combination in between. The model equations are solved in spherical

polar coordinates and the latitude-longitude grid is rotated so that the equator lies inside the region of interest in order to obtain quasi-uniform grid box area throughout the region. The horizontal resolution is 0.44×0.44 degrees, which gives a minimum resolution of $\sim 50\text{km}$ at the equator of the rotated grid. The model requires a time step of 5 minutes to maintain numerical stability. Physical parameterizations and numerical diffusion are represented by three dimensional source and sink vector functions of the prognostic variables. Horizontal diffusion is applied everywhere in order to represent unresolved sub-grid scale processes and to control the accumulation of noise and energy at the grid scale. A representation of the sulphur cycle is also modelled.

PRECIS has been run at the Hadley Centre and CEH for a number of 30-year ‘time slices’. These cover the near present day control (1961-1990) and future (2071-2100) for the IPCC Special Report on Emission Scenarios (SRES) A2 and B2 scenarios.

8.3 Regional model temperature and surface pressure results

The increase in regional mean atmospheric surface temperature between the first decade of the control and future SRES A2 simulation is 3.77°C over land (Figure 40). As expected, the land warms more than the sea, which is a consequence of the large thermal inertia of the ocean and differences in surface and atmospheric feedbacks over the ocean and land. This latter cause means that even in stabilisation simulations, the eventual warming is likely to exhibit a land/sea contrast. The regional mean surface warming in the SRES B2 scenario was 2.52°C

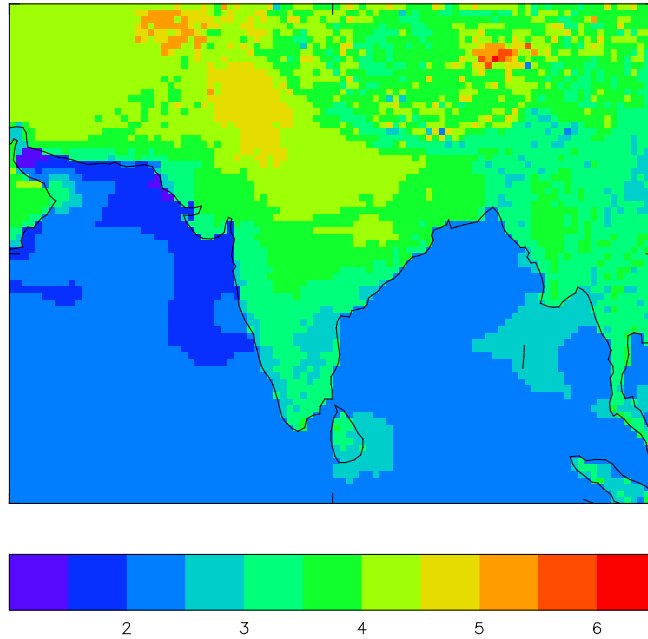


Figure 40 Temperature rise ($^{\circ}\text{C}$) between baseline and future simulation (SRES B2 Scenario)

The changes in surface and atmospheric temperature are likely to occur concomitantly with changes in surface pressure.

Figure 41 shows the pressure at mean sea level during the evolution and transit of a typical tropical cyclone in the control simulation. As the simulations progressed, the winds at 10m above the surface and the pressure at mean sea level were archived at the high temporal resolution needed to simulate storm surges. In total 240 Gb of data were archived during this study.

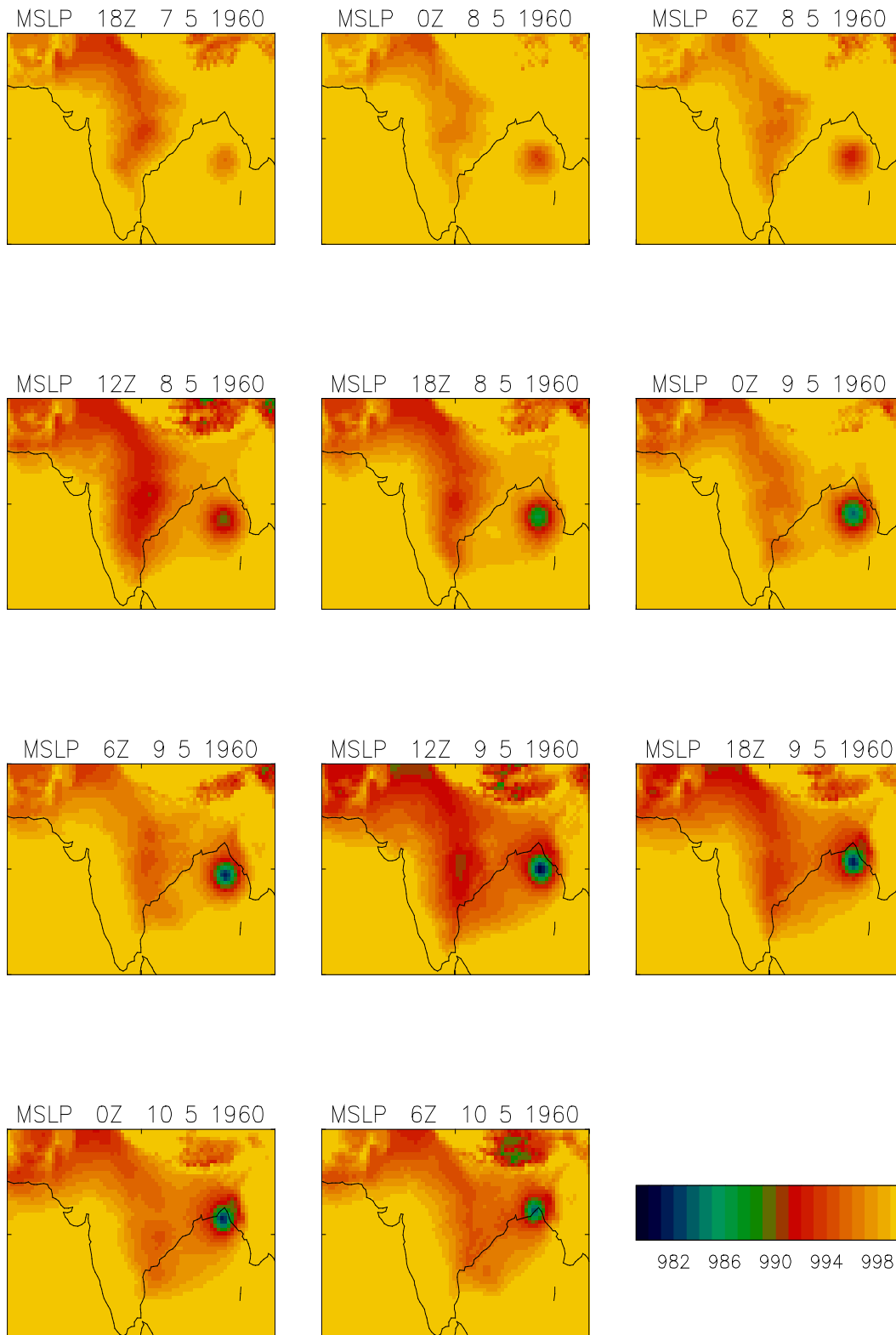


Figure 41 A typical RCM simulated cyclone in the new control simulation. Frames show the evolution at 6 hour intervals. Pressure at mean sea level is in mb

8.4 Representation of cyclones in the PRECIS climate model

Work in this area comprises two strands, an investigation into the ability of the regional climate model to represent the near surface wind and pressure field, and a comparison of cyclone tracks from the control and future experiments. The former is reported first.

Comparison of RCM and analytical cyclone results

A number of analytical cyclone models have been developed; we have selected two and fitted them to the regional model results.

Holland (1980) described an extension to the Schloemer (1954) model which has been widely adopted. Holland's model has two adjustable parameters and, in common with other parametric models, is associated with a description of the cyclone in terms of maximum wind speed, central pressure and the radius of maximum wind speed. In earlier surge modelling work, some authors have used the Holland model and related some of these parameters to each other using empirical formulae derived from historical data. One advantage of Holland's model is its popularity which will facilitate comparison of our data with the results of other workers.

The mean sea level pressure profile is given in the Holland model by:-

$$p = p_c + \Delta p \exp(-A/r^B)$$

where p_c is the central pressure, $\Delta p = (p_n - p_c)$, p_n being the ambient pressure, r is the radius and A and B are the tuneable parameters. The maximum tangential wind, w_m , can then be approximated by assuming that the cyclostrophic term dominates the strongest winds:

$$w_m = \left(\frac{B\Delta p}{2.72\rho} \right)^{\frac{1}{2}}$$

where ρ is the air density. The shape parameter B may be estimated by assuming a relationship between w_m and Δp of the form $w_m = K_p \Delta p^\beta$ and fitting a regression line to observed data. Jacobsen and Madsen (2004) present such a regression for cyclone data from the Bay of Bengal and so we have adopted their K_p and β to determine B . The scale parameter, A , can then be determined if the radius of maximum wind, r_m , is known. To complete our analytical model we impose a typical value of r_m for cyclones in the Bay of Bengal, 83 km, chosen following inspection of Joint Typhoon Warning Centre (JTWC) data for the region (http://metocph.nmci.navy.mil/jtwc/best_tracks/foindex.html). From the Holland model we can obtain geostrophic tangential winds.

For the input to the storm surge model, however, we require winds at 10m above the sea surface. In order to accommodate the boundary layer and estimate the radial wind we follow the more complex model of Jacobsen and Madsen (2004). Our 10 m tangential and radial winds are thus:

$$w_t = 0.8 \left\{ \left[\frac{AB\Delta p}{\rho r^B} \exp\left(\frac{-A}{r^B}\right) + \frac{r^2 f^2}{4} \right]^{\frac{1}{2}} - \frac{rf}{2} \right\}$$

and

$$w_r = w_t \left[\frac{B(BR^{-2B} + (1-3B)R^{-B} + B-1)k - 2k - 2Rc}{B(R^{-B} - 1) + 2 + 2fr/w_t} \right]$$

where $R = r/r_m$ and $c=0.013$. Δp and p_n are fitted to the RCM data: p_c is taken from the centre of the storm as diagnosed by the tracking algorithm and p_n is taken to be the mean of the pressure at 4 points located $5r_m$ North, South, East and West of the storm centre.

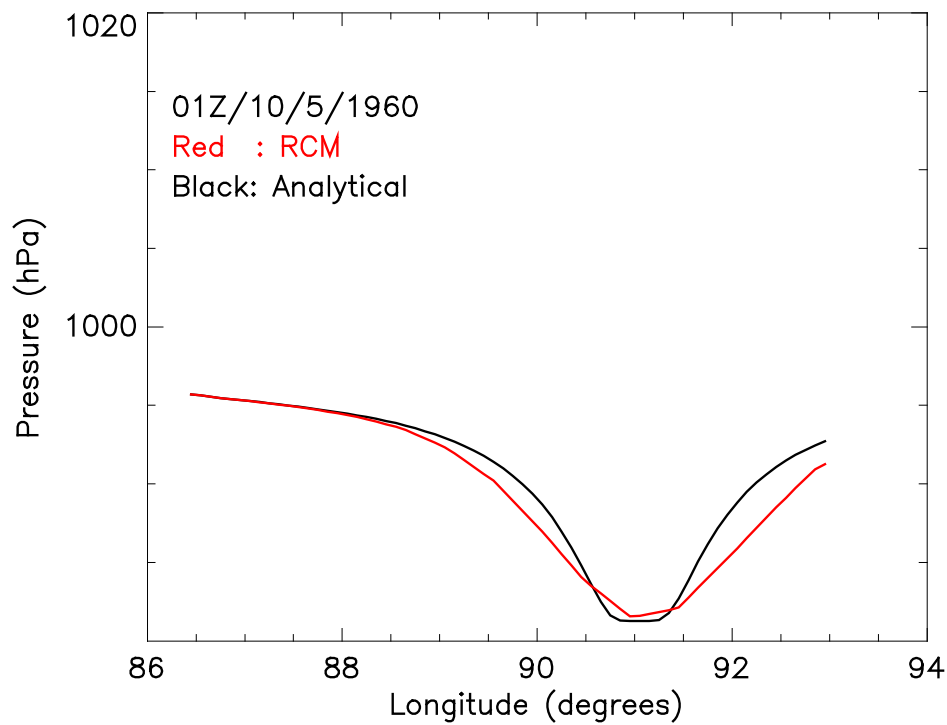


Figure 42 RCM simulated pressure and fitted Holland model along a line from the centre of the cyclone.

The wind field from the Holland model is shown in Figure 43 and shows remarkably good agreement between the RCM and the analytical model, considering that r_m in the analytical model is imposed rather than fitted to the RCM data although the eye is much more pronounced in the analytical model. Thus, we conclude that the large scale surface features of tropical cyclones in the Bay of Bengal are credibly represented in PRECIS.

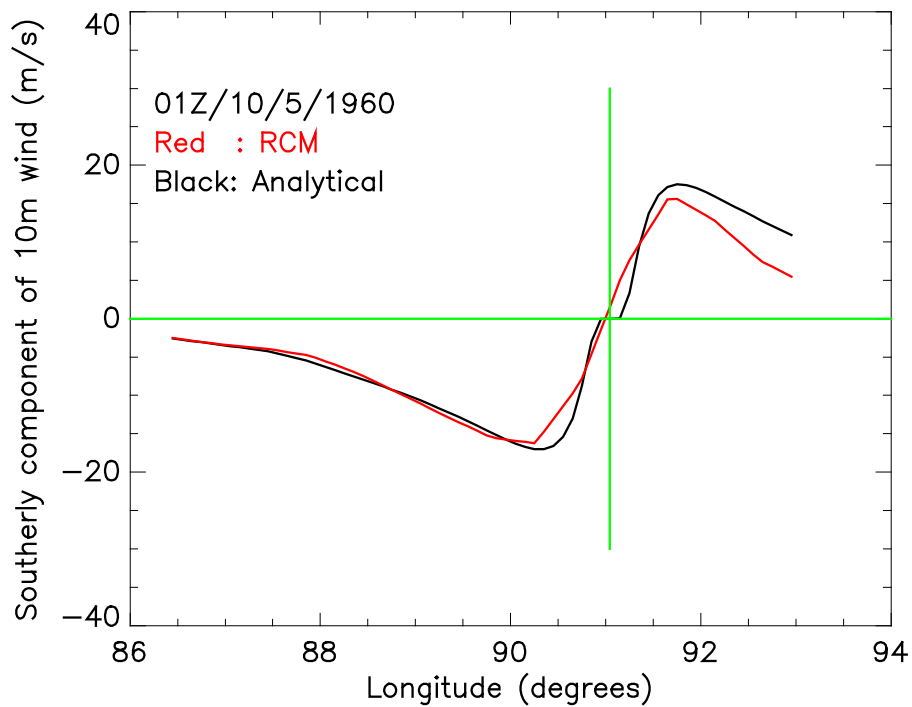


Figure 43 RCM simulated wind and fitted Holland model along a line from the centre of the cyclone.

Tropical Cyclone Storm Tracks – validation

The software package TRACK (Hodges, 1994), developed at the Centre for Global Atmospheric Modelling, was used to track minima in mean sea level pressure in the regional climate model output, which we take as indicating the location of the centre of each modelled tropical storm.

Figure 44 and Figure 45 show the locations of 30 years of diagnosed tracks from model baseline and A2 runs, respectively. Figure 46 shows 28 years of observed tracks taken from the Joint Typhoon Warning Centre (JTWC) database. The main purpose of the colour scheme is to distinguish between tracks: the first storm each year is shown in red, the second in green, the third in blue.

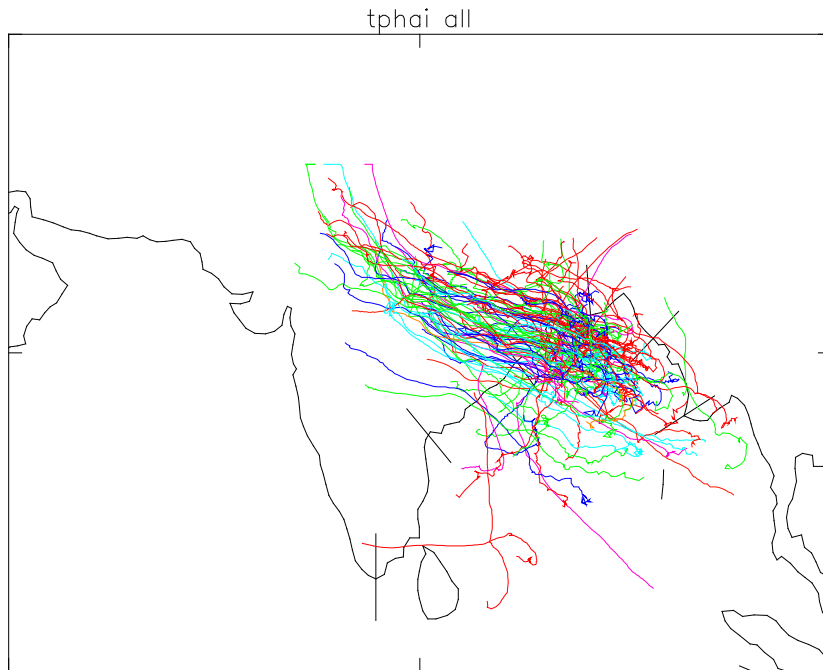


Figure 44: 30 years of modeled cyclone tracks from the Baseline run.

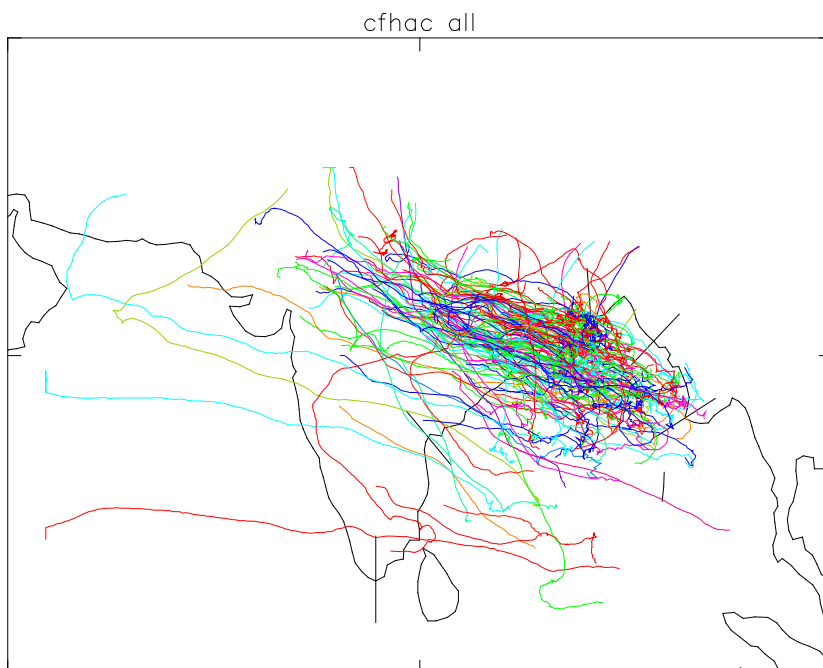


Figure 45: 30 years of modeled cyclone tracks from the A2 run.

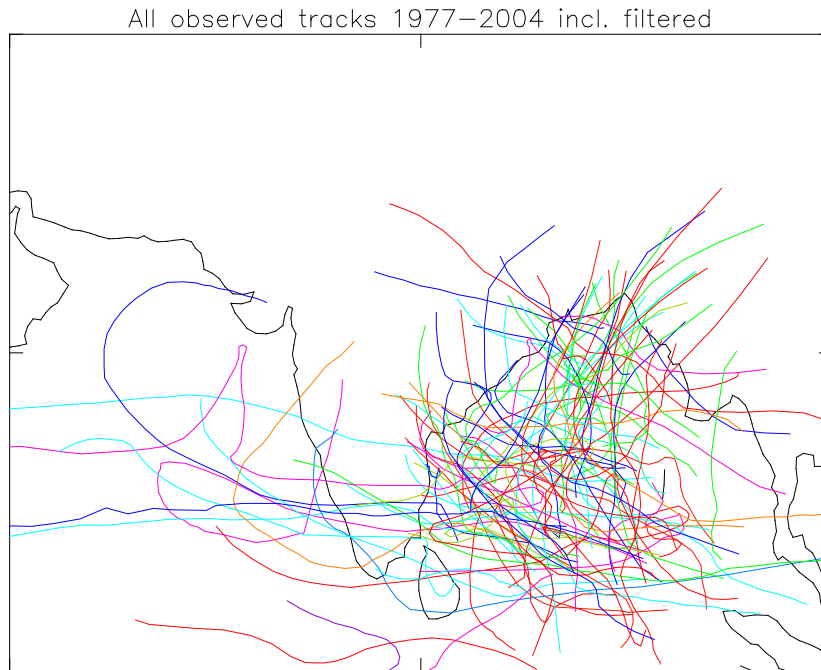


Figure 46: 28 years of observed cyclone tracks from the JTWC database

The depth of a minimum in MSLP relative to some representative average is known as the central pressure deficit. The largest value of this over the lifetime of a storm is the maximum central pressure deficit. In order to make meaningful comparisons with observations, we tuned our maximum central pressure deficit threshold to give the same mean number of storms per year in our baseline run as in the JTWC database of observations. This was necessary because the “cut off” value of maximum central pressure deficit was not clear for all of the observed storms.

To test the ability of the model to reproduce realistically the year-on-year variability in the number of storms we compared the variance of our 30 year baseline distribution with the 28 year observed distribution using an F-test. The difference was not statistically significant (68% probability that the two samples were drawn from populations with identical variances).

We then used a T-test to compare the mean number of storms in the A2 simulation with that of the baseline and found a statistically significant increase under the future climate (only 1.6% probability that the samples were drawn from populations with identical means). This is summarised in the Figure 47. We did a similar test on the B2 model results and found the smaller increase to be still significant (approx 6% probability that the samples come from the same distribution) over the baseline. However the mean number of storms in the A2 and B2

results were not statistically separable from each other by this test. Similar results were also found when non parametric tests were used on the data.

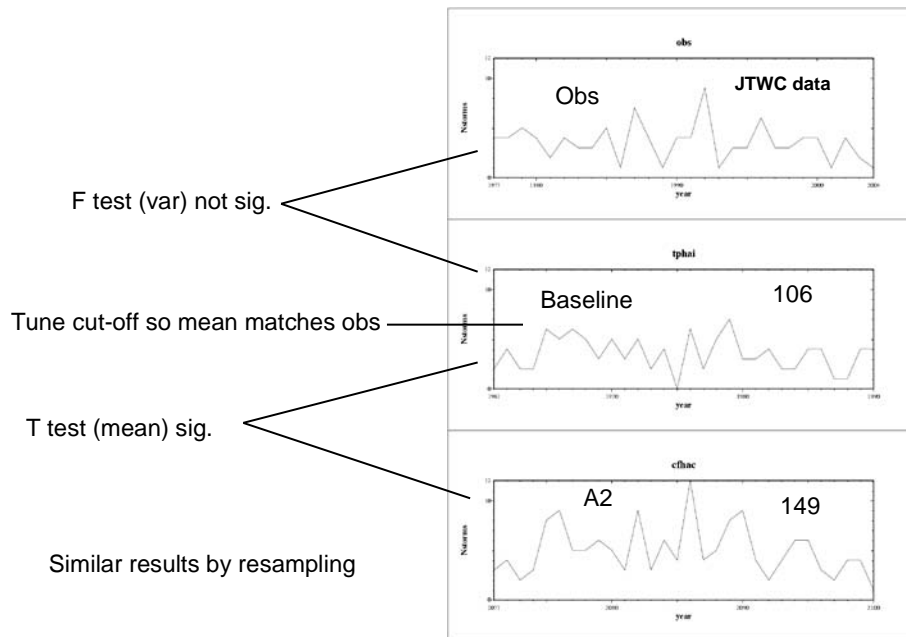


Figure 47: Summarising the results of significance testing on the number of storms per year.

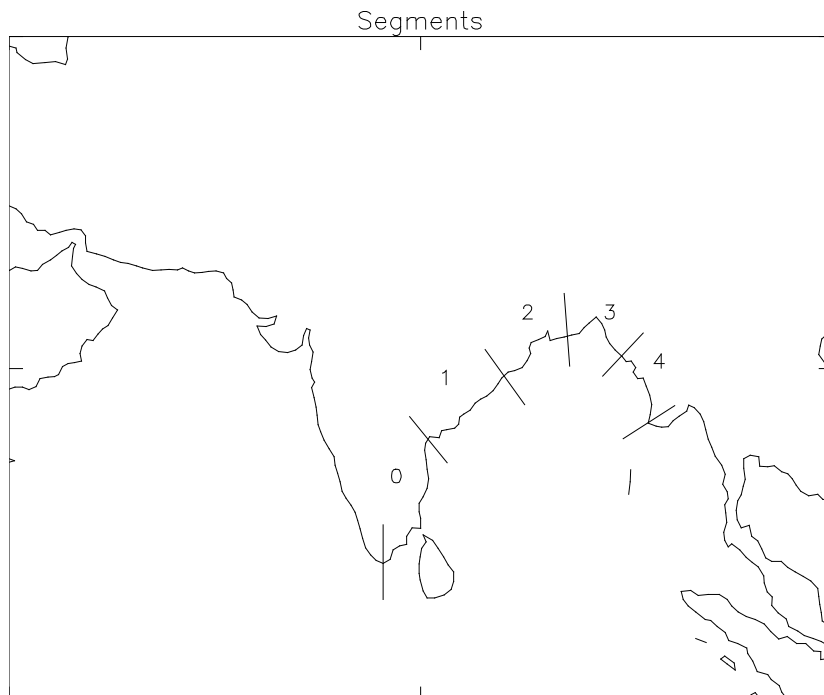


Figure 48: Division of the coastline into segments.

Next we examined the spatial distribution of the storm land fall points. First the coastline of the bay was divided into five segments (labelled 0,1,2,3,4 and shown in Figure 48) and significance tests performed on the mean number of storms per year crossing the coastline in each segment.

These results are shown in the two bar charts (Figure 49). It could be argued that this test was unnecessary in the case of baseline versus observations because the differences are so gross that they are immediately apparent from the track plots, but they are included here for completeness. The probability that model and observations agree are largest for segment 1 on the West of the bay. For all other segments it appears highly unlikely that the storm counts in the model and observations were drawn from identical populations. Thus, there are clear limitations on PRECIS’s ability to replicate the precise detail of storm tracks in this region. The reasons for this are the subject of further work.

While there are clear differences between the A2 scenario and the baseline, it is statistically quite difficult to isolate the spatial detail of the signal at the 90% level (right hand Figure).

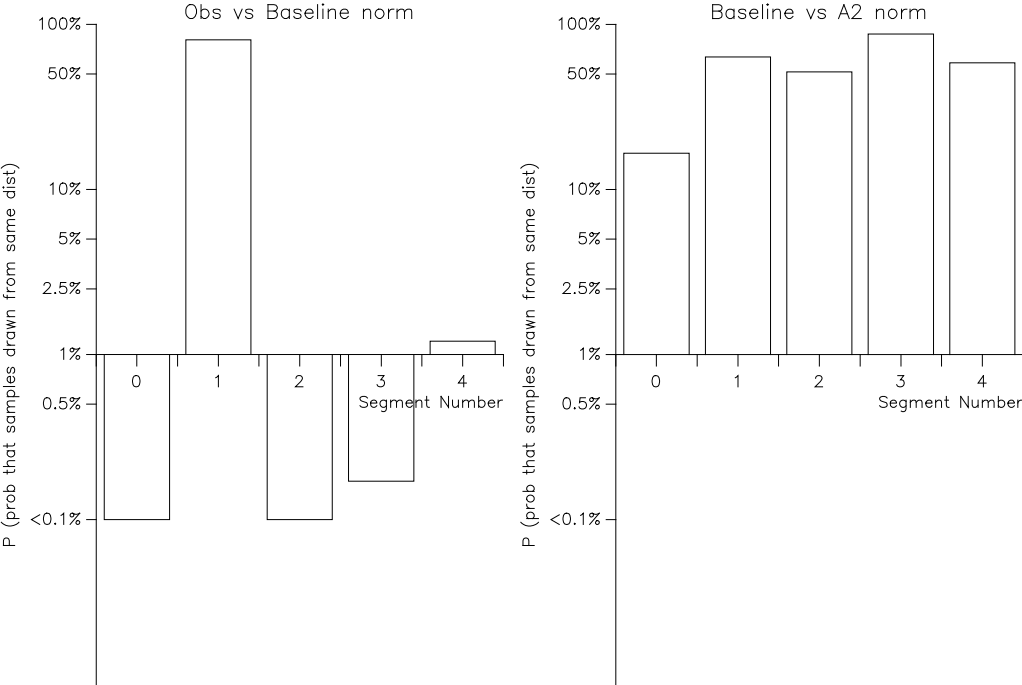


Figure 49: Significant model bias in the spatial distribution of storms (left) and no significant change in the normalized spatial distribution of storms under the changed climate (right)

In conclusion we note that in the baseline scenario we are able to reproduce some observed features of tropical cyclones but there is a bias in the coastal distribution of landfall. We also note that the spatial distribution of tracks and the accompanying track counts clearly show increases in the predicted number of storms under future emissions scenarios, SRES A2 and B2.

9 Extreme Water Level Modelling

A POL storm surge model of the northern Bay of Bengal has been set up and has been validated for tidal simulation and against idealised cyclones. The model is based on that of Flather (1994), which was used in a previous study of the devastating storm surge that struck Bangladesh in April 1991.

The depth mean storm surge model used in the current study remains similar to that of Flather (1994). The height of the water surface above mean sea level and the depth mean currents are determined using a continuity equation and a momentum conservation equation. The surface wind stress is parameterised as a quadratic of the 10-m horizontal wind speed. In order to include the change in roughness of the ocean surface as the wave height varies, the surface drag coefficient increases with wind speed as in the parameterisation of Smith and Banke (1975). The bottom stress is parameterised as a quadratic of the depth mean current. The surge model equations were solved using a finite difference method with a time step of 45 seconds on a regular latitude-longitude grid of approximately 10 km resolution. The region represented by the model was approximately 20°N to 23°N by 86°E to 93°E. Changes in sea surface elevation were applied at the open boundary to represent the effect of tides. At the coastal boundaries, the normal component of the depth mean current was set to zero. The meteorological forcing from the regional climate model was linearly interpolated in space onto the surge model grid and linearly interpolated in time at every surge model time step between the hourly results of the regional climate model. Two separate surge model runs were carried out for each climate scenario. The first run was driven by both tidal and meteorological forcings. The second run was driven by tidal forcing alone. Surge heights were determined by subtracting the tide only results from the tide plus meteorological forcing results. This approach made it possible to include non-linear interactions between the tide and surge components. Depth mean currents and surface elevations, relative to mean sea level, were output from the surge model as instantaneous values at hourly intervals.

The model was modified to use high resolution (200-600m) bathymetry (supplied by IWM Bangladesh). The fine resolution bathymetry can be used to improve the representation of sub-grid scale channel features in the 10 km resolution model. Although the channels in the delta are now better represented in the model physics, considerable tuning is required to correctly parameterise the effective lateral friction of the channels, and this was not part of the scope of this program. The effect of having large channels in the current study is mainly to reduce the potential height of positive surges along the coast line by providing an additional

reservoir for coastal water. However, the channel treatment is too simplistic for the simulated surge heights within any particular channel to be considered realistic. It is for this reason that the locations chosen for the pixels in sections 9.1 and 9.2 are all on the 'open sea' coastline of the model, and not on channels.

At POL and the Hadley Centre, software was developed to match driving data from the regional climate model automatically to the surge model and to facilitate automatic 30-year consecutive runs of the surge model.

Analysis software has been developed to extract the upper extreme percentiles of total water level and surge residual. These are shown in section 9.1 for the different time slices. At point locations, annual maxima have been fitted to a Gumbel extreme value distribution. This enables the extreme water level results to be extrapolated to longer return periods. The results of this are shown in section 9.2.

In addition to the changes in extreme water level caused by the changes in storminess, local relative sea level will also be affected by changes in the time average sea level and by vertical land movement. Estimates of the time average sea level change can be taken from the Third Assessment Report of the Intergovernmental Panel on Climate Change (Church, 2001), the key result of which is reproduced in Figure 50 for ease of reference. Vertical land movement estimates, obtained from observations, can be found in Warwick (1993).

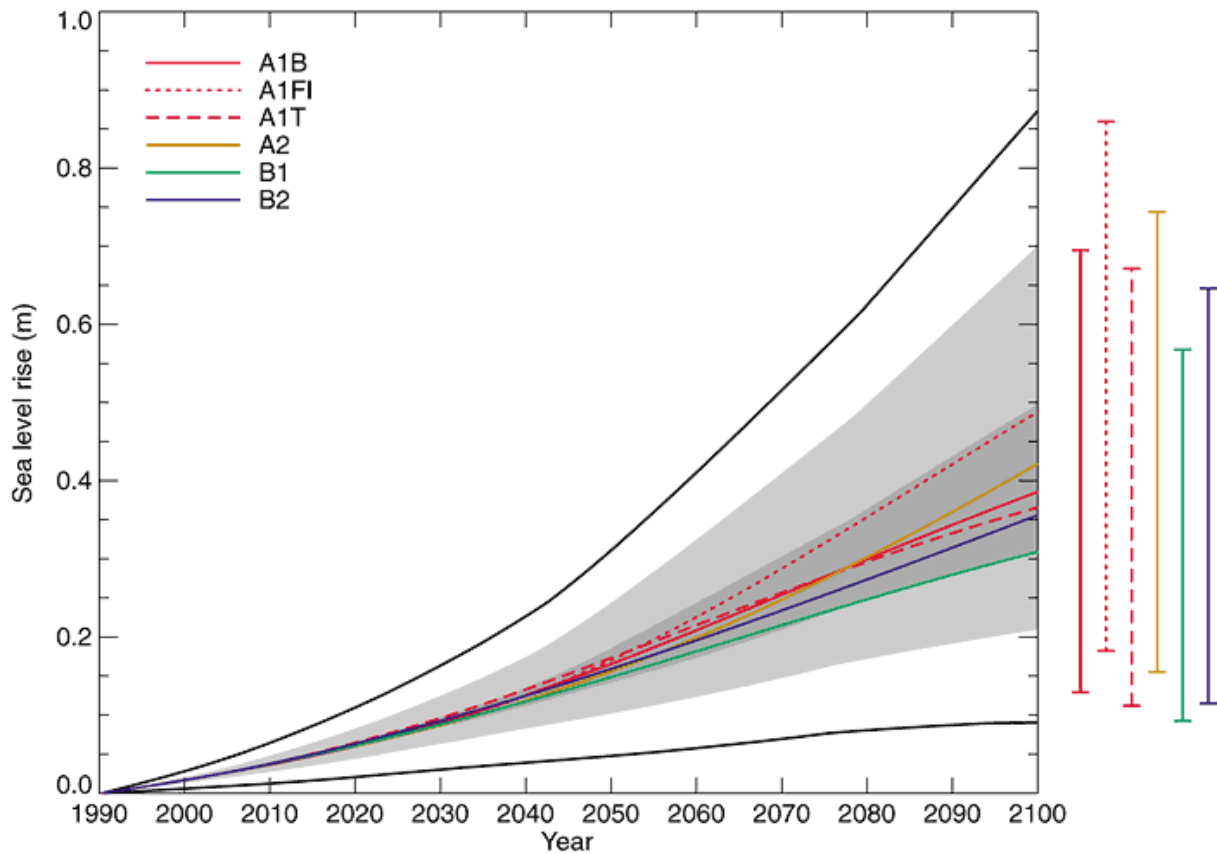


Figure 50: Global average sea level rise 1990 to 2100 for the SRES scenarios.
 (Reproduced from IPCC TAR Figure 11.12; see there for full details.)

9.1 Regional Distribution of Rxtreme Water Levels

In a given 30 years time slice there are 259,200 hours (owing to the use of a 360 day year in the climate model). Results from the surge model were stored at each hour and at each point in the surge domain from which the 99th, 99.9th and 99.99th percentile level were determined. No attempt was made to correct for a lack of independence between adjacent ranked hourly results, which since the extremes are driven by atmospheric effects that persist for more than one hour, may sometimes be driven by the same storm. Spatial distributions of the percentiles are shown in Figure 51. This was repeated for the residual; the results of this are shown in Figure 52.

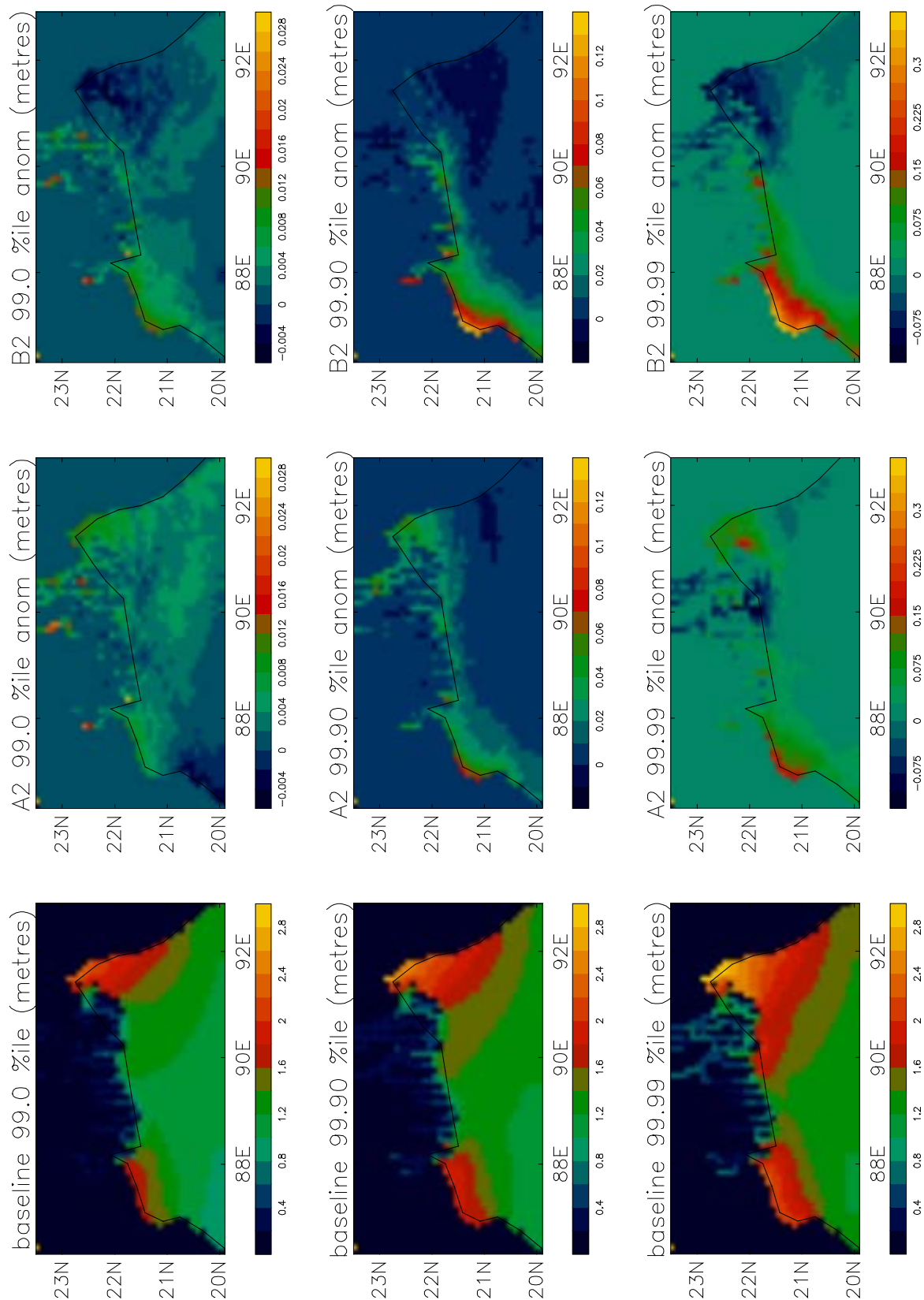


Figure 51: Percentiles of extreme water levels in the surge domain, showing values from the baseline time slice and changes arising under the two different future scenarios.

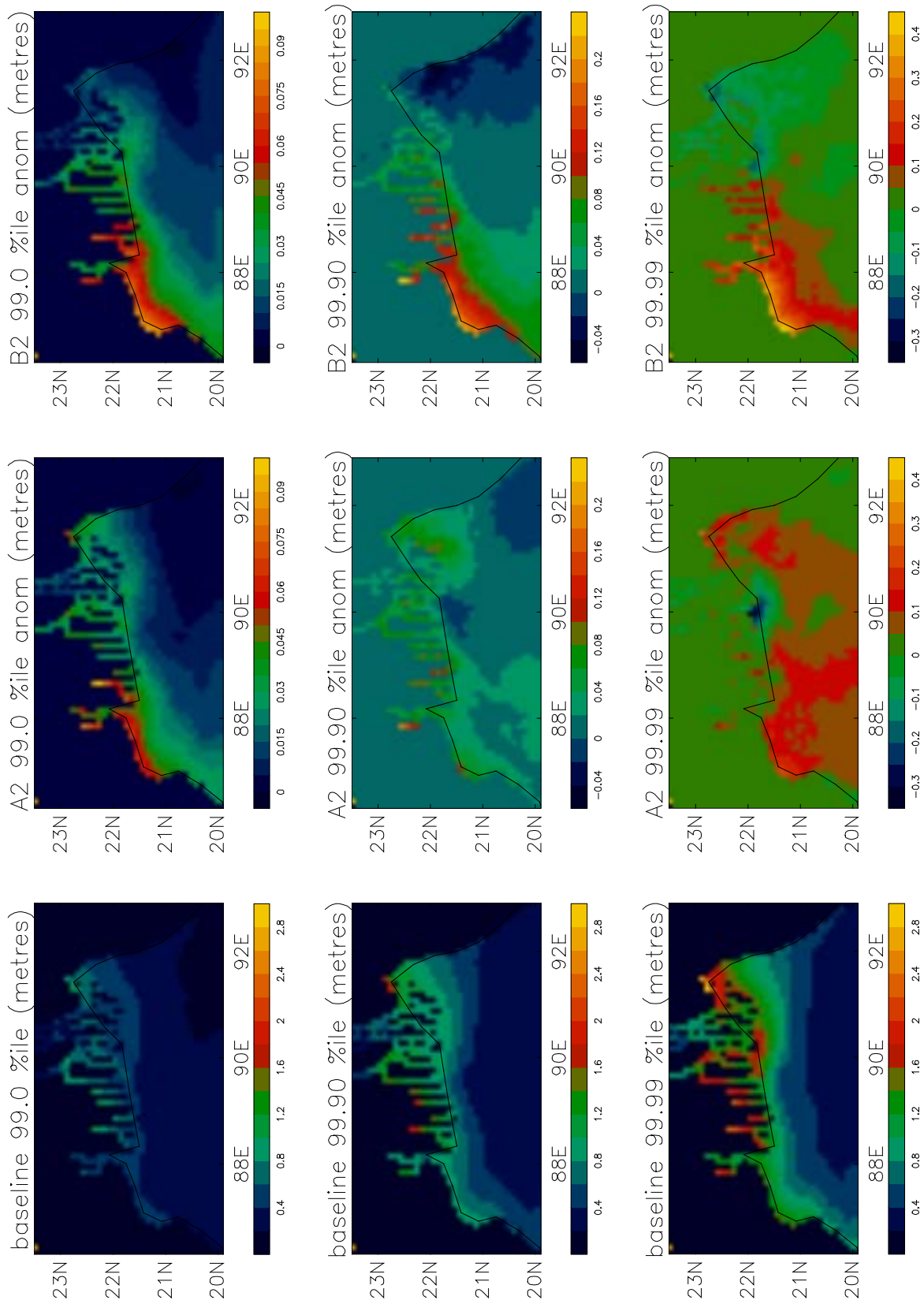


Figure 52: As fig 30 but for residual elevation (i.e. after removal of the tide component).

In general, extreme percentiles of water level and surge residual increase under either of the future scenarios, except in parts of the east of the bay where they decrease under the B2 scenario. Furthermore, although concentrations of greenhouse gases are smaller in the B2 scenario, extreme values in the west of the bay are larger.

The model seems to be suggesting that the regional response does not scale linearly with regional temperature rise, perhaps indicating a dominant role of natural variability. To investigate this we plotted anomalies in mean sea level pressure for each season between the B2 run and the pressure which would be obtained by interpolation between the baseline and A2, taking the mean temperature at 1.5 metres (averaged over the sea and the full 30 years time slice in the regional climate model domain) as the independent variable with which to make the interpolation. For comparison the change in seasonal mean sea level pressure under the two future scenarios compared to the baseline simulation is shown in Figure 53 and Figure 54. This scaling result is shown in Figure 55 and does indeed show some nonlinearity in the scaling of regional surface pressure response, which is likely to affect the surface results.

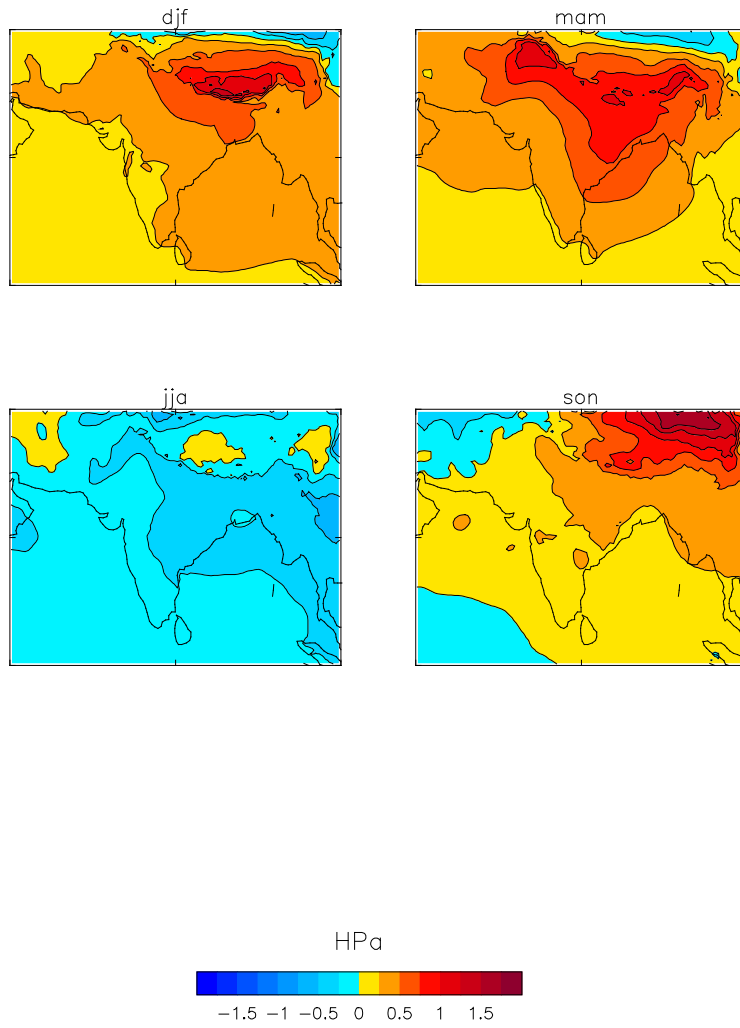
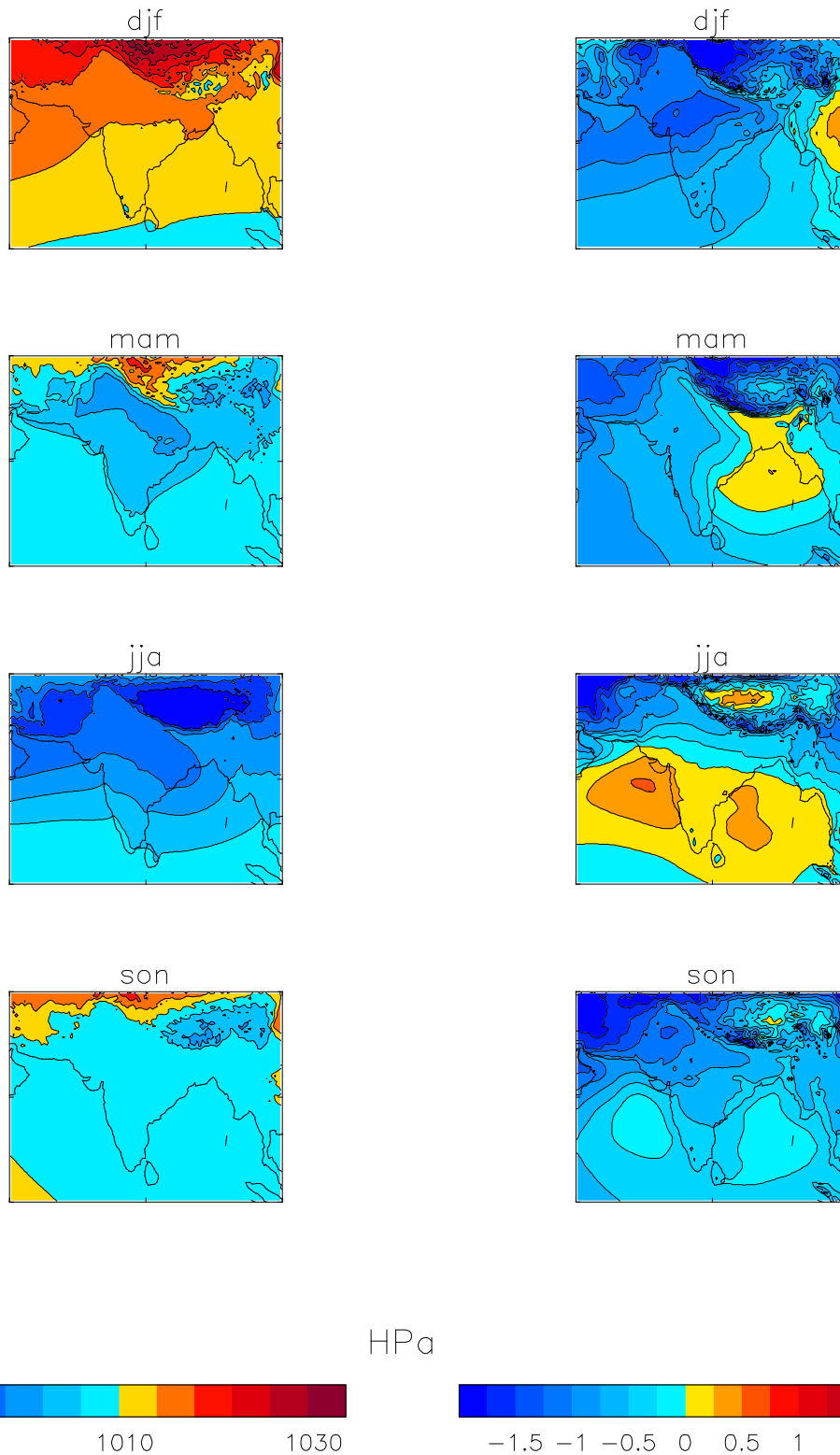
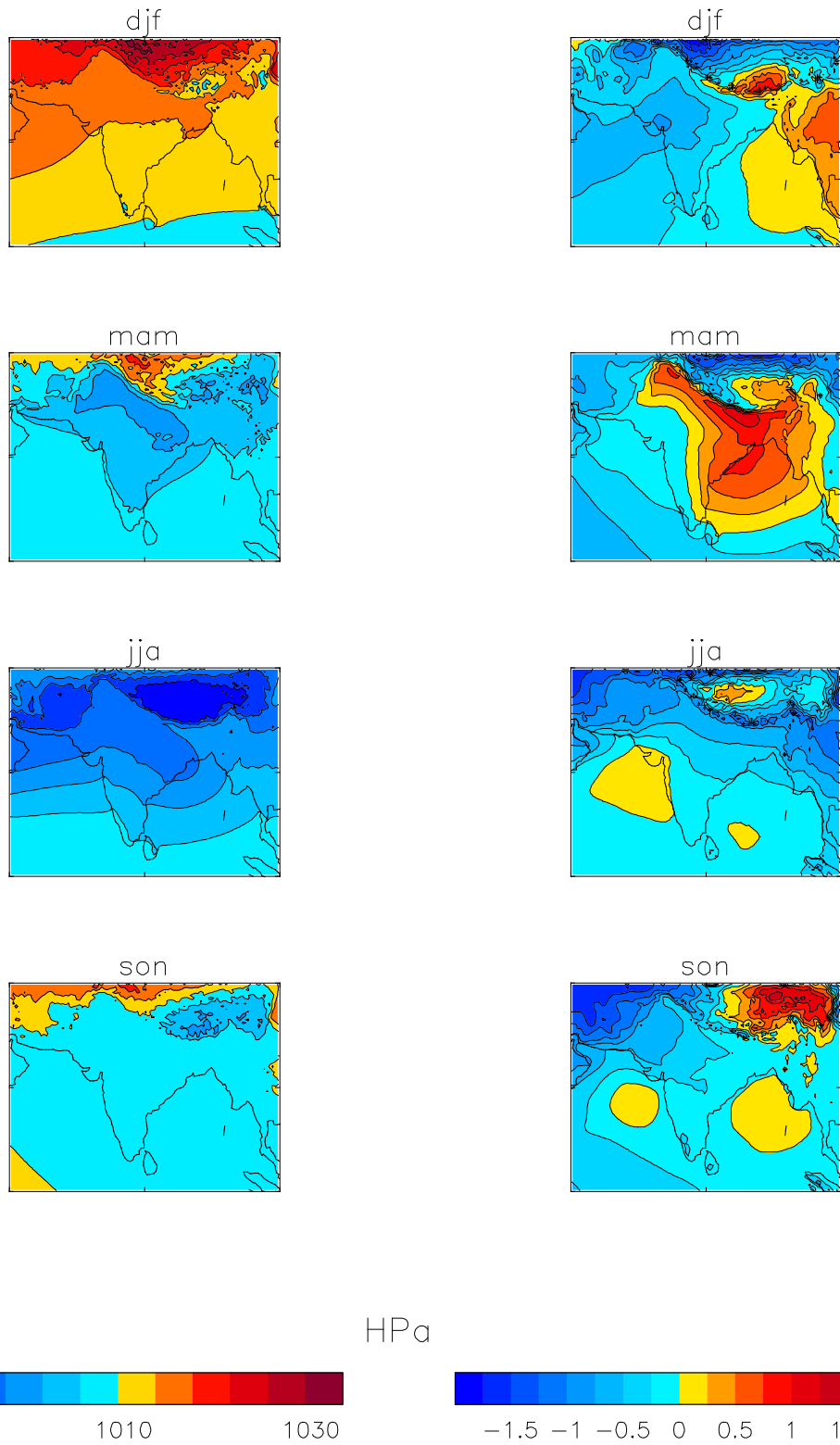


Figure 53: MSLP anomaly by season between B2 model run and an “idealised B2” derived from linearly interpolated MSLP changes between the baseline and A2 run, taking the mean 1.5 metre temperature over the sea as the independent variable.



30 year seasonal mean PMSL (Control 1, left)
and increase in PMSL (from Control 1 to A2, right)

Figure 54: Modelled Baseline MSLP and changes in MSPL under the A2 scenario



30 year seasonal mean PMSL (Control 1, left)
and increase in PMSL (from Control 1 to B2, right)

Figure 55: Modelled Baseline MSLP and changes in MSPL under the B2 scenario.

9.2 Local Analysis of Extreme Water Levels

We selected model pixels around the bay and, for each one, analysed the percentiles and the highest modelled water levels per year. For reference, we gave the name of a nearby place to each pixel we considered. The place names, and the corresponding pixel centres, are:

Baleshwar	87.05E	21.45N
Cox's Bazaar	91.85E	21.65N
Chittagong	91.75E	22.35N
Noakhali	91.05E	22.55N

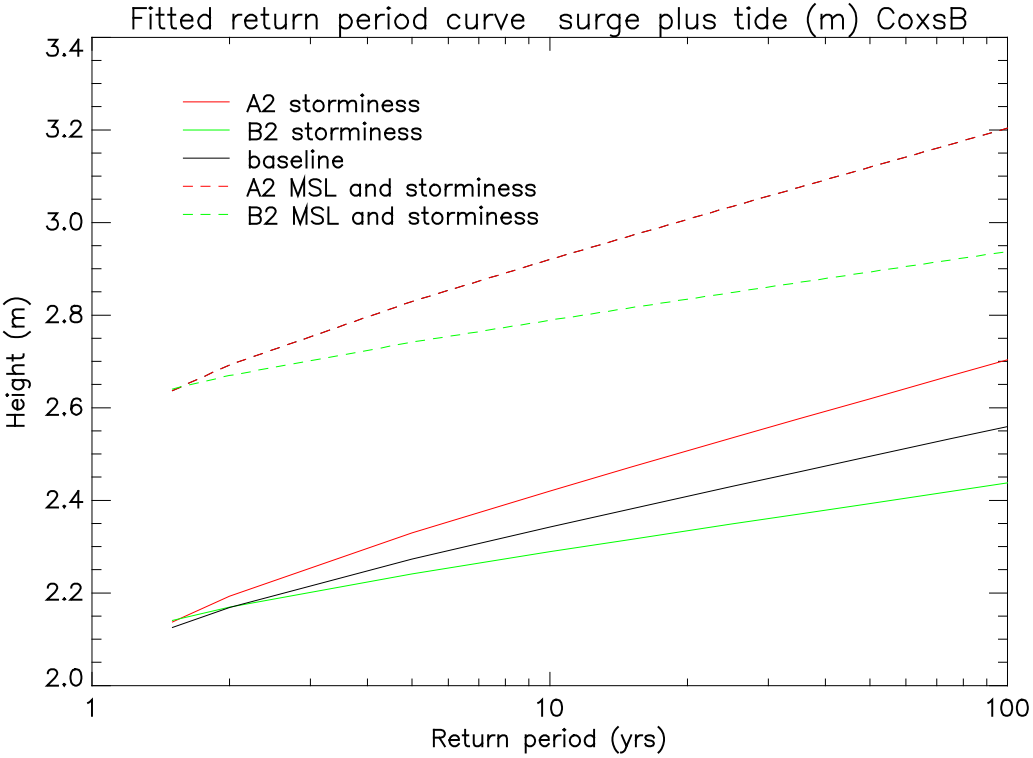
We consider first the extreme percentiles at these locations. Figure 57 shows all the percentiles above the 99th, ranked for A2 and B2 scenarios. These confirm the results seen in the patterns for the 99th, 99.9th and 99.99th percentiles and discussed in section 9.1. At the locations on the East of the bay the A2 signal is greatest. However, on the West of the bay B2 is larger.

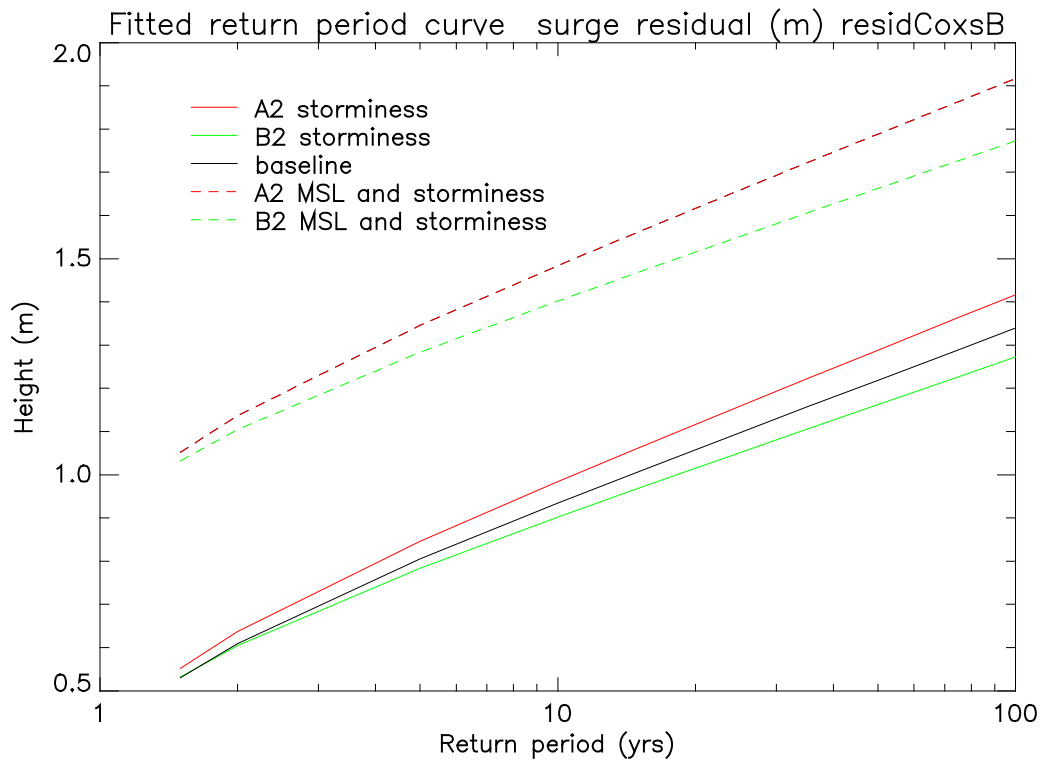
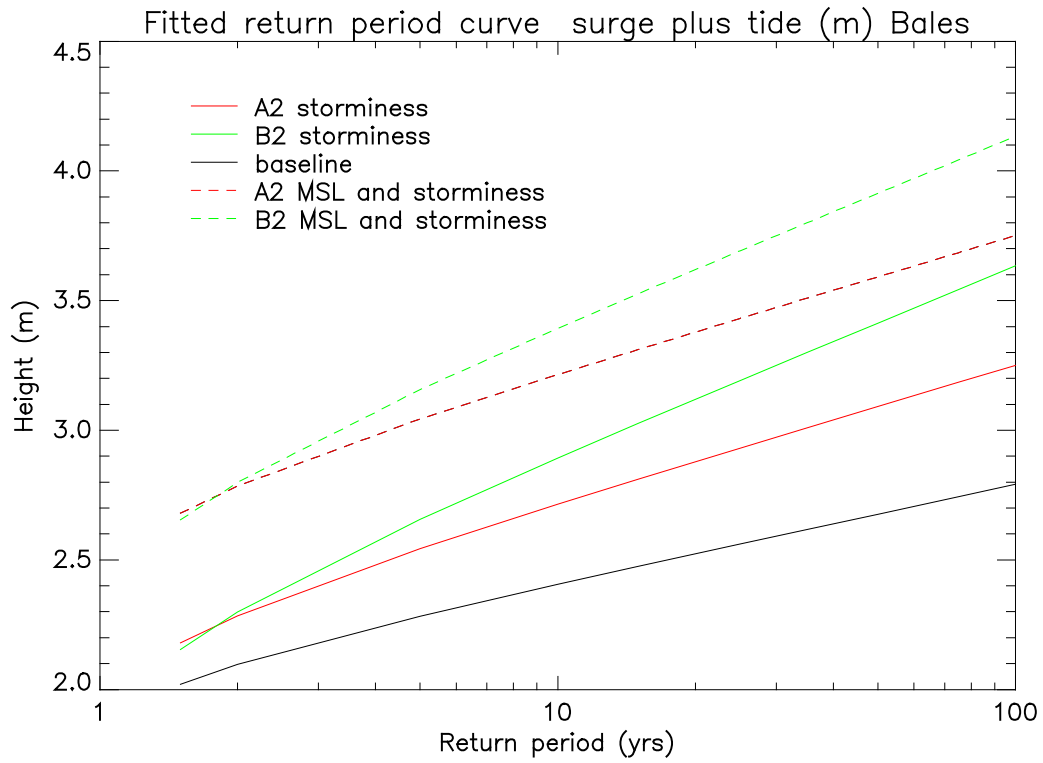
Next we analysed in detail the annual average maximum water level (surge plus tide relative to mean sea level) and surge residual (relative to mean sea level). For the surge plus tide results on the East of the Bay at Cox's Bazaar the most extreme water levels are higher in the A2 simulation than in the baseline simulation. Conversely, in B2 they are lower than in present day. Without a change in mean sea level being added neither future water level result is separable from the baseline at the 90% level (using a t-test) and they are not separable from each other. However, adding in a change in mean sea level of 50cm does make the future periods separable from the baseline. We draw a similar conclusion from the surge residuals, but the significance levels of the t-test are lower. So, it appears that the change in storminess (as manifested in the change seen in local water levels) is too small at this site to be isolated from the variability using this technique and experimental design.

On the West of the Bay, at Baleshwar, there is a significant signal in water levels, with both A2 and B2 results separable from baseline at a 90% significance level using a t-test. However they are not separable from each other. Both A2 and B2 extremes are greater than the baseline extremes (the sign of the change is similar on this side of the bay). But, the magnitude of the B2 change is greater than for A2. Since they are not separable this may again indicate a

sizeable part of the change is due to natural variability. The A2 and B2 signals are more difficult to separate from the baseline in the residual although they are still significant at a 90% level.

The final part of our analysis involved fitting Gumbel distributions to the annual maximum water levels and residuals and examining the change in return period of particular events between the baseline and future simulations (Figure 56). Clearly the largest changes in extreme water levels is due to the rise in time mean sea level. However, the storminess changes on the west of the bay can alter the return period of surge residuals by more than a factor of two. Thus future work should focus on better understanding of the driving storms and there changes in RCMs and characterising the uncertainty in mean sea level. Improvements in the baseline (present day) return period curves using higher resolution surge models may also be useful.





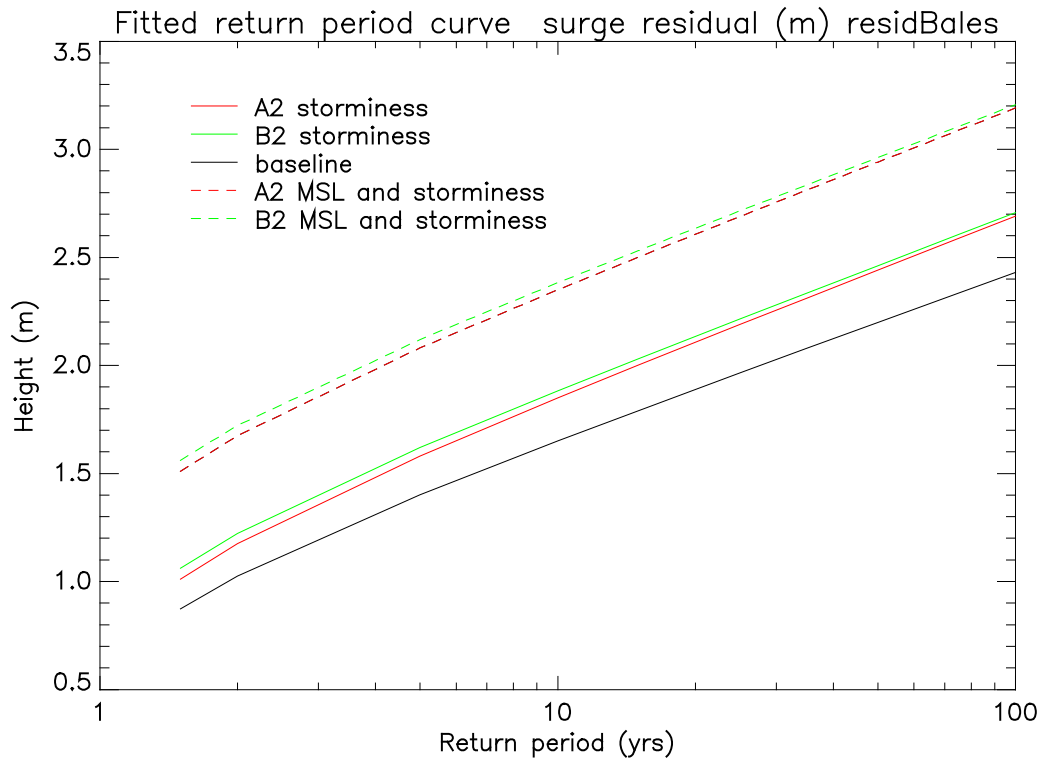


Figure 56 Return period curves for baseline and future changes under A2 and B2 scenarios for changes in storminess alone, and changes in time average sea level (neglecting non linear depth effects of mean sea level on surges). Panel 1 is for Cox's Bazar surge plus tide results. Panel 2 is for Baleswar surge plus tide result. Panel 3 and 4 are as panels 1 and 2 but for surge residuals only.

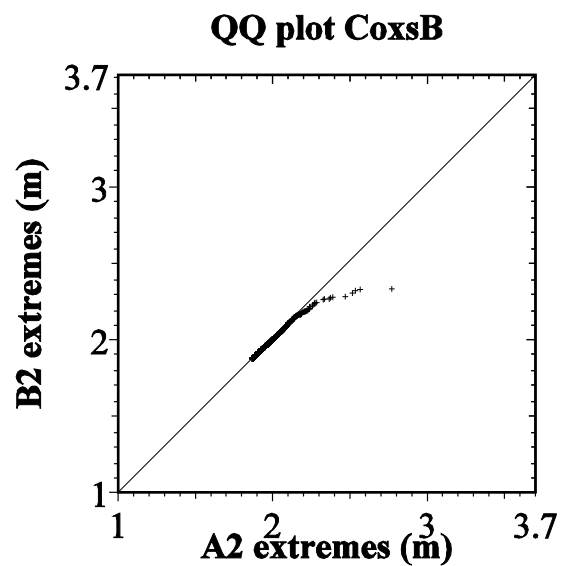
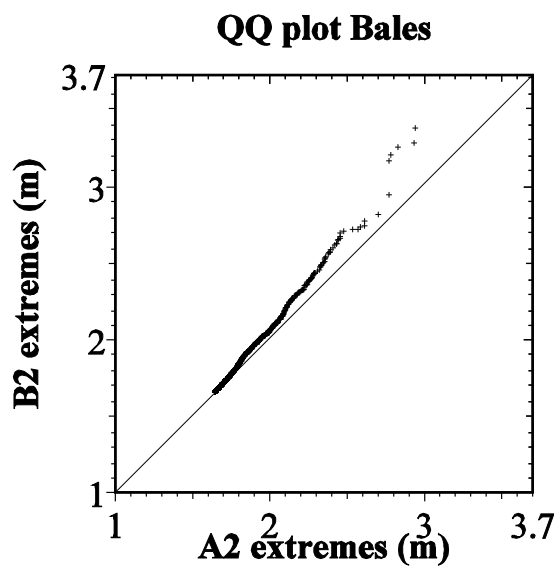
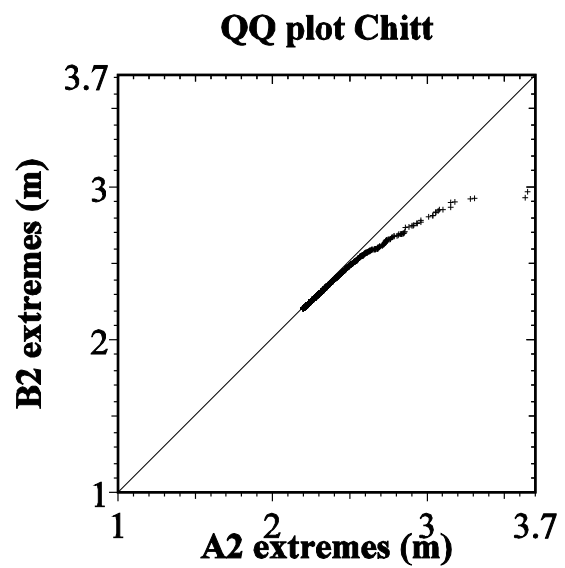
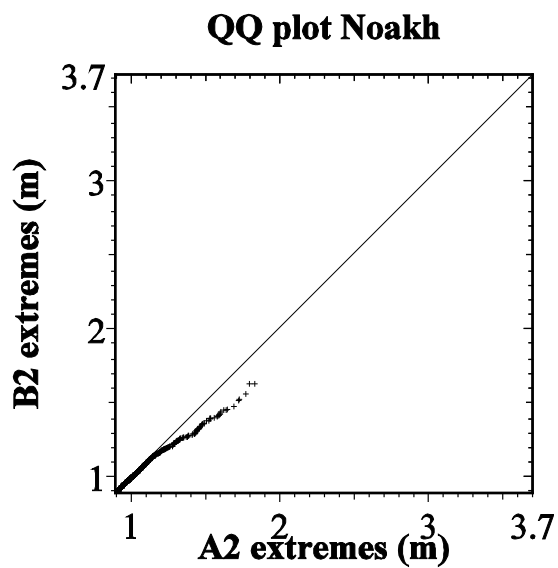


Figure 57: Quantile-Quantile plots for four of the pixels described in Section 9.2. Only extreme water levels above the 99 percentile are shown. Notice that in three cases the extreme water levels are larger under the A2 scenario, as expected, but that at Baleshwar in the west of the bay, the opposite is true.

9.3 Discussion

10 Conclusions

It was clear from the launch workshop in Dhaka on 30th January 2003 that there is a real need for the outputs of the CLASIC project. The fact that the meeting was so well attended, and that so much enthusiasm was evident during the meeting, indicates that there is a general awareness of the issues, and interest in having access to tools to begin to address these problems. It was unfortunate that the project did not in fact start until some 8 months later once the contract was signed. The delay was caused by a number of reasons, and has led to problems throughout, since we tried to compress the original three year project duration into a little over two years, with a planned end date of the end of September 2005.

It has not been possible to meet this shortened deadline, partly because collecting the necessary local data and setting up models has taken longer than anticipated. However, the real delay to the project has been caused by the delays in obtaining the necessary regional climate change data from those groups throughout the region who should have been generating scenario data using the PRECIS model. Because of the very slow take-up of this model by regional partners, we have now had to start a number of model runs here in the UK. Whilst it might have been sensible for us to have taken up this option earlier, we were prevented from doing so by apparent agreements between Defra, DFID, and the Hadley Centre that restricted use of the PRECIS model to groups in developing countries. It took considerable time and negotiation to overcome this obstacle, such that we could only initiate runs in the UK in late October, a month after the official end of the project.

Throughout the project, there has been very positive collaboration between the UK team and partners in Bangladesh, who have helped enormously during the project. We are confident that the models that will be handed over to the local partners at the end of the project will be used effectively over the coming years. The fact that we have managed to involve the Water Resources Planning Organisation in the study is a real bonus, and ensures that outputs will be made available through appropriate Government of Bangladesh agencies. It is to be hoped that the partnerships forged during the project can be maintained after the current KaR funding ceases, and we must endeavour to find supplementary funding over the next two years to ensure effective take-up of the project outputs and ‘products’ (the GWAVA model and the storm surge model). For the project to be fully effective, such continued support to the Bangladeshi partners will be important over the next two years, to provide the support that they need to be able to extend the scope of work initiated during the project.

Whilst recognising that the DFID KaR programme ends on 31st March 2006, we hope that there can be as much leeway as possible within this financial year to enable us to deliver the planned outputs.

11 Dissemination of Results

Results of the project will be presented to an audience in late January or early February in Dhaka. We are planning to invite 150 people representing stakeholders from various sectors, public representatives, research organizations, NGOs and development partners. It will include all of the 67 delegates from 41 organizations who attended the Launch Workshop on the 30th January 2003 at BUET, Dhaka. It will be a two day programme. There will be a workshop on the first day where project approach and results will be presented to all invitees. A meeting of water resources and disaster managers will be organized on the second day. This will be attended by a selected audience of about 30. The purpose is to discuss what needs to be done and to frame recommendations in the light of project results and comments and suggestions received in the workshop. A tentative programme of workshop and meeting is given in Appendix B.

12 References

Adam, J., Clark, E.A. and Lettermaier, D. P., 2006, "Correction of Global Precipitation Products for Orographic Effects", *Journal of Climate*, 19, pp. 15-38.

Ahmed, M. F. and Rahman, M.M., (2000). "Water supply & sanitation, Rural and low income urban communities", ITN-Bangladesh, Centre for Water Supply and Waste Management, BUET, Dhaka, Bangladesh.

Bangladesh Agricultural Development Board (BADC), 2003. "Survey report on irrigation equipment and irrigated area in Boro/2003 season", Survey and Monitoring Project for Development of Minor Irrigation. Bangladesh Agricultural Development Board.

Bangladesh Bureau of Statistics (BBS), 1998. "Agricultural Statistical Year Book of Bangladesh - 1998", Bangladesh Bureau of Statistics.

Bell, V.A. and Moore, R.J., 1999, "An elevation-dependent snowmelt model for upland Britain", *Hydrological Processes*, 12, pp. 1887-1903, 1999.

Calder, I.R. 1990. "Evaporation in uplands". Wiley, Chichester.

Center for International Earth Science Information Network (CIESIN), Columbia University; International Food Policy Research Institute (IFPRI); and World Resources Institute (WRI). 2000. "Gridded Population of the World (GPW), Version 2". Palisades, NY: CIESIN, Columbia University. Available at <http://sedac.ciesin.columbia.edu/plue/gpw>.

Church, J.A. et al., 2001. In "Climate Change 2001: The Scientific Basis. Contribution of Working Group 1 to the Third Assessment Report of the Intergovernmental Panel on Climate Change", J. T. Houghton et al., Eds. (Cambridge Univ. Press, Cambridge, 2001), pp. 639-694

Department of Public Health Engineering (DPHE), 1998. "Data book 1998, Urban water supply system", Department of Public Health Engineering, Bangladesh.

Department of Public Health Engineering (DPHE), 2002. “Year book 2000-2001, Rural water supply”, Department of Public Health Engineering, Bangladesh.

Directorate of Economics and Statistics (DES), 2004. “Agricultural Statistics at a Glance”, Government of India, New Delhi

Döll, P. and Lehner, B., 2001. ”Validation of a new global 30-minute drainage direction map”, *Journal of Hydrology*, submitted March 2001.

Environmental Systems Research Institute (ESRI), 1993. *Digital Chart of the World – Data Dictionary*, November.

Food and Agriculture Organization (FAO), 1997. *Digital Soil Map of the World and Derived Soil Properties., Version 3.5 November 1995*, FAO Land and Water Digital Material Series 1 (CD-ROM). Derived from the FAO/UNESCO 1:5 000 000 Soil Map of the World.

FAO, 2001. *Rural population in South Asia*, First edition., GeoNetwork, 1 May 2001. Available at <http://www.fao.org/geonetwork/>.

FAO, 2005. FAOSTAT data.

FAO, 2005(a). *Irrigation Cropping Calendar, Review of global agricultural water use per country*, AQUASTAT, Land and Water Development Division. Available at http://www.fao.org/ag/agl/aglw/aquastat/water_use/index4.stm.

FAO, 2005(b)., *AQUASTAT Online Database*, Land and Water Development Division. Available at http://www.fao.org/ag/agl/aglw/aquastat/water_use/index4.stm

Flather, R. A., 1994. “A storm surge prediction model for the northern Bay of Bengal with application to the cyclone disaster in April 1991”. *Journal of Physical Oceanography*, **24**, 172-190.

Flood Plan Coordination Organization (FPCO), 1993. “Final report on Geographic Information System”, ISPAN, Ministry of Irrigation, Water Development and Flood Control, Bangladesh.

Gaffin, S. R., Rosenzweig, C., Xing, X. and Yetman G., 2004. “Downscaling and geo-spatial gridding of socio-economic projections from the IPCC Special Report on Emissions Scenarios (SRES)”, *Global Environmental Change*, **14**, pp.105-123.

Hassel, D. and Jones, R.G., 1999. “Simulating climatic change of the southern Asian monsoon using a nested regional climate model (HadRM2)”. HCTN 8. Hadley Centre for Climate Prediction and Research, Bracknell, UK.

Hodges, K.I., 1994. “A general method for tracking analysis and its application to meteorological data”. *Monthly Weather Review* 122: 2573–2586.

Holland, G.J., 1980. “An analytic model of the wind and pressure profiles in hurricanes”. *Monthly Weather Rev.*, 108:1212-1218.

Houghton, J.T., 1997. “Global warming: the complete briefing”. 2nd edition. Cambridge University Press. ISBN 05216208991997.

Houghton, J.T., 2004. “Global warming: the complete briefing”. 3rd edition, Cambridge, Cambridge University Press. ISBN 0521528747.

IPCC. 2006. SRES scenario runs included in the IPCC-DCC, SRES-TAR GCM data from www.mad.zmaw.de/IPCC_DDC/html/SRES_TAR/index.html

Jakobsen, F. and Madsen, H., 2004. “Comparison and further development of parametric tropical cyclone models for storm surge modelling”. *J. Wind Engineering Industrial Aerodynamics*, 92:375-391.

Lerner, J., E. Matthews, and I. Fung. “Methane Emission from Animals: A Global High Resolution Database. Camel, caribou, dairy and non-dairy cow, goat, horse, pig, sheep, and water buffalo densities; and total methane emissions”. Digital raster data on a 1-degree grid (180x360 cells). Eleven independent single-attribute spatial layers. 2,869,843 bytes in 25 files. [incorporates original data published in 1988 by NASA Goddard Space Flight Center]

Liu, C. and Ding, L., 1986. “The Newly Progress of Glacier Inventory in Tianshan Mountains”. *Journal of Glaciology and Geocryology* 8(2): 168-169.

Lowe, J.A., and Gregory, J.M., 2002. “Simulating tropical cyclones and storm surges in the Northern Bay of Bengal: The effect of increased concentrations of atmospheric greenhouse gases”. A Hadley Centre report to DEFRA. Hadley Centre.

Master Plan Organization (MPO), 1987. “Irrigation water requirements”, MPO Technical Report 2, Ministry of Irrigation, Water Development and Flood Control, Bangladesh.

Meigh, J.R., McKenzie, A.A., Austin, B.N., Bradford, R.B. and Reynard, N.S., 1998. “Assessment of global water resources – phase II. Estimates of present and future water availability for Eastern and Southern Africa”, Technology Development & Research Programme, DFID Report 98/4.

Mitchell, T.D., Carter, T.R., Jones, P.D., Hulme, M., New, M., 2003: “A comprehensive set of high-resolution grids of monthly climate for Europe and the globe: the observed record (1901-2000) and 16 scenarios (2001-2100)”. *Journal of Climate*: submitted (August 2003)

Moore R.J., 1985. “The probability-distributed principle and runoff production at point and basin scales”, *Hydrol. Sci. J.*, 30, 2, 273-297

Nash, J. E. and J. V. Sutcliffe (1970), “River flow forecasting through conceptual models part I — A discussion of principles”, *Journal of Hydrology*, 10 (3), 282–290.

New, M., Hulme, M. and Jones, P.D., 1999: “Representing twentieth century space-time climate variability. Part 1: development of a 1961-90 mean monthly terrestrial climatology”. *Journal of Climate* **12**, 829-856 ([abstract](#))

Nijssen, B., O’Donnell, G., Lettermaier, D.P., Lohmann, D. and Wood, E.F., 2001, “Predicting the discharge of global rivers”, *Journal of Climate*, 14, pp. 3307-3323.

Noman, N.S., 1997. “Optimal operation of the Kaptai reservoir, Bangladesh”, M.Engg. Thesis,

Asian Institute of Technology, School of Civil Engineering, Bangkok, Thailand.

Prudhomme, C., 2006, “GCM and downscaling uncertainty in modelling of current river flow: why is it important for future impacts?”, *Climate Variability and Change—Hydrological Impacts* (Proceedings of the Fifth FRIEND World Conference held at Havana, Cuba, November 2006), IAHS Publ. 308.

Ramankutty, N. and Foley, J.A., 1998. “Characterizing patterns of global land use: an analysis of global croplands data”, *Global Biogeochemical Cycles* 12(4), 667-685.

Rees, G. and Collins, D.N., 2004. “An assessment of the potential impacts of deglaciation on the water resources of the Himalaya”, SAGARMATHA Technical report, Centre for Ecology and Hydrology, 2004.

Saxton, K.E., Rawls, W.J., Romberger, J.W. and Papendick, R.I. (1986) Estimating generalised soil water characteristics from texture. *Soil Sci. Soc. Am. J.* **50**(4), 1031-1036.

Schloemer, R. W., 1954. “Analysis and synthesis. of hurricane wind patterns over Lake Okechobee, Florida”. Hydromet. Report No. 31 [Govt. Printing Office, No. C30 70:31].

Siebert, S., Döll, P. and Hoogeveen, J., 2001. *Global map of irrigated areas version 2.0*, Center for Environmental Systems Research, University of Kassel, Germany / Food and Agriculture Organization of the United Nations, Rome, Italy

<http://www.fao.org/ag/AGL/aglw/aquastat/irrigationmap/index.stm>

Smith, S. D. and Banke, E. G., 1975. “Variation of the sea surface drag coefficient with wind speed”. *Quart. J. Roy. Meteor. Soc.* 101: 665-673

UN-HABITAT, 2004. *The Human Settlements Statistical Database version 4 at the national level*, (HSDB4-99), Human Settlements Indicators (HSI) Model. Available at http://www.unhabitat.org/programmes/guo/guo_hsd4.asp.

UNPD, 2005. *World Population Prospects: The 2004 Revision*, Department of Economic and Social Affairs, Population Division, United Nations, New York. Available at <http://esa.un.org/unpp/>.

United States Geological Survey (USGS), 2001. *HYDRO1k Elevation Derivative Database – Asia*. Distributed by the Land Processes Distributed Active Archive Center (LP DAAC), located at the USGS EROS Data Centre <http://LPDAAC.usgs.gov>.

United States Geological Survey (USGS), 2005. *Global Land Cover Characteristics Database, Version 2.0*, National Center for Earth Resources Observation & Science (EROS), <http://edcsns17.cr.usgs.gov/glcc/>.

Vörossmarty, C.J., Moore, B., Grace, A.L., Gildea, M.P., Melillo, J.M., Peterson, B.J., Rasetter, E.B. and Steudler, P.A. 1989. “Continental scale models of water balance and fluvial transport: an application to South America. *Global Biogeochemical Cycles*, 3, pp. 241-265.

Warwick, R. A., Barrow, E. M. & Wigley, T. M. L., 1993. “Climate and sea level change: observations, projections and implications”. Cambridge: Cambridge University Press.

Willmott, C. J. and Matura K.. 2001, Terrestrial air temperature and precipitation: monthly and annual time series (1950-1999) (version 1.02). Center for Climate Research. University of Delaware. Newark, DE.

Wint, W. 2005. “Global Livestock Distributions”, Data archive prepared by Environmental Research Group Oxford Limited for the Pro-poor Livestock Policy Initiative of the Animal Production and Health Division of the Food and Agriculture Organisation of the United Nations, Rome, Italy. Available at <http://ergodd.zoo.ox.ac.uk/agaagdat/>.

Appendix A Data Sources for Areas Outside of Bangladesh

Physiological Parameters

Data	Source	Details
Cell code	-	Calculated from co-ordinates
Sub-catchments	-	Determined from calibration sites
Mountain Cells	Identified using DEM from Hydro1k	see later
Cell area	-	Calculated using formula and latitude
Flow directions	Based on DDM30 by Döll & Lehner (2001)	Gridded data at 0.5 degrees resolution
Soil Texture	FAO Digital Soil Map of the World (FAO, 1994)	ArcGIS Coverage
Land Use	Global Land Cover Characteristics Data Base (USGS, 2005)	BSQ image file at 1km resolution, Lambert Azimuthal Equal Area Projection
Proportional Loss	-	Assumed/ Calibration parameter
Muskingham Parameter	Based on Hydro1k DEM (see later)	Assumed/ Calibration parameter.
Lakes	Digital Chart of the World (ESRI, 1993)	ArcGIS Coverage
	<i>Tibet Map Institute, (TMI, 2000) www.tibetmap.com</i>	<i>Digitised maps</i>
	US Tactical Pilotage Charts	
Elevation	Hydro1k DEM, (USGS, 2001)	BSQ image file at 1km resolution, Lambert Azimuthal Equal Area Projection

Snow and Glacier Data

Data	Source	Type
------	--------	------

Climate data elevation	relevant climate data source, e.g. CRU for 61-90 baseline	Raster
Elevation, mountain identification, glacier max/min/mean elevation	Hydro1k (USGS, 2001)	1km in Lambert- Azimuth equal-area projection
Glacier Location, Percentage ice	Digital Chart of the World and Global Land Cover Characteristics (ESRI, 1993)	Coverage

Estimation of water demands

Data	Source	Type
Total Population	Gridded Population of the World (CIESIN et al, 2000)	Raster at resolution 2.5 minute
	FAO Total Population density in South Asia (FAO, 2001)	Raster 5 minute
	World Population Prospects (UNPD, 2005)	National
Urban Population	Based on FAO Rural Population in South Asia (FAO, 2001)	Raster 5 minute
	World Population Prospects (UNPD, 2005)	National
Cattle/Sheep/Goat Population	FAO Bovine/Small Ruminant Population Density (Wint, 2005)	Raster at 5km resolution
	FAOSTAT (FAO, 2005)	National statistics
Urban/Rural demand	AQUASTAT (FAO, 2005)	National
Industrial demand	AQUASTAT (FAO, 2005)	National
	Distribution based on urban population density	See urban population
Crop area/type/planting month	Distribution based on global map of irrigated areas (FAO, 2001) and global cropland data (Ramankutty and Foley, 1998)	Raster 5 minute resolution

Data	Source	Type
	Agricultural Statistics at a Glance (DES, 2004)	State-wise data
	AQUASTAT (FAO)	National Statistics
Annual Irrigation	FAO – AQUASTAT	National Statistics
	Distribution based on FAO - global map of irrigated areas	Raster 5 minute resolution

Climate Data

The climate data required to drive the hydrological model

Source	Time Frame	Details
CRU (Mitchell et al, 2000)	1901-2000 observed	0.5 degree geographic projection
PRECIS (Hadley Centre, 2005)	1979-1993 “Observed” Baseline (ERA-15)	Met. Office PP format, 0.44 degree resolution, Rotated-Polar Co-ordinates
	1961-1990 Baseline	
	2070-2100 SRES A2	
HadRM2 (Hassell and Jones, 1999)	2041-2060 control	ASCII, 0.44 degree resolution, Rotated-Polar Co-ordinates
	2041-2060 perturbed (+1%/yr CO ₂)	

Appendix B Provisional programme for final Dissemination Workshop

(To be organised and hosted by BUET in May 2007)

Day 1: Final Workshop on Impact of CLimate and Sea level change in the Indian sub-Continent (CLASIC)

Session 1: Inauguration (Time: 9:15 – 10:15)

Chief Guest: Vice-Chancellor, BUET

Special Guest: from DFID

- a) Welcome Address – IWFM
- b) Project overview – CEH
- c) Speech by - Chief Guest
- d) Speech by - Special Guest
- e) Vote of thanks - CEGIS

Refreshment: 12:30 – 1:30

Session 2: Project Approach (Time: 1:30 – 3:45)

- a) Climate model – Hadley Centre
Discussion on paper a
- b) Hydrological model – CEH & IWFM
Discussion on paper b
- c) Sea level and storm surge model - POL
Discussion on paper c
- d) Water demand scenario – CEGIS & WARPO
Discussion on paper d
- e) Remarks by Chairman

Lunch break: 1:15 – 2:15

Session 3: Impact Prediction (Time: 1:30 – 3:40)

- a) Climate change - CEH
Discussion on paper a
- b) Water availability – IWFM & CEH
Discussion on paper b
- c) Riverine flooding – IWFM & CEGIS
Discussion on paper c
- d) Sea level rise and storm surge flooding – CEH & POL
Discussion on paper d
- e) Implications on National Water Management Plan – WARPO & IWFM
Discussion on paper e
- f) Remarks by Chairman
- g) Vote of thanks

Day 2: Meeting with Water Resources and Disasters Managers

(Time: 11:00 - 1:00)

- a) Purpose of Meeting
- b) Summary of project findings and workshop opinion
- c) Discussion on what needs to be done and recommendations
- d) Closing remarks by Chairman
- e) Vote of thanks

Lunch: 1:00– 1:30

Appendix C: Land cover to soil capacity conversion

Soil texture class	Root depth (m)				Field capacity (mm)				Saturation capacity (mm)			
	Forest	Shrub	Grass	Bare soil	Forest	Shrub	Grass	Bare soil	Forest	Shrub	Grass	Bare soil
Sand	2.5	2.0	1.0	0.5	369	296	148	74	886	709	354	177
Sandy loam	2.0	1.6	1.0	0.5	420	336	210	105	825	660	412	206
Silt loam	2.0	1.7	1.3	0.5	590	501	383	147	935	795	608	234
Clay loam	1.6	1.4	1.0	0.5	533	466	333	167	806	705	504	252
Clay	1.2	1.0	0.7	0.5	580	484	339	242	653	544	381	272
Lithosol	0.1	0.1	0.1	0.1	27	27	27	27	50	50	50	50
Organic	-	-	-	-	50	50	50	50	100	100	100	100

Table C.1 Rooting depths and corresponding field and saturated capacities

IGBP-DIS class	% of Universal Components											
	1	2	3	4	5	6	7	8	9	10	11	12
1 Evergreen needleleaf forests			80		5					15		
2 Evergreen broadleaf forests	90									10		
3 Deciduous needleleaf forests				80	5					15		
4 Deciduous broadleaf forests		80			15					5		
5 Mixed forests		40	40		10					10		
6 Closed shrublands					15		70			15		
7 Open shrublands					35		35			30		
8 Woody savannas		45			50					5		
9 Savannas		20			75					5		
10 Grasslands					90					10		
11 Permanent wetlands												100
12 Croplands						80				20		
13 Urban & built-up								100				
14 Cropland/Nat.Veg.Mosaic						80				20		
15 Snow & ice											100	
16 Barren										100		
17 Water bodies									100			
Universal Class	Broadleaf evergreen tree	Broadleaf deciduous tree	Needleleaf evergreen tree	Needleleaf deciduous tree	Grass	Crop	Shrub	Urban	Water	Bare soil	Land ice	Wetland
GWAVA Class	Tree				Grass/Crop		Shrub	Bare Soil	Water	Bare soil	Bare Soil	Wetland

Table C.2 Conversion of land cover types

Appendix D: Water Availability Indices for GBM

The following is a set of the surface water availability indices for the whole of the Ganges-Brahmaputra-Meghna basin for the baseline, 2020s and 2050s.

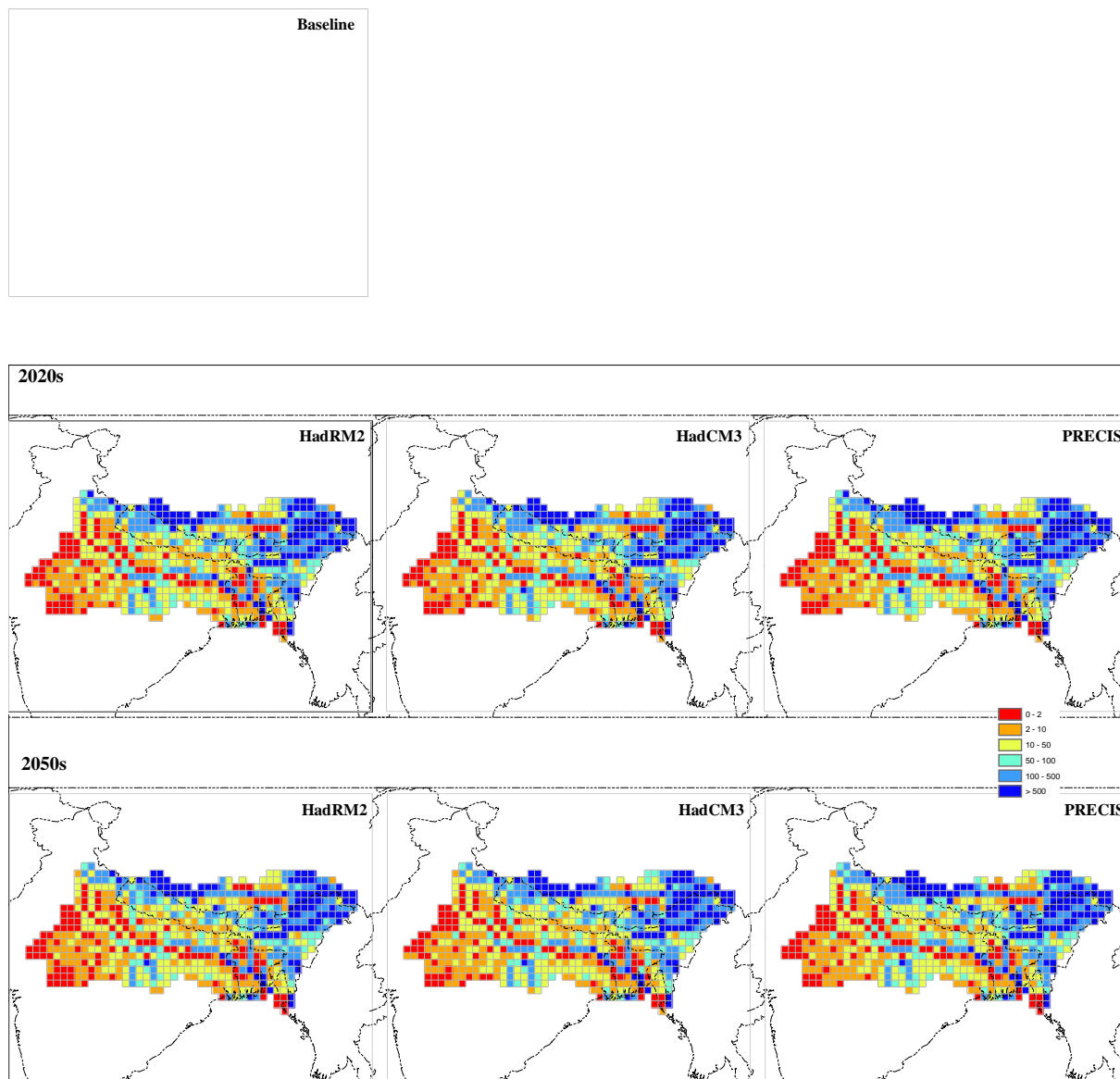


Figure D.1 SWAI-1 for Hadley Centre climate models

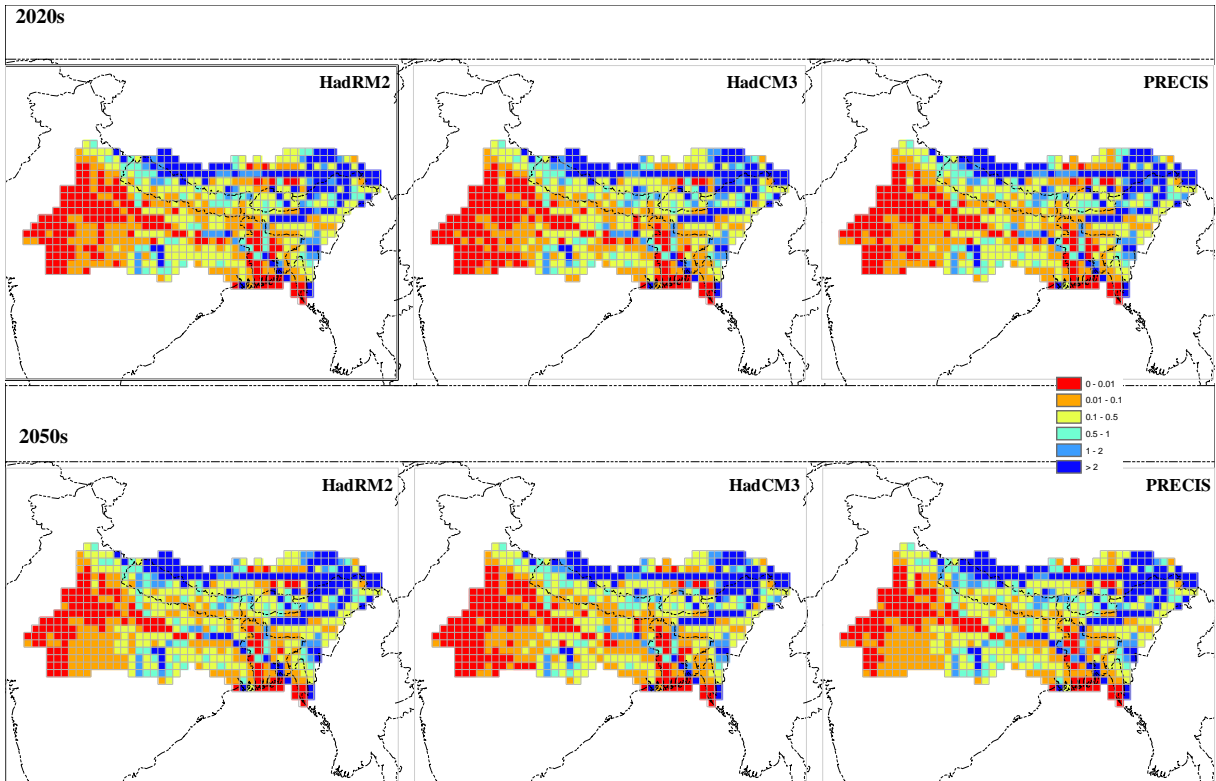
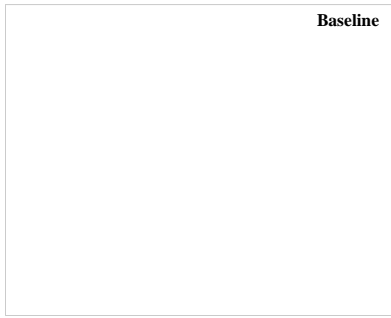


Figure D.2 SWAI-2 for Hadley Centre climate models

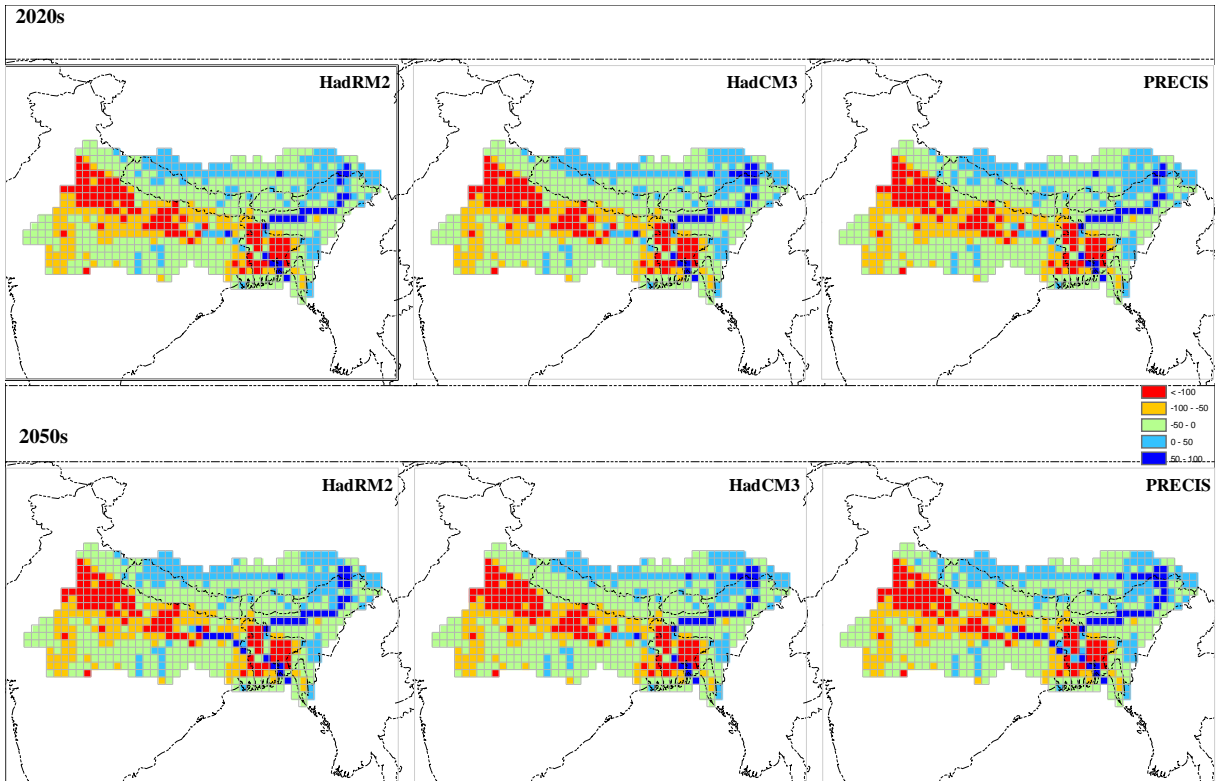
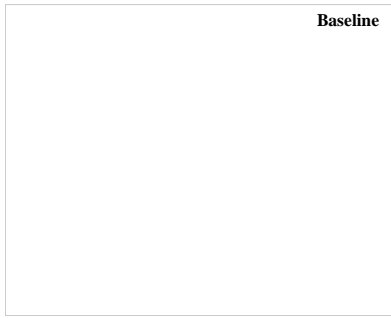


Figure D.3 SWAI-3 in Mm^3 for Hadley Centre climate models

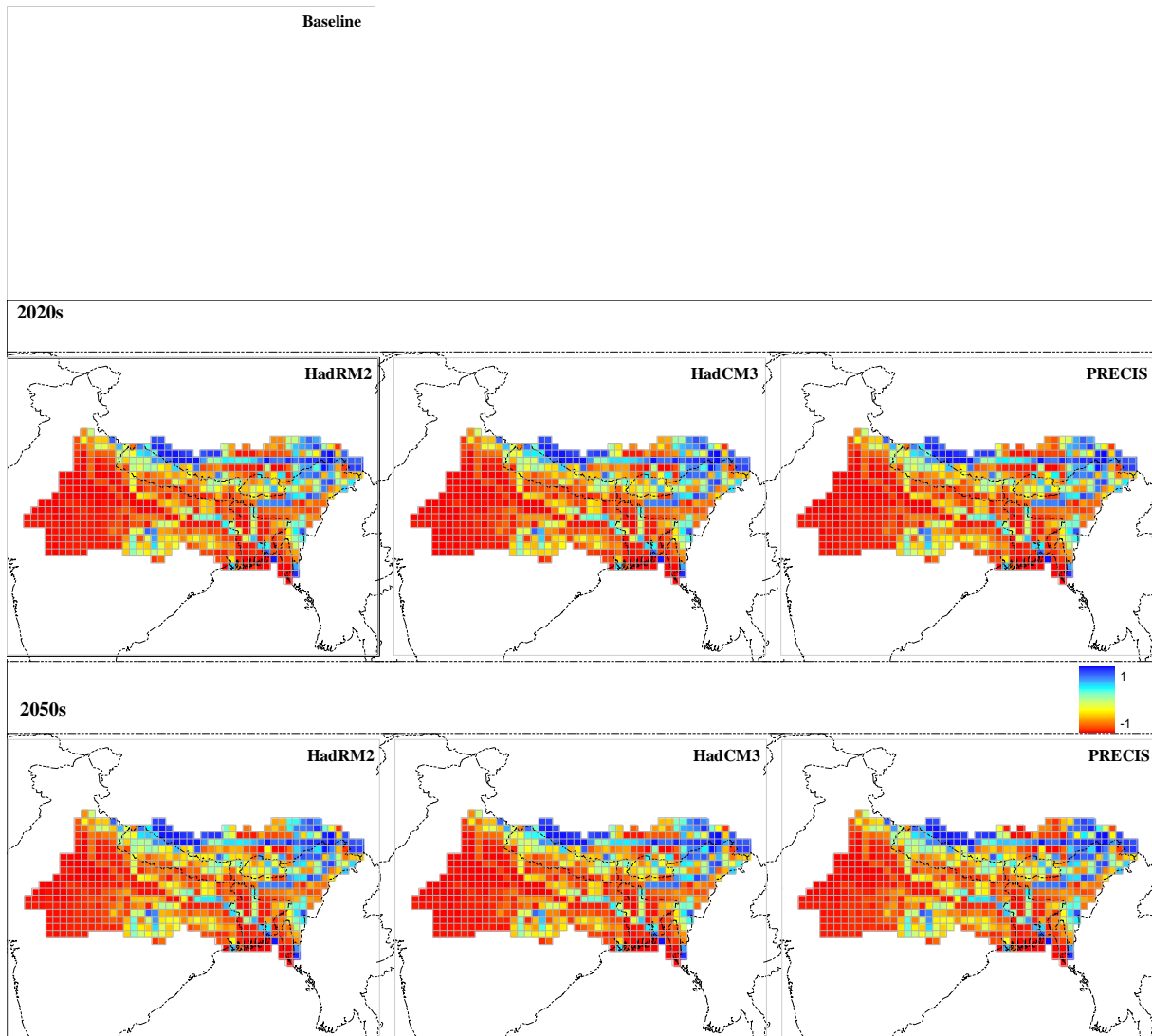


Figure D.4 SWAI-4 for Hadley Centre climate models